General Disclaimer

One or more of the Following Statements may affect this Document

- This document has been reproduced from the best copy furnished by the organizational source. It is being released in the interest of making available as much information as possible.

- This document may contain data, which exceeds the sheet parameters. It was furnished in this condition by the organizational source and is the best copy available.

- This document may contain tone-on-tone or color graphs, charts and/or pictures, which have been reproduced in black and white.

- This document is paginated as submitted by the original source.

- Portions of this document are not fully legible due to the historical nature of some of the material. However, it is the best reproduction available from the original submission.

ENGINEERING ANALYSIS, INC.

SPACE SHUTTLE

SIMULATION MODEL

Summary Report

Contract NAS8-33818

Prepared For:

National Aeronautics and Space Administration
George C. Marshall Space Flight Center
Marshall Space Flight Center, Alabama 35812

Prepared By:

Frank B. Tatom
S. Ray Smith

November 17, 1980

ENGINEERING ANALYSIS, INC.

2109 Clinton Ave. W., Suite 432
Huntsville, Alabama 35805
(205)533-9391

TABLE OF CONTENTS

LIST OF ILLUSTRATIONS

LIST OF ILLUSTRATIONS
(Continued)

LIST OF ILLUSTRATIONS
(Continued)

LIST OF TABLES

LIST OF TABLES
(Continued)

1. INTRODUCTION

The effects of atmospheric turbulence in both horizontal and near-horizontal flight, during the return of the Space Shuttle, are important for determining design, control, and "pilot-in-the-loop" effects. A non-recursive model (based on von Karman spectra) for atmospheric turbulence along the flight path of the Shuttle Orbiter has been developed which provides for simulation of instantaneous vertical and horizontal gusts at the vehicle center-of-gravity, and also for simulation of instantaneous gust gradients. Based on this model the time series for both gusts and gust gradients have been generated and stored on a series of magnetic tapes which are entitled Shuttle Simulation Turbulence Tapes (SSTT). The time series are designed to represent atmospheric turbulence from ground level to an altitude of 10,000 meters.

A description of the turbulence generation procedure is provided in Section 2. The results of validating the simulated turbulence are described in Section 3. Conclusions and recommendations are presented in Section 4 with Section 5 containing references cited. Appendix A contains the tabulated one-dimensional von Karman spectra while Appendices B and C present the results of spectral and statistical analyses of the SSTT. A more detailed description of the proper use of the tapes is provided elsewhere [1].

2. TURBULENCE GENERATION PROCEDURE

The non-recursive turbulence model used to generate the SSTT is based on von Karman spectra with finite upper limits corresponding to the dimensions of the Space Shuttle, relative to the scale of turbulence in the atmosphere. Because the scale of turbulence increases with altitude while the dimensions of the Space Shuttle are fixed, the finite upper limits of the von Karman spectra increase with altitude. In order to take into account the resulting spectral changes, the atmosphere, extending from ground level to 10,000 meters, was divided into four altitude bands. The subsections which follow provide a description of the development and application of the turbulence generation procedures.

2.1 SELECTION OF ATMOSPHERIC BANDS

The standard deviations $(\sigma_1, \sigma_2, \sigma_3)$ and the scales (L_1, L_2, L_3) of atmospheric turbulence are functions of altitude, increasing with increasing altitude as shown in Table 2-1. Notice should be taken that the values for σ_i and L_i presented in this table are designed for use with von Karman spectral models and therefore differ somewhat from previously tabulated values [2] which were designed for use with Dryden spectra. The von Karman σ_i and L_i have been computed based on the requirement for local isotropy, which can be expressed as

$$\frac{\sigma_1^2}{L_1^{2/3}} = \frac{\sigma_2^2}{L_2^{2/3}} = \frac{\sigma_3^2}{L_3^{2/3}} \tag{2-1}$$

This method of computation is consistent with the established procedure [3].

Based on the variation of σ_i and L_i presented in Table 2-1, the atmosphere was divided into four altitude bands as presented in Table 2-2. Within each band, as also indicated in Table 2-2, characteristic scales of turbulence were selected for use in calculating the finite upper limit of the turbulence spectral model discussed in subsection 2.2.

ALTITUDE (m)	STANDARD DEVIATION OF TURBULENCE			INTEGRAL SCALES OF TURBULENCE		
	σ_1(m/sec)	σ_2(m/sec)	σ_3(m/sec)	L_1(m)	L_2(m)	L_3(m)
10	1.79	1.49	1.12	19	10	5
20	2.15	1.80	1.48	34	20	11
30	2.39	2.06	1.74	47	30	18
40	2.57	2.26	1.95	59	40	26
50	2.73	2.43	2.14	70	50	34
60	2.86	2.58	2.30	82	60	42
70	2.98	2.72	2.44	92	70	51
80	3.09	2.84	2.58	103	80	60
90	3.19	2.95	2.70	113	89	69
100	3.28	3.05	2.81	123	99	78
200	3.93	3.83	3.71	214	197	180
300	4.37	4.37	4.36	296	295	294
304.8						
400						
500	4.39	4.39	4.39	300	300	300
600						
700						
762						
800						
900	5.7	5.7	5.7			
1524						
2000	5.79	5.79	5.79			
3048						
4000						
5000	5.52	5.52	5.52	533	533	533
6096						
7000	5.27	5.27	5.27			
8000						
9144						
10000	4.22	4.22	4.22			

TABLE 2-2. TURBULENCE PARAMETERS FOR ALTITUDE BANDS

Band #	Lower Limit (m)	Upper Limit (m)	Time Interval (dimensionless)	Finite Limit of Spectrum (dimensionless)			Von Karman Length Scale (m)		
			T	Ω_{1MAX}	Ω_{2MAX}	Ω_{3MAX}	L_1	L_2	L_3
1	0	30	.6018	5.22	3.38	7.22	47	30	18
2	30	100	.2300	13.66	11.14	31.27	123	99	78
3	100	762	.09431	33.31	33.76	120.27	300	300	300
4	762	10000	.05309	59.18	59.97	213.68	533	533	533

2.2 DEVELOPMENT OF VON KARMAN SPECTRA WITH FINITE UPPER LIMITS

As developed previously [4] the basic three-dimensional von Karman relation to be integrated for the dimensionless gust spectra is,

$$\phi_{ii}(\Omega_1, \Omega_2, \Omega_3) = \frac{55}{36a\pi^2} \frac{(\Omega^2 - \Omega_i^2)}{(1+\Omega^2)^{17/6}} \tag{2-2}$$

The corresponding von Karman relation for dimensionless gust gradient spectra is

$$\phi_{ii/jj}(\Omega_1, \Omega_2, \Omega_3) = \frac{55}{36\pi^2 a^3} \frac{\Omega_j^2(\Omega^2 - \Omega_i^2)}{(1+\Omega^2)^{17/6}} \tag{2-3}$$

These three-dimensional spectral relations must be integrated over certain ranges of values of Ω_2 and Ω_3 to obtain one-dimensional spectral models $\phi_{ii}(\Omega_1)$ and $\phi_{ii/jj}(\Omega_1)$.

2.2.1 Upper Limits of Integration

The upper limits of integration are calculated according to the relation [5]

$$\Omega_{imax} = aL_i / \ell_i \qquad\qquad (2\text{-}4)$$

where

      a = 1.339

      L_i = scale of the ith component of atmospheric turbulence

      ℓ_i = characteristic length of Space Shuttle in ith direction

Values of L_i for the four bands are given in Table 2-2 while the characteristic lengths, ℓ_i, are presented in Table 2-3. The resulting values of Ω_{imax} are included in Table 2-?.

<div align="center">

TABLE 2-3. CHARACTERISTIC DIMENSIONS
OF THE SPACE SHUTTLE [6]

</div>

Characteristic Length	Magnitude (ft)	(m)	Explanation
ℓ_1	39.56	12.06	mean aerodynamic chord
ℓ_2	39.05	11.9	1/2 wingspan
ℓ_3	10.95	3.34	1/2 fuselage thickness

2.2.2 One-Dimensional Spectra

As indicated in Table 2-4, there are six spectra of primary interest for turbulence simulation. Based on second-order numerical integration, the six corresponding three-dimensional gust and gust gradient spectral relations were integrated over Ω_3 and Ω_2 (with the appropriate upper limits). The resulting one-dimensional spectra for all altitude bands are presented in Appendix A. These spectra are used in establishing the impulse response functions associated with digital filter simulation processes described in subsection 2.3.

TABLE 2-4. TYPES OF SIMULATED TURBULENCE

Type	Corresponding Spectrum	Comments
u_1	ϕ_{11}	longitudinal gust
u_2	ϕ_{22}	transverse gust
u_3	ϕ_{33}	vertical gust
$\partial u_2/\partial x_1$	$\phi_{22/11}$	yaw
$\partial u_3/\partial x_1$	$\phi_{33/11}$	pitch
$\partial u_3/\partial x_2$	$\phi_{33/22}$	roll

2.2.3 Dimensionless Energy Content

The total dimensionless energy content of each one-dimensional spectra in each altitude band was established by integrating the corresponding spectra over the appropriate finite limit, Ω_{1max}, indicated in Table 2-2. The resulting energy content is presented in Table 2-5. As might be expected the total dimensionless energy content of each of the turbulent gust series is less than unity. The dimensionless energy[*] content for each gust gradient, however, is not limited in such a manner and range as high as 54.125. For both gusts and gust gradients the total energy content increases with altitude because of similar increases in the limits of integration.

---

[*]Actually the term "energy" is not precise when dealing with gust gradients.

TABLE 2-5.   DIMENSIONLESS ENERGY CONTENT
FOR GUSTS AND GUST GRADIENTS

Spectrum	Altitude Band			
	1	2	3	4
Φ_{11}	.5388	.7841	.8956	.9298
Φ_{22}	.5772	.7942	.8952	.9296
Φ_{33}	.5225	.7646	.8809	.9197
$\Phi_{22/11}$	1.2832	6.6484	24.768	54.125
$\Phi_{33/11}$	1.1321	5.9699	22.644	49.528
$\Phi_{33/22}$	.7049	4.9954	22.893	50.057

2.3   DIGITAL FILTER SIMULATION

The simulated turbulence, $Y(t)$, can be interpreted as the response or output of a control system [7] with double-sided impulse response functions, $h(t)$, subject to an input consisting of Gaussian white noise $I(t)$. This response can be represented by the convolution integral

$$Y(t) = \frac{1}{2\pi} \int_{-\infty}^{\infty} h(\tau) \, I(t-\tau) \, d\tau \qquad (2-5)$$

Based on filter theory the double-sided spectrum, $\Phi_{DY}(\Omega)$, of the simulated turbulence satisfies the relation

$$\Phi_{DY}(\Omega_1) = H(\Omega_1) H^*(\Omega_1) \Phi_{DI}(\Omega_1) \qquad (2-6)$$

where

$$H(\Omega_1) = F[h(t)]$$

$$\Phi_{DI}(\Omega_1) = \text{double-sided power spectrum for white noise}$$

Generally the standard deviation of any white signal has a value of unity[*]. Furthermore in most practical situations the white noise is defined to occur over some interval extending from $-\Omega_{1max}$ to $+\Omega_{1max}$.

For this case,

$$\Phi_{DI}(\Omega_1) = \frac{1}{2\Omega_{1max}}$$

$$= \frac{T}{2\pi} \tag{2-7}$$

where

T = time interval associated with generation process $(=\pi/\Omega_{1max})$

By substitution,

$$\Phi_{DY}(\Omega_1) = H(\Omega_1)H^*(\Omega_1)\frac{T}{2\pi} \tag{2-8}$$

If $H(\Omega_1)$ is limited to real values,

$$\Phi_{DY}(\Omega_1) = H^2(\Omega_1)\frac{T}{2\pi} \tag{2-9}$$

Rearrangement of Eq (2-9) yields

$$H(\Omega_1) = \sqrt{\frac{2\pi}{T}\Phi_{DY}(\Omega_1)} \tag{2-10}$$

---

[*]In some derivations [7,8,9], the standard deviation of the white noise signal has been set equal to $2\Omega_{1max}$. In this case the standard deviation of the input becomes very large as $\Omega_{1max} \to \infty$.

Then based on the definition of the inverse Fourier transform, the double-sided impulse response function h(t) can be expressed as

$$h(t) = F^{-1}[H(\Omega_1)]$$

$$= \int_{-\infty}^{\infty} \sqrt{\frac{2\pi}{T} \phi_{DY}(\Omega_1)} \; \cos(\Omega_1 t) \; d\Omega_1$$

$$= 2\int_{0}^{\infty} \sqrt{\frac{2\pi}{T} \phi_{DY}(\Omega_1)} \; \cos(\Omega_1 t) \; d\Omega_1$$

$$= 2\int_{0}^{\infty} \sqrt{\frac{2\pi}{T} \frac{\phi_{Y}(\Omega_1)}{2}} \; \cos(\Omega_1 t) \; d\Omega_1$$

$$= 2\sqrt{\frac{\pi}{T}} \int_{0}^{\infty} \sqrt{\phi_{Y}(\Omega_1)} \; \cos(\Omega_1 t) \; d\Omega_1 \qquad (2\text{-}11)$$

where

$$\phi_{Y}(\Omega_1) = \text{single-sided spectrum of } Y(t)$$

The single-sided spectra tabulated in Appendix A correspond to $\phi_{Y}(\Omega_1)$

The discrete version of the convolution integral given in Eq (2-5) yields

$$Y(k) = \sum_{j=-N}^{+N} h(j) \; I(k-j) \; T \qquad (2\text{-}12)$$

where

$Y(k)$ = discrete sampled turbulence output

$h(j)$ = discrete double-sided impulse response function h(jT)

$I(k)$ = discrete sampled white noise input

2-8

Eq (2-12) represents the basic, non-recursive relation for the generation
of simulated turbulence*. The impulse response functions $h(t)$ were evaluated
by means of second-order numerical integration of Eq (2-11) using the six
spectra from Appendix A. The values of dimensionless time increment, T, used
for the four altitude bands are included in Table 2-2 and are based on the
values of Ω_{1max} shown in the same table. Thus the Nyquist generation fre-
quencies Ω_{NG} for the simulated turbulence correspond to the upper frequency
limits for Ω_1 as computed by Eq (2-4) for each altitude band.

2.4   EFFECTS OF DIGITIZATION

        The effects of digitization in turbulence simulation have been
considered by a number of investigators [7-10]. As a result of these studies
two basic digitization effects have been generally identified.

        The first effect results from the assumption of a white noise
spectrum with unit strength instead of unit power, noted in subsection 2.3.
To correct for such an "effect" the proposed procedure is to divide the series
approximation of the convolution integral by ΔT. This "effect" disappears
when the white noise spectrum has unit power.

        The second effect involves the tapering of the spectrum of simulated
white noise, Φ_1', in the vicinity of the Nyquist generation frequency, Ω_{NG}. Some
investigators [8,10] have considered it necessary, because of the tapering
effect, to generate the simulated turbulence time series at a rate from four
to ten times the rate at which the series will be sampled.

        The second effect arises from the discrete processes associated
with both the generation and sampling of the simulated turbulence. In the
case of discrete white noise with unit variance, the time series involved is
basically a train of step functions as shown in Figure 2-1. The autocorre-
lation function of the train of step functions depicted in Figure 2-1 can

---

*In certain references [7,9] to correct for the "effect of digitizing", the series
represented by Eq (2-12) has been divided by ΔT. This process can be seen to be
dimensionally incorrect and actually results from the use of a white noise
spectrum with unit strength instead of a strength of $T/2\pi$.
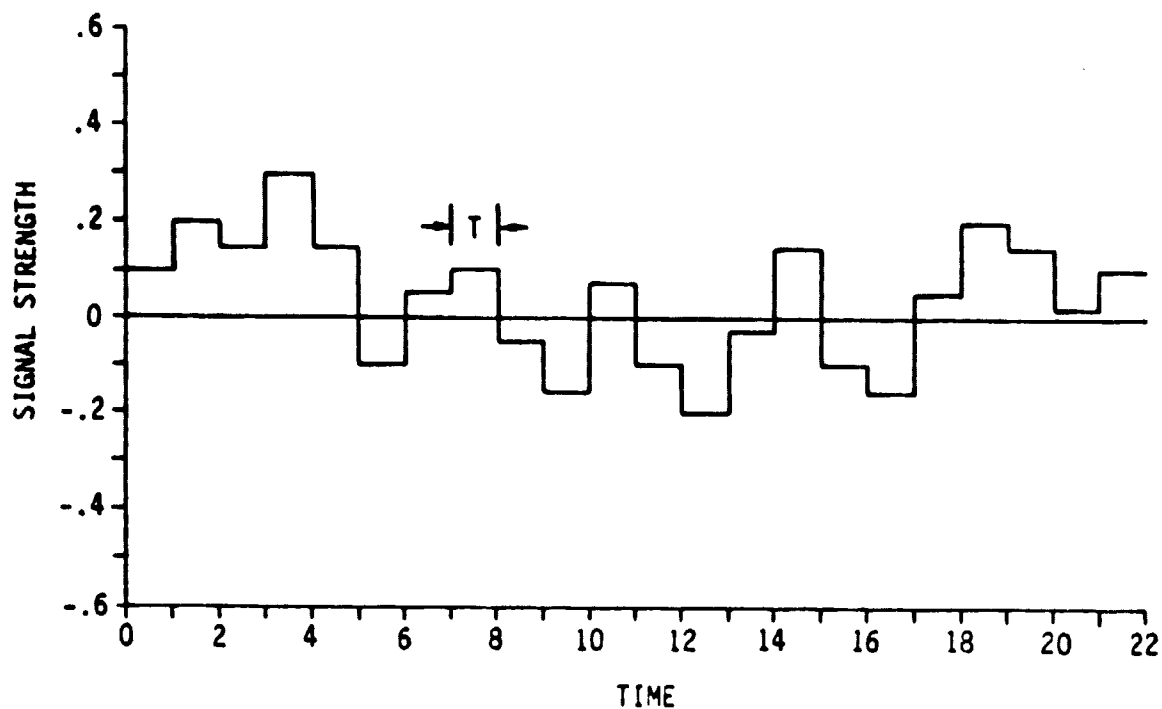
Figure 2-1. Discrete White Noise Series

be shown to be

$$
R_{DI}(\tau) \;=\; \begin{cases} 1 - \dfrac{|\tau|}{T_G} & (\,|\tau| \le T_G\,) \\[2ex] 0 & (\,|\tau| > T_G\,) \end{cases}
\tag{2-13}
$$

The corresponding double-sided power spectrum by definition is

$$
\begin{aligned}
\phi'_{DI}(\Omega) &\equiv F[R_{ID}(\tau)] \\[1ex]
&= \frac{T_G}{2\pi}\,\frac{\sin^2(\Omega T_G/2)}{(\Omega T_G/2)^2} \\[1ex]
&= \frac{1}{2\Omega_{NG}}\,\frac{\sin^2(\Omega\pi/2\Omega_{NG})}{(\Omega\pi/2\Omega_{NG})^2}
\end{aligned}
\tag{2-14}
$$

The single-sided version of this power spectrum is shown in Figure 2-2.
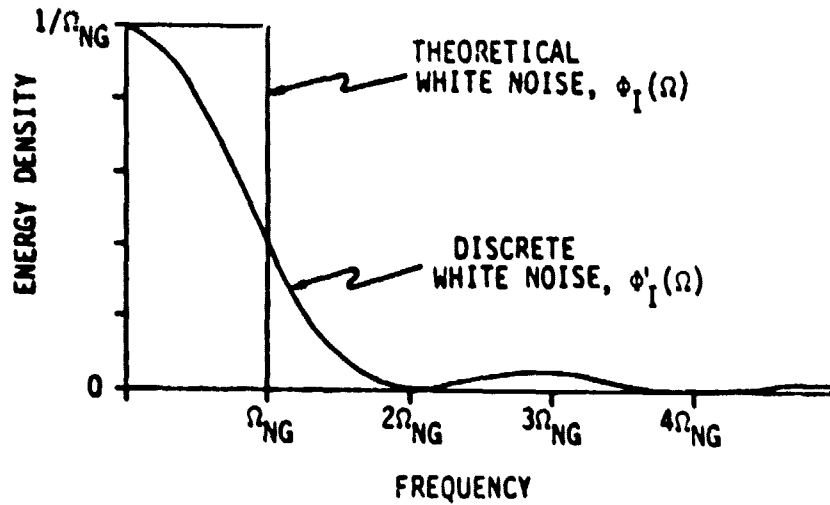
Figure 2-2. White Noise Spectra

Theoretical white noise, be definition, is characterized by a uniform power spectral distribution. In order to avoid infinite power, such a spectral distribution is normally restricted to the finite frequency band $(-\Omega_{NG} \leq \Omega \leq \Omega_{NG})$ for a double-sided spectrum. For a signal with unit power the spectral density function for such white noise is

$$\Phi_{DI}(\Omega) = \begin{cases} \dfrac{1}{2\Omega_{NG}} & (-\Omega_{NG} \leq \Omega \leq \Omega_{NG}) \\ \\ 0 & (\Omega_{NG} < |\Omega|) \end{cases} \qquad (2\text{-}15)$$

Such a theoretical distribution in single-sided form is also shown in Figure 2-2.

It is important to note that the two power spectra shown in Figure 2-2 are both normalized and thus

$$\int_{-\infty}^{\infty} \Phi_{DI}(\Omega)d\Omega = \int_{-\infty}^{\infty} \Phi'_{DI}(\Omega)d\Omega \qquad (2\text{-}16)$$

$$= 1$$

The theoretical spectrum is basically a rectangular pulse function while the discrete spectrum is characterized by tapering. The difference between these two spectra is generally considered the basis for the second digitization effect.

The preceding descriptions of the two spectra $\phi_I(\Omega)$ and $\phi_{DI}(\Omega)$ are based purely on mathematical theory. To observe such spectra in reality the corresponding time series would have to be sampled with an infinitesimal sampling interval. Actually, finite sampling intervals, T_S, must be used but this finite (or discrete) sampling process results in *aliasing*. The aliased spectrum, $\phi^+(\Omega)$, based on the finite sampling process, is related to the original spectrum according to the relation [11]

$$\phi^+(\Omega) = \sum_{k=-\infty}^{\infty} \phi(\Omega + 2k\Omega_{NS}) \qquad (2\text{-}17)$$

where

$$\Omega_{NS} = \text{Nyquist sampling frequency} \quad (=\pi/T_S)$$

For the case of the discrete white noise

$$\phi'^+_{DI}(\Omega) = \sum_{k=-\infty}^{\infty} \phi'_{DI}(\Omega + 2k\Omega_{NS})$$

$$= \frac{1}{2\Omega_{NG}} \sum_{k=-\infty}^{\infty} \frac{\sin^2[(\Omega + 2k\Omega_{NS})\pi/2\Omega_{NG}]}{[(\Omega + 2k\Omega_{NS})\pi/2\Omega_{NG}]^2} \qquad (2\text{-}18)$$

Numerical evaluation of this series has been carried out for $\Omega_{NG} = 100$ with various ratios of Ω_{NS}/Ω_{NG}, including .5, 1, 2, and 4. The resulting aliased spectra are presented in Figure 2-3. It is important to note that the figure indicates that

$$\phi'^+_{DI}(\Omega) = \left\{ \begin{array}{ll} \frac{1}{2\Omega_{NG}} & (-\Omega_{NG} \leq \Omega \leq \Omega_{NG}) \\ \\ 0 & (\Omega_{NG} < |\Omega|) \end{array} \right\} \quad (\Omega_{NG} = \Omega_{NS}) \qquad (2\text{-}19)$$
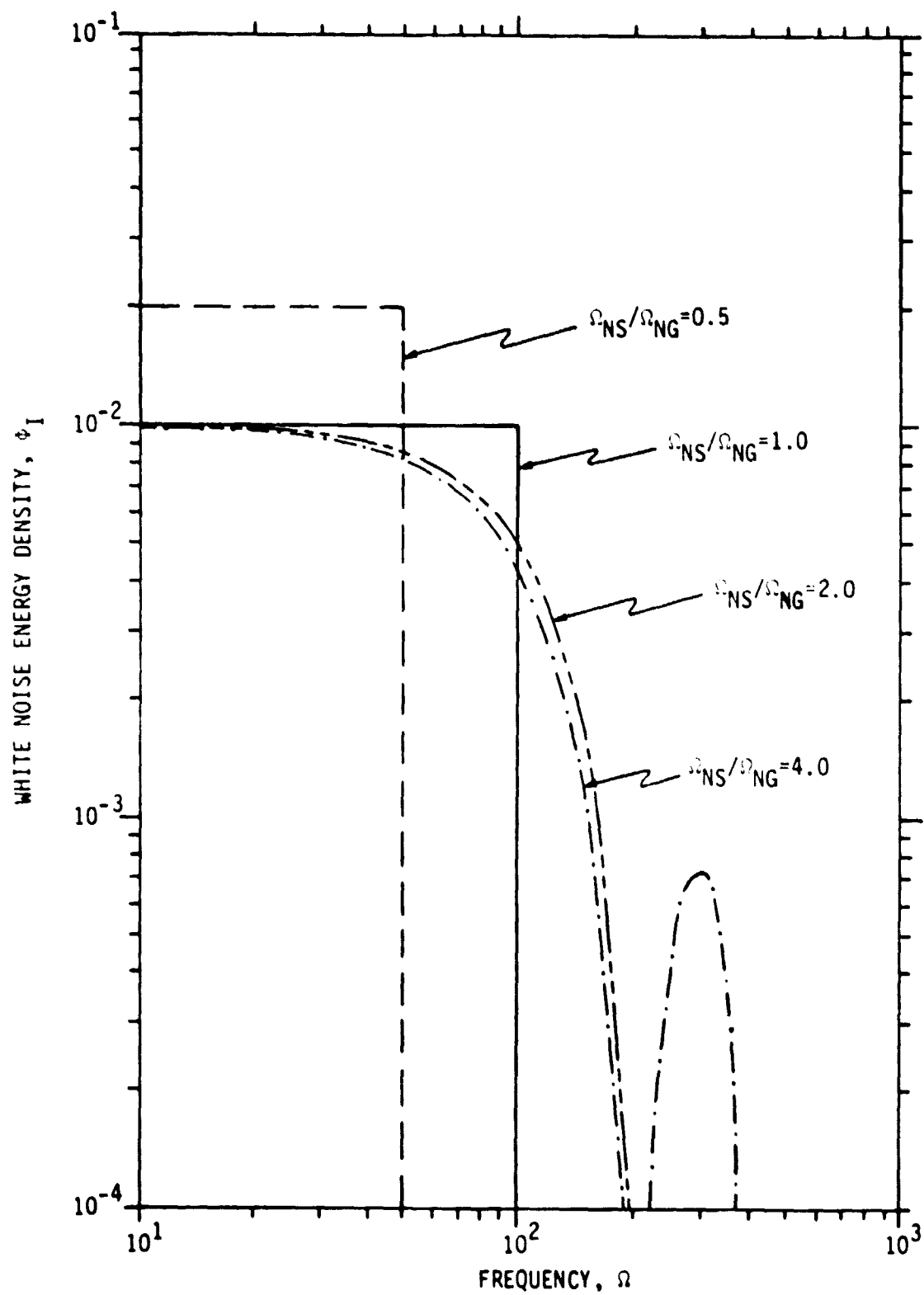
2-12

Figure 2-3. Effects of Aliasing on White Noise Spectrum

In this case, by comparison with $\phi_{DI}(\Omega)$,

$$\phi'^+_{DI}(\Omega) = \phi_{DI}(\Omega) \qquad (\Omega_{NG} = \Omega_{NS}) \qquad (2\text{-}20)$$

Thus for white noise *the aliasing due to discrete sampling exactly offsets the tapering due to discrete generation when the sampling frequency equals the generation frequency.* Based on this fundamental point, it is clear that in the simulation of white noise no tapering of the spectrum occurs as long as the sampling rate equals the generation rate. Under most conditions this equality is automatically satisfied.

The process of convolving the white noise with the appropriate impulse response function is also carried out in a discrete manner. The process involves selecting (or sampling) values of the white noise signal and the impulse response function at equal intervals in time and then approximating the convolution integral by a summation of products. It is important to note that the discrete sampling of both the white noise and the impulse response function normally occurs at the same rate as the generation rate for the white noise. Thus the resulting spectra for the sampled discrete white noise, as previously shown, will be uniform. According to the convolution theorem, the spectrum of the output signal equals the spectrum of the input white noise multiplied by the product of the Fourier transform of the inpulse response function and its complex conjugate. Thus, as previously noted in subsection 2.3, for a continuous signal,

$$\phi_{DY}(\Omega) = \phi_{DI}(\Omega)H(\Omega)H^*(\Omega) \qquad (2\text{-}6)$$

The Fourier transform $H(\Omega)$ for the *continuous* impulse function, h(t), is

$$H(\Omega) = F[h(t)]$$

$$= \sqrt{\frac{2\pi}{T} \phi_{DY}(\Omega)} \qquad (2\text{-}10)$$

The corresponding output spectrum for a discrete signal would be

$$\phi'_{DY}(\Omega) = \phi'_{DI}(\Omega)H'(\Omega)H'^*(\Omega) \qquad (2\text{-}21)$$

The Fourier transform $H'(\Omega)$ of the *discrete* impulse response function, $h'(t)$, is

$$H'(\Omega) = F[h'(t)] \qquad (2\text{-}22)$$

Based on the preceding development, for cases in which the sampling frequency equals the generation frequency, any difference between the discrete turbulence spectrum and the continuous spectrum apparently originates because of some difference between $H(\Omega)$ and $H'(\Omega)$.

3. SIMULATED TURBULENCE TAPES

The turbulence generation procedure described in Section 2 has been used to generate six dimensionless simulated turbulence time series which are stored on magnetic tapes as summarized in Table 3-1. The appropriate procedures for using the tapes are described elsewhere [1]. Subsection 3.1 provides a description of the results of validating the tapes while subsection 3.2 presents an explanation of the process for converting from dimensionless to dimensional values.

TABLE 3-1. INDEX OF SHUTTLE SIMULATED
TURBULENCE TAPES (SSTT)

Tape	Time Series	Comments
SSTT-1	u_1 - gust	longitudinal gust
SSTT-2	u_2 - gust	transverse gust
SSTT-3	u_3 - gust	vertical gust
SSTT-4	$\partial u_2/\partial x_1$ - gust gradient	yaw
SSTT-5	$\partial u_3/\partial x_1$ - gust gradient	pitch
SSTT-6	$\partial u_3/\partial x_2$ - gust gradient	roll

3.1   VALDIATION OF SIMULATED TURBULENCE

A spectral analysis of each of the dimensionless time series has been carried out by means of a Fast Fourier Transform FFT4 [12]. The results, which are presented in Appendix B, demonstrate that the simulated turbulence possesses the proper von Karman spectral characteristics.

All of the dimensionless time series have also been analyzed statistically to determine the gust and gust gradient probability density functions. As shown in Appendix C the results of these analyses indicate that both the simulated gusts and gust gradients are normally distributed, with near-zero means and standard deviations consistent with the energy content presented in Table 2-5.

3.2   CONVERSION TO DIMENSIONAL VALUES

The dimensionless time series on each tape must be converted to
dimensional form before actual use in a simulation exercise. The conversion
process generally involves multiplication and/or division by the appropriate
turbulence parameters. For dimensionless gusts, u_i, the corresponding standard
deviation, σ_i, should be used. Thus

$$u_i^* = \sigma_i u_i \qquad (3-1)$$

where

$$u_i^* = \text{dimensional gust}$$

For dimensionless gust gradient, $\dfrac{\partial u_i}{\partial x_j}$, the parameters σ_i and L_j are used.
Thus

$$\frac{\partial u_i^*}{\partial x_j^*} = \frac{\sigma_i}{L_j} \frac{\partial u_i}{\partial x_j} \qquad (3-2)$$

where

$$\partial u_i^*/\partial x_j^* = \text{dimensional gust gradient}$$

In the case of dimensionless time it is necessary to develop the
procedures for converting both from dimensionless to dimensional form and also
to dimensionless from dimensional. In proceeding from dimensionless to dimen-
sional time the dimensionless time step represents the basic unit to be
converted. The conversion involves the vehicle velocity, V, and the x_1-component
of turbulence scale, L_1. Thus

$$\Delta t^* = a L_1 T/V \qquad (3-3)$$

where

$$\Delta t^* = \text{dimensional time step}$$

It is important to note that because both L_1 and V vary with altitude, the resulting dimensional time step Δt^* is not a constant. To obtain dimensional time, t^*, a summation process is involved as follows:

$$t_N^* = \sum_{n=1}^{N} \Delta t_n^* \qquad (3\text{-}4)$$

$$= aT \sum_{n=1}^{N} L_{1n}/V_n$$

where

$$L_{1n} = L_1(Z_n)$$
$$V_n = V(Z_n)$$
$$Z_n = \text{altitude at } n\text{th step}$$

In converting to dimensionless from dimensional time the basic unit, the dimensional time step, δt^*, will normally be a constant. The corresponding dimensionless time interval, T_m, will be

$$T_m = \frac{V_m \delta t^*}{a L_{1m}} \qquad (3\text{-}5)$$

The total dimensionless time, t_M, will be

$$t_M = \sum_{m=1}^{M} T_m$$

$$= \sum_{m=1}^{M} \frac{V_m \delta t^*}{a L_{1m}}$$

$$= \frac{\delta t^*}{a} \sum_{m=1}^{M} V_m/L_{1m} \qquad (3\text{-}6)$$

3-3

The dimensional time, t_M, corresponds to some M' dimensionless time intervals, T, plus some fractional interval, T', as follows:

$$t_M = M'T + T' \tag{3-7}$$

where

$$0 \leq T' \leq T$$

Thus the number of intervals (of dimensionless time), M', can be computed as

$$M' = \text{Int}(t_M/T)$$

$$= \text{Int}\left(\frac{\delta t^*}{aT} \sum_{m=1}^{M} V_m/L_{1m}\right) \tag{3-8}$$

where

$$\text{Int}(\ ) = \text{integer value of }(\ )$$

The fractional interval, T', can be computed by the relation

$$T' = t_M - M'T \tag{3-9}$$

The interpolation process will involve interpolating between $t_{M'}$ and $t_{M'+1}$ at the point t_M as shown in Figure 3-1.
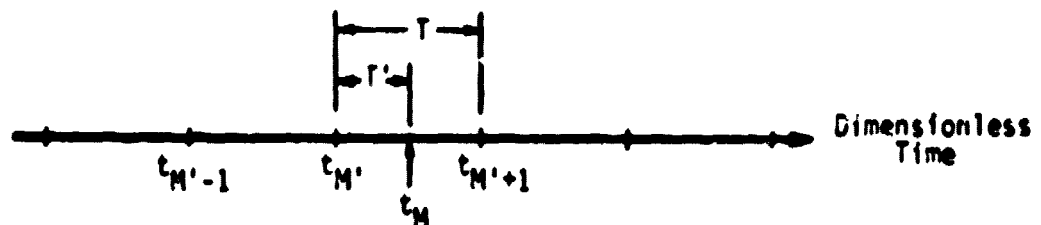

Figure 3-1. Relationship Between t_M, $t_{M'}$, and $t_{M'+1}$

The variation of the turbulence standard deviation, σ_i, with altitude was presented in Table 2-1. The same table contains the turbulence scale, L_i, as a function of altitude. The vehicle speed, V, is a function of altitude but also may vary from one trajectory to another. Table 3-2 provides *representative* values of V as a function of altitude.

TABLE 3-2. TYPICAL VARIATION OF SHUTTLE VELOCITY
WITH ALTITUDE [10]

ALTITUDE (m)	V (m/sec)
100	152
300	156
500	158
2000	170
4000	188
6000	200
8000	240
10000	300

3-5

4. CONCLUSIONS AND RECOMMENDATIONS

By means of a non-recursive discrete generation process, based on a von Karman spectral model with finite upper limits, dimensionless simulated turbulence time series have been developed and stored on six magnetic tapes. Longitudinal, transverse, and vertical gusts are simulated as well as the gust gradients associated with yaw, pitch, and roll. For each gust or gust gradient four separate time series (corresponding to the four altitude bands extending from ground level to 10,000 meters) have been stored on each tape.

The results of spectral analyses of each tape reveals that the simulated turbulence possesses the appropriate von Karman spectral characteristics. Statistical analyses of the tapes indicate that both the simulated gust and gust gradients are normally distributed with near-zero means. Furthermore the standard deviation of each series is consistent with the theoretical energy content.

The Shuttle Simulated Turbulence Tapes (SSTT) are now ready for actual use for simulating turbulence at altitudes below 10,000 meters. Appropriate steps should be taken to incorporate the SSTT into existing simulation systems. In addition, simulated turbulence should be generated for altitudes between 10,000 and 100,000 meters.

5. REFERENCES CITED

1. Tatom, Frank B., and Smith, S. Ray, "Shuttle Simulation Turbulence Tapes (SSTT) Users Guide", *EAI-TR-80-002A*, Engineering Analysis, Inc., Huntsville, Alabama, October 27, 1980.

2. Space Shuttle Program: Natural Environment Design Requirements. Appendix 10.10, Space Shuttle Flight and Ground Specification, Level II Program Definition and Requirements, *JSC 07700*, vol. X, Revision B. NASA-Lyndon B. Johnson Space Center, Houston, TX, August 18, 1975.

3. Chalk, C. R., et al, "Background Information and User Guide for MIL-F-8785B(ASG), 'Military Specification - Flying Qualities of Piloted Airplanes'", Air Force Flight Dynamics Laboratory, Air Force Systems Command, Wright-Patterson Air Force Base, Ohio, *AFFDL-TR-69-72*, August 1969.

4. Tatom, Frank B., and Smith, S. Ray, "Atmospheric Turbulence Simulation for Shuttle Orbiter", *EAI-TR-79-004*, Engineering Analysis, Inc., Huntsville, Alabama, August 31, 1979.

5. Etkin, B., *Dynamics of Atmospheric Flight*, John Wiley & Sons, Inc., New York, 1972.

6. Rockwell International Corporation, "Aerodynamic Design Substantiation Report", *SD74-SH-0206*, 1974.

7. Fichtl, George H., Perlmutter, Morris, and Frost, Walter, "Monte Carlo Turbulence Simulation", *Handbook of Turbulence*, Vol. 1, Chapter 14, Plenum Publishing Corporation, 1977.

8. Neuman, Frank, and Foster, John D., "Investigation of a Digital Automatic Aircraft Landing System in Turbulence", *NASA TN D-6066*, National Aeronautics and Space Administration, Washington, D.C., October 1970.

9. Perlmutter, Morris, "Stochastic Simulation of Ocean Waves for SRB Simulation", *NASA TR-230-1446*, George C. Marshall Space Flight Center, Marshall Space Flight Center, Alabama, May 1975.

10. Fichtl, George H., "A Technique for Simulating Turbulence for Aerospace Vehicle Flight Simulation Studies", *NASA TM 78141*, George C. Marshall Space Flight Center, Marshall Space Flight Center, Alabama, November 1977.

11. Bloomfield, Peter, *Fourier Analysis of Time Series: An Introduction*, John Wiley & Sons, Inc., 1976.

12. Maynard, Harry W., "An Evaluation of Ten Fast Fourier Transform (FFT) Programs", *Research and Development Technical Report ECOM-5476*, U.S. Army Electronics Command, Fort Monmouth, NJ, March 1973.

APPENDIX A

DIMENSIONLESS VON KARMAN SPECTRA
WITH FINITE UPPER LIMITS

For each altitude band, the three-dimensional spectral model
for gusts, as given by Eq (2-2), and the three-dimensional model for gust
gradients, as given by Eq (2-3), have been integrated with respect to Ω_2
and Ω_3 over the finite limits indicated in Table 2-2. The six resulting
one-dimensional spectra are presented in Tables A-1 through A-4, corres-
ponding to Altitude Bands #1 through 4 respectively. These spectra were
used in the numerical evaluation of the impulse response functions described
in subsection 2.3

TABLE A-1. DIMENSIONLESS SPECTRUM FOR ALTITUDE BAND #1

Dimensionless Wave Number Ω_1	Dimensionless Spectrum					
	ϕ_{11}	ϕ_{22}	ϕ_{33}	$\phi_{22/11}$	$\phi_{33/11}$	$\phi_{33/22}$
0.000	.41284	.21598	.19686	0.0000	0.0000	.28145
.010	.41280	.21600	.19688	.12047E-04	.10981E-04	.28144
.020	.41269	.21606	.19694	.48203E-04	.43938E-04	.28143
.030	.41249	.21616	.19704	.10851E-03	.98910E-04	.28141
.040	.41222	.21630	.19718	.19302E-03	.17597E-03	.28138
.050	.41186	.21647	.19736	.30184E-03	.27519E-03	.28135
.060	.41144	.21669	.19758	.43509E-03	.39672E-03	.28131
.070	.41093	.21694	.19783	.59289E-03	.54067E-03	.28126
.080	.41035	.21723	.19812	.77542E-03	.70722E-03	.28120
.090	.40969	.21755	.19845	.98286E-03	.89656E-03	.28114
.100	.40896	.21791	.19881	.12154E-02	.11089E-02	.28106
.190	.39915	.22248	.20343	.44796E-02	.40959E-02	.28004
.280	.38420	.22858	.20959	.99952E-02	.91651E-02	.27831
.370	.36523	.23481	.21592	.17929E-01	.16487E-01	.27582
.460	.34349	.23989	.22112	.28311E-01	.26097E-01	.27250
.550	.32020	.24290	.22429	.40982E-01	.37842E-01	.26834
.640	.29636	.24339	.22496	.55604E-01	.51394E-01	.26337
.730	.27280	.24132	.22310	.71726E-01	.66311E-01	.25765
.820	.25008	.23691	.21894	.88850E-01	.82109E-01	.25127
.910	.22859	.23058	.21288	.10650	.98325E-01	.24433
1.000	.20854	.22277	.20538	.12425	.11455	.23696
1.422	.13461	.17793	.16235	.20068	.18310	.19973
1.844	.87928E-01	.13588	.12241	.25770	.23216	.16375
2.266	.58773E-01	.10319	.91862E-01	.29552	.26308	.13268
2.688	.40239E-01	.78984E-01	.69629E-01	.31830	.28060	.10721
3.110	.28168E-01	.61179E-01	.53547E-01	.33004	.28886	.86805E-01
3.532	.20114E-01	.47931E-01	.41804E-01	.33385	.29087	.70622E-01
3.954	.14617E-01	.38082E-01	.33107E-01	.33207	.28869	.57810E-01
4.376	.10789E-01	.30562E-01	.26566E-01	.32642	.28374	.47641E-01
4.798	.80741E-02	.24779E-01	.21571E-01	.31816	.27696	.39532E-01
5.220	.61177E-02	.20380E-01	.17702E-01	.30821	.26904	.33026E-01

A-2

TABLE A-2. DIMENSIONLESS SPECTRUM FOR ALTITUDE BAND #2

Dimensionless Wave Number Ω_1	Dimensionless Spectrum					
	ϕ_{11}	ϕ_{22}	ϕ_{33}	$\phi_{22/11}$	$\phi_{33/11}$	$\phi_{33/22}$
0.000	.46500	.23421	.23079	0.0000	0.0000	.92864
.010	.46496	.23423	.23081	.13064E-04	.12873E-04	.92864
.020	.46484	.23429	.23087	.52269E-04	.51507E-04	.92862
.030	.46464	.23439	.23097	.11766E-03	.11594E-03	.92859
.040	.46436	.23453	.23111	.20929E-03	.20625E-03	.92855
.050	.46400	.23471	.23129	.32727E-03	.32251E-03	.92849
.060	.46356	.23493	.23151	.47172E-03	.46486E-03	.92843
.070	.46304	.23519	.23177	.64277E-03	.63343E-03	.92835
.080	.46245	.23549	.23207	.84059E-03	.82839E-03	.92825
.090	.46178	.23582	.23240	.10654E-02	.10499E-02	.92815
.100	.46103	.23619	.23277	.13173E-02	.12983E-02	.92803
.190	.45102	.24086	.23745	.48497E-02	.47809E-02	.92642
.280	.43575	.24711	.24370	.10806E-01	.10656E-01	.92373
.370	.41640	.25352	.25011	.19357E-01	.19097E-01	.91990
.460	.39425	.25876	.25535	.30539E-01	.30137E-01	.91488
.550	.37050	.26192	.25851	.44191E-01	.43616E-01	.90866
.640	.34623	.26252	.25912	.59973E-01	.59196E-01	.90125
.730	.32222	.26051	.25712	.77430E-01	.76421E-01	.89274
.820	.29906	.25614	.25275	.96061E-01	.94790E-01	.88323
.910	.27712	.24982	.24644	.11539	.11382	.87283
1.000	.25660	.24201	.23863	.13498	.13310	.86169
1.900	.12447	.15040	.14713	.30283	.29623	.73268
2.800	.69125E-01	.93005E-01	.89880E-01	.40669	.39302	.60944
3.700	.42724E-01	.61869E-01	.58936E-01	.47241	.45001	.50614
4.600	.28382E-01	.43779E-01	.41064E-01	.51667	.48463	.42166
5.500	.19816E-01	.32441E-01	.29958E-01	.54734	.50545	.35279
6.400	.14344E-01	.24881E-01	.22633E-01	.56841	.51706	.29658
7.300	.10673E-01	.19588E-01	.17570E-01	.58221	.52223	.25056
8.200	.81170E-02	.15740E-01	.13940E-01	.59028	.52278	.21275
9.100	.62859E-02	.12856E-01	.11258E-01	.59378	.51999	.18157

Dimensionless Wave Number Ω_1	Dimensionless Spectrum					
	ϕ_{11}	ϕ_{22}	ϕ_{33}	$\phi_{22/11}$	$\phi_{33/11}$	$\phi_{33/22}$
10.000	.49428E-02	.10642E-01	.92297E-02	.59357	.51478	.15575
10.366	.44998E-02	.98878E-02	.85453E-02	.59260	.51214	.14654
10.732	.41049E-02	.92028E-02	.79273E-02	.59118	.50924	.13799
11.098	.37519E-02	.85792E-02	.73678E-02	.58936	.50614	.13004
11.464	.34356E-02	.80102E-02	.68599E-02	.58716	.50284	.12266
11.830	.31515E-02	.74897E-02	.63978E-02	.58462	.49939	.11578
12.196	.28957E-02	.70127E-02	.59763E-02	.58178	.49580	.10937
12.562	.26649E-02	.65745E-02	.55910E-02	.57866	.49209	.10340
12.928	.24562E-02	.61714E-02	.52381E-02	.57528	.48829	.97832E-01
13.294	.22671E-02	.57997E-02	.49142E-02	.57169	.48440	.92631E-01
13.660	.20954E-02	.54566E-02	.46164E-02	.56789	.48045	.87771E-01

TABLE A-3. DIMENSIONLESS SPECTRUM FOR ALTITUDE BAND #3

Dimensionless Wave Number Ω_1	Dimensionless Spectrum					
	ϕ_{11}	ϕ_{22}	ϕ_{33}	$\phi_{22/11}$	$\phi_{33/11}$	$\phi_{33/22}$
0.000	.47307	.23698	.23610	0.0000	0.0000	1.8736
.010	.47303	.23700	.23612	.13218E-04	.13169E-04	1.8736
.020	.47291	.23706	.23618	.52887E-04	.52691E-04	1.8736
.030	.47271	.23716	.23628	.11905E-03	.11861E-03	1.8736
.040	.47243	.23730	.23642	.21177E-03	.21098E-03	1.8735
.050	.47207	.23748	.23660	.33114E-03	.32991E-03	1.8735
.060	.47164	.23770	.23682	.47728E-03	.47551E-03	1.8734
.070	.47112	.23796	.23708	.65034E-03	.64793E-03	1.8733
.080	.47052	.23826	.23737	.85047E-03	.84733E-03	1.8732
.090	.46985	.23859	.23771	.10779E-02	.10739E-02	1.8731
.100	.46911	.23896	.23807	.13328E-02	.13279E-02	1.8730
.190	.45909	.24363	.24275	.49055E-02	.48878E-02	1.8713
.280	.44382	.24988	.24900	.10927E-01	.10888E-01	1.8684
.370	.42447	.25629	.25541	.19569E-01	.19502E-01	1.8644
.460	.40230	.26153	.26066	.30866E-01	.30762E-01	1.8591
.550	.37855	.26469	.26381	.44658E-01	.44510E-01	1.8525
.640	.35426	.26529	.26441	.60606E-01	.60406E-01	1.8447
.730	.33025	.26328	.26241	.78253E-01	.77995E-01	1.8357
.830	.30707	.25891	.25804	.97099E-01	.96774E-01	1.8257
.910	.28512	.25259	.25172	.11666	.11626	1.8147
1.000	.26458	.24477	.24391	.13652	.13604	1.8029
1.900	.13222	.15316	.15235	.30838	.30675	1.6641
2.800	.76534E-01	.95746E-01	.95000E-01	.41867	.41541	1.5255
3.700	.49712E-01	.64591E-01	.63915E-01	.49319	.48803	1.4020
4.600	.34906E-01	.46476E-01	.45867E-01	.54851	.54132	1.2931
5.500	.25860E-01	.35110E-01	.34555E-01	.59238	.58301	1.1966
6.400	.19915E-01	.27517E-01	.27002E-01	.62864	.61688	1.1102
7.300	.15792E-01	.22187E-01	.21700E-01	.65945	.64496	1.0324
8.200	.12812E-01	.18295E-01	.17825E-01	.68613	.66848	.96184
9.100	.10588E-01	.15363E-01	.14902E-01	.70956	.68828	.89757

TABLE A-3. DIMENSIONLESS SPECTRUM FOR ALTITUDE BAND #3 (Continued)

Dimensionless Wave Number Ω_1	Dimensionless Spectrum					
	ϕ_{11}	ϕ_{22}	ϕ_{33}	$\psi_{22/11}$	$\psi_{33/11}$	$\phi_{33/22}$
10.000	.88842E-02	.13095E-01	.12639E-01	.73036	.70497	.83878
12.331	.59522E-02	.91366E-02	.86902E-02	.77486	.73700	.70777
14.662	.42188E-02	.67483E-02	.63162E-02	.80914	.75733	.60132
16.993	.31087E-02	.51878E-02	.47783E-02	.83552	.76958	.51383
19.324	.23566E-02	.41067E-02	.37254E-02	.85532	.77590	.44133
21.655	.18260E-02	.33242E-02	.29732E-02	.86945	.77765	.38084
23.986	.14401E-02	.27382E-02	.24176E-02	.87866	.77578	.33011
26.317	.11528E-02	.22874E-02	.19961E-02	.88361	.77105	.28735
28.648	.93461E-03	.19332E-02	.16692E-02	.88491	.76407	.25117
30.979	.76625E-03	.16499E-02	.14112E-02	.88312	.75537	.22043
33.310	.63449E-03	.14199E-02	.12044E-02	.87872	.74537	.19421

A·9

TABLE A-4. DIMENSIONLESS SPECTRUM FOR ALTITUDE BAND #4

Dimensionless Wave Number Ω_1	ϕ_{11}	ϕ_{22}	ϕ_{33}	$\phi_{22/11}$	$\phi_{33/11}$	$\phi_{33/22}$
0.000	.47403	.23725	.23678	0.0000	0.0000	2.5188
.010	.47399	.23727	.23680	.13234E-04	.13207E-04	2.5188
.020	.47387	.23733	.23686	.52949E-04	.52843E-04	2.5188
.030	.47367	.23744	.23696	.11919E-03	.11895E-03	2.5188
.040	.47339	.23758	.23710	.21201E-03	.21159E-03	2.5187
.050	.47303	.23776	.23728	.33152E-03	.33086E-03	2.5187
.060	.47259	.23798	.23750	.47784E-03	.47688E-03	2.5186
.070	.47208	.23824	.23776	.65109E-03	.64979E-03	2.5185
.080	.47148	.23853	.23805	.85146E-03	.84976E-03	2.5184
.090	.47081	.23886	.23839	.10791E-02	.10770E-02	2.5183
.100	.47006	.23923	.23875	.13343E-02	.13317E-02	2.5182
.190	.46005	.24391	.24343	.49111E-02	.49014E-02	2.5164
.280	.44478	.25016	.24968	.10939E-01	.10918E-01	2.5136
.370	.42542	.25656	.25609	.19590E-01	.19554E-01	2.5095
.460	.40326	.26181	.26133	.30899E-01	.30843E-01	2.5041
.550	.37951	.26496	.26449	.44704E-01	.44625E-01	2.4975
.640	.35522	.26556	.26509	.60669E-01	.60561E-01	2.4897
.730	.33120	.26356	.26309	.78336E-01	.78196E-01	2.4806
.820	.30803	.25919	.25872	.97204E-01	.97028E-01	2.4705
.910	.28607	.25287	.25240	.11679	.11658	2.4594
1.000	.26553	.24505	.24459	.13668	.13642	2.4476
1.900	.13316	.15344	.15301	.30895	.30809	2.3075
2.800	.77440E-01	.96030E-01	.95655E-01	.41992	.41827	2.1669
3.700	.50590E-01	.64876E-01	.64556E-01	.49537	.49292	2.0407
4.600	.35757E-01	.46762E-01	.46492E-01	.55188	.54870	1.9285
5.500	.26687E-01	.35394E-01	.35166E-01	.59716	.59331	1.8280
6.400	.20721E-01	.27797E-01	.27599E-01	.63503	.63052	1.7371
7.300	.16579E-01	.22463E-01	.22284E-01	.66765	.66234	1.6542
8.200	.13584E-01	.18567E-01	.18398E-01	.69632	.68999	1.5781
9.100	.11346E-01	.15631E-01	.15465E-01	.74519	.73587	1.4422

TABLE A-4. DIMENSIONLESS SPECTRUM FOR ALTITUDE BAND #4 (Continued)

Dimensionless Wave Number	Dimensionless Spectrum					
Ω_1	ϕ_{11}	ϕ_{22}	ϕ_{33}	$\phi_{22/11}$	$\phi_{33/11}$	$\phi_{33/22}$
10.000	.96272E-02	.13361E-01	.13194E-01	.74519	.73587	1.4422
14.918	.47318E-02	.68100E-02	.66211E-02	.84529	.82184	1.1505
19.836	.27883E-02	.41832E-02	.39941E-02	.91802	.87652	.93466
24.754	.18075E-02	.28453E-02	.26686E-02	.97244	.91203	.76798
29.672	.12439E-02	.20619E-02	.19002E-02	1.0125	.93313	.63634
34.590	.89249E-03	.15597E-02	.14134E-02	1.0408	.94317	.53100
39.508	.66058E-03	.12169E-02	.10853E-02	1.0594	.94487	.44596
44.426	.50103E-03	.97193E-03	.85425E-03	1.0699	.94037	.37685
49.344	.38768E-03	.79063E-03	.68580E-03	1.0737	.93133	.32035
54.262	.30505E-03	.65273E-03	.55962E-03	1.0719	.91902	.27389
59.180	.24352E-03	.54553E-03	.46299E-03	1.0656	.90441	.23549

APPENDIX B

SPECTRAL ANALYSIS OF SIMULATED TURBULENCE

By means of a Fast Fourier Transform [12] spectral analyses of all simulated turbulence have been performed. The results are presented in dimensionless form in Figures B-1 through B-24. Table B-1 provides a summary of these figures. Also included in each figure is the theoretical von Karman spectra. The agreement between the theoretical spectra and the computed spectra is quite satisfactory.

TABLE B-1. MATRIX OF SPECTRAL ANALYSIS FIGURES

SERIES TYPE	ALTITUDE BAND			
	1	2	3	4
u_1	B-1	B-2	B-3	B-4
u_2	B-5	B-6	B-7	B-8
u_3	B-9	B-10	B-11	B-12
$\partial u_2/\partial x_1$	B-13	B-14	B-15	B-16
$\partial u_3/\partial x_1$	B-17	B-18	B-19	B-20
$\partial u_3/\partial x_2$	B-21	B-22	B-23	B-24
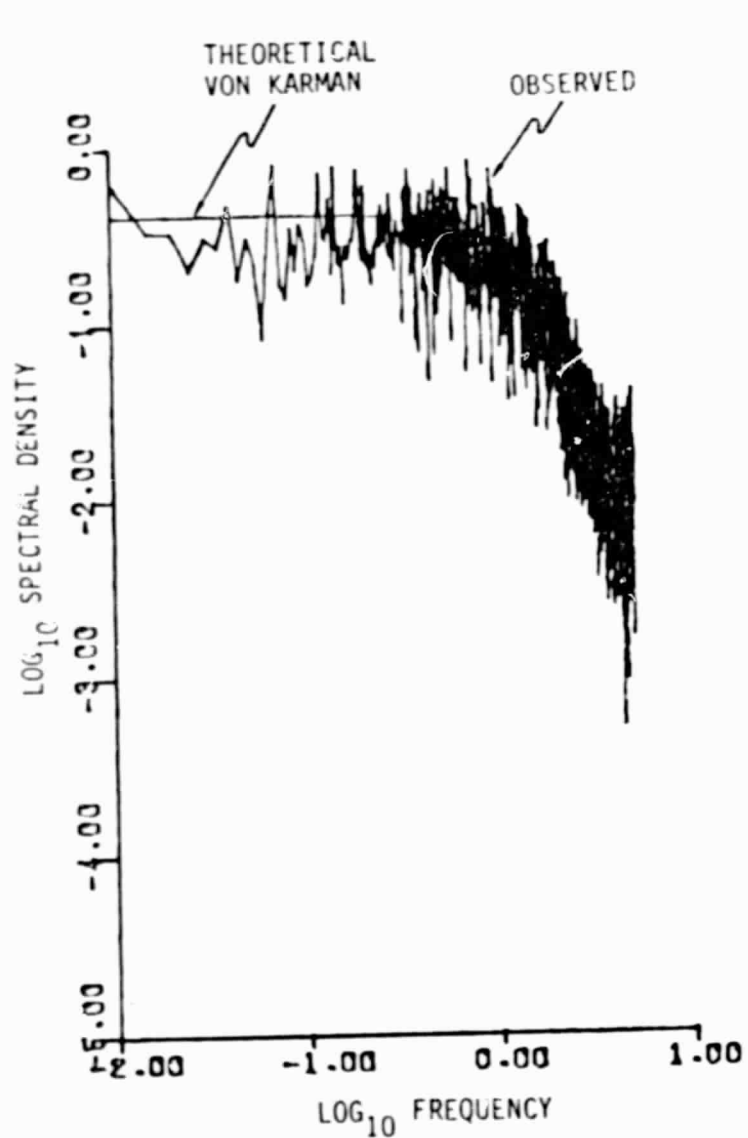
Figure B-1. u_1 - Gust Spectrum, Altitude Band #1
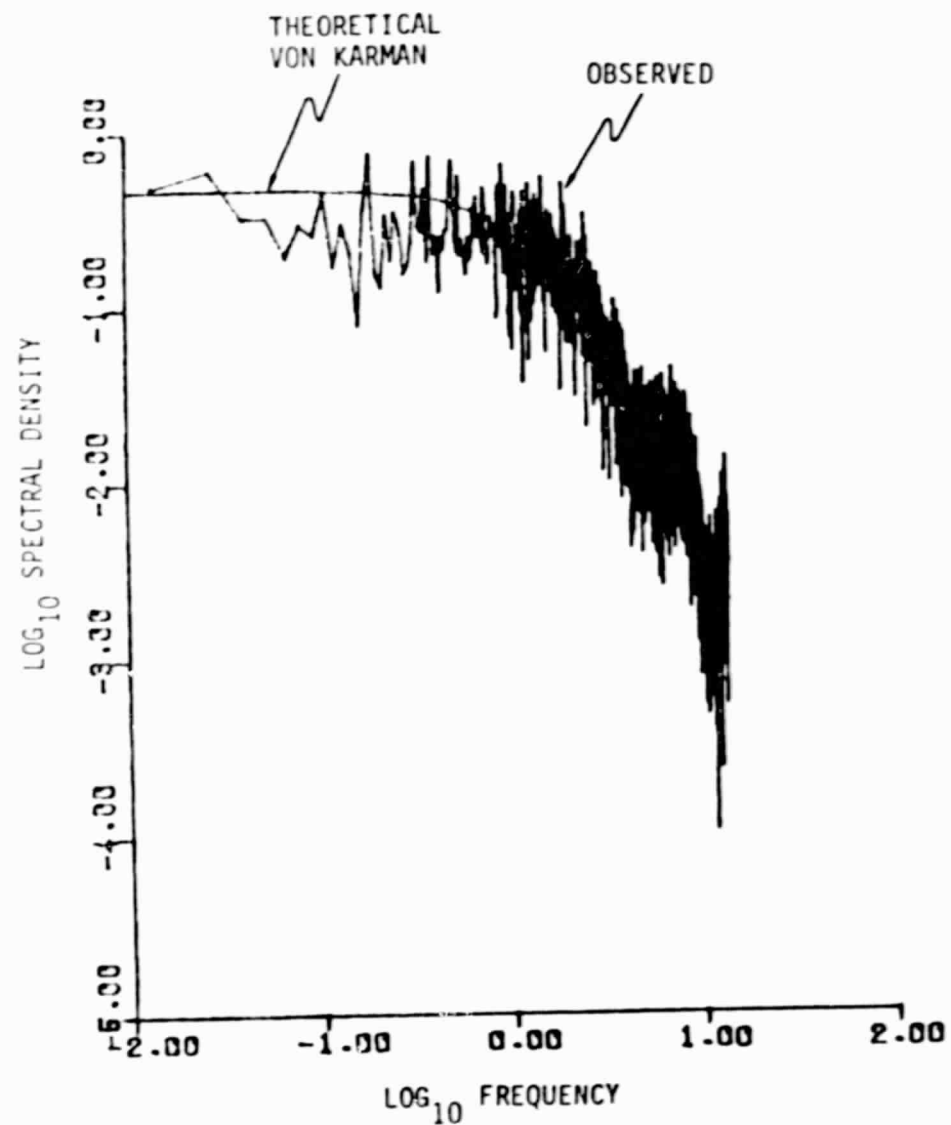
Figure B-2. u_1 - Gust Spectrum, Altitude Band #2

B-2
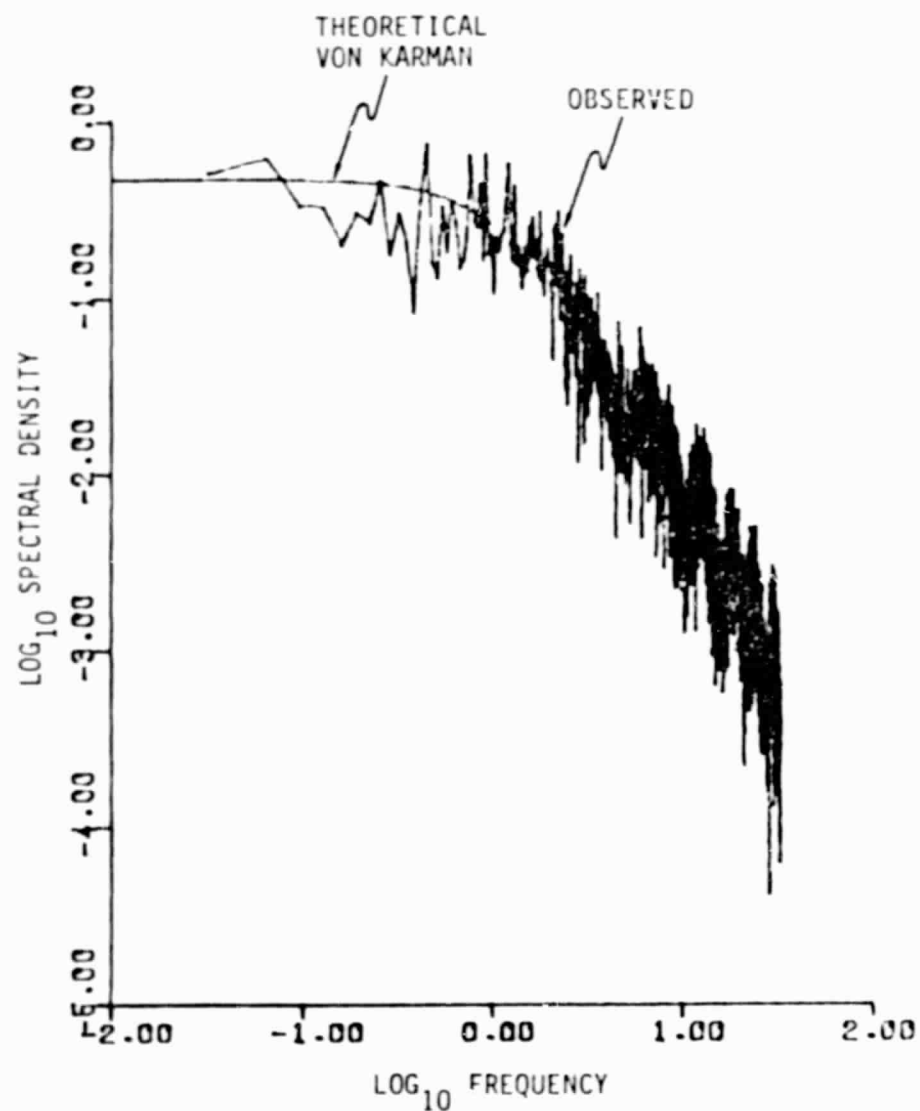
Figure B-3. u_1 - Gust Spectrum, Altitude Band #3
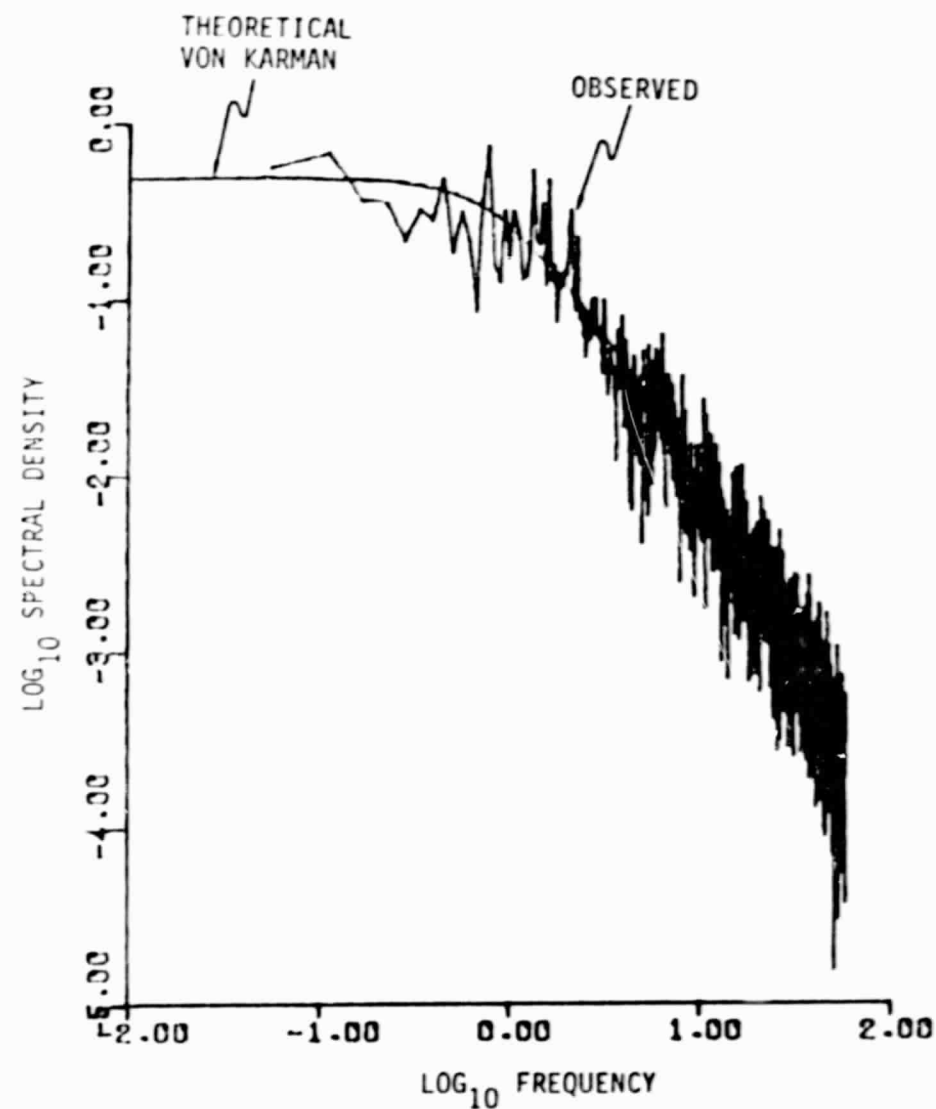
Figure B-4. u_1 - Gust Spectrum, Altitude Band #4

B-3
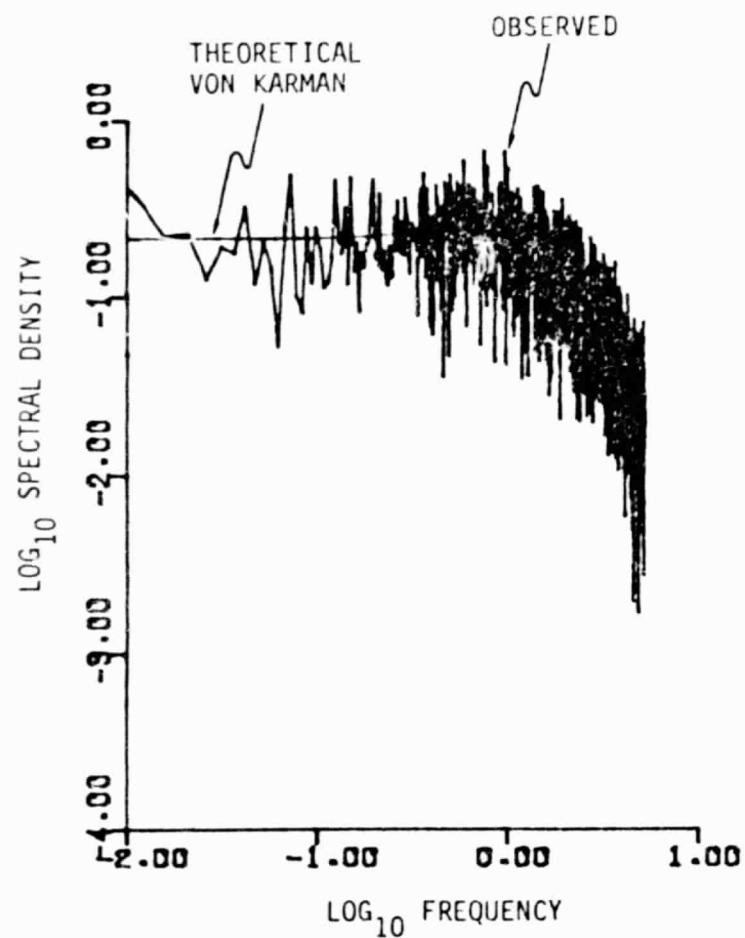
Figure B-5. u_2 - Gust Spectrum, Altitude Band #1
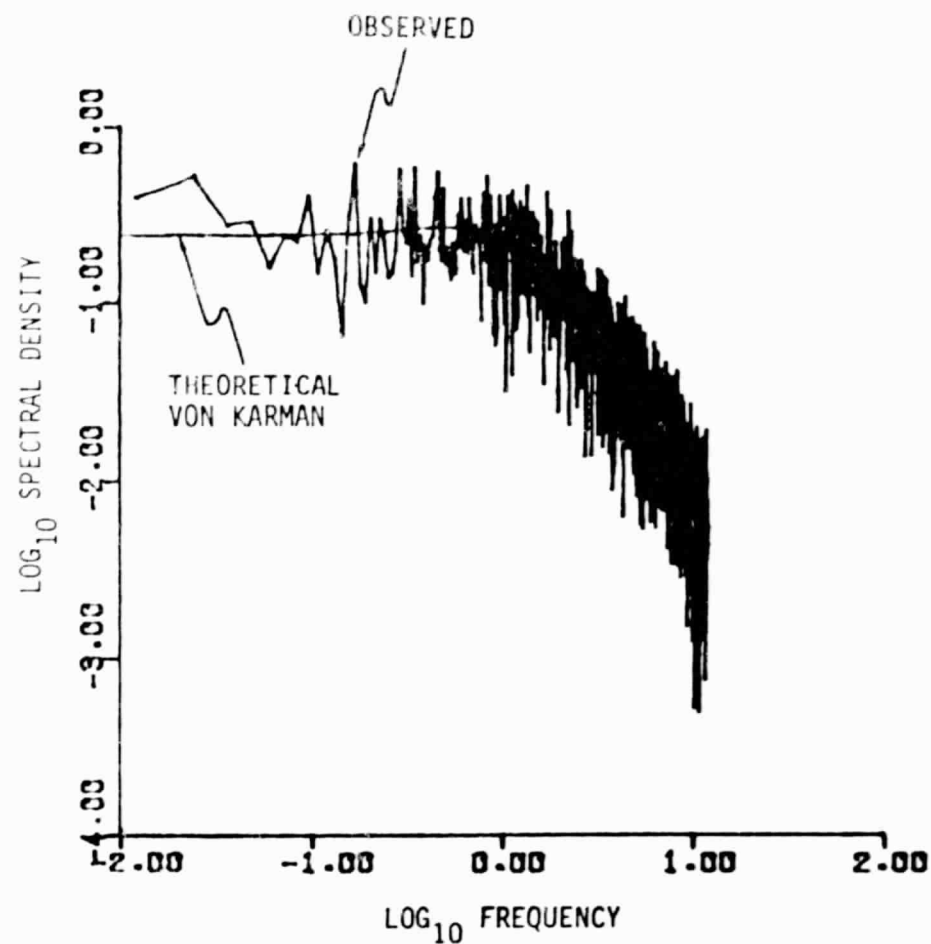
Figure B-6. u_2 - Gust Spectrum, Altitude Band #2
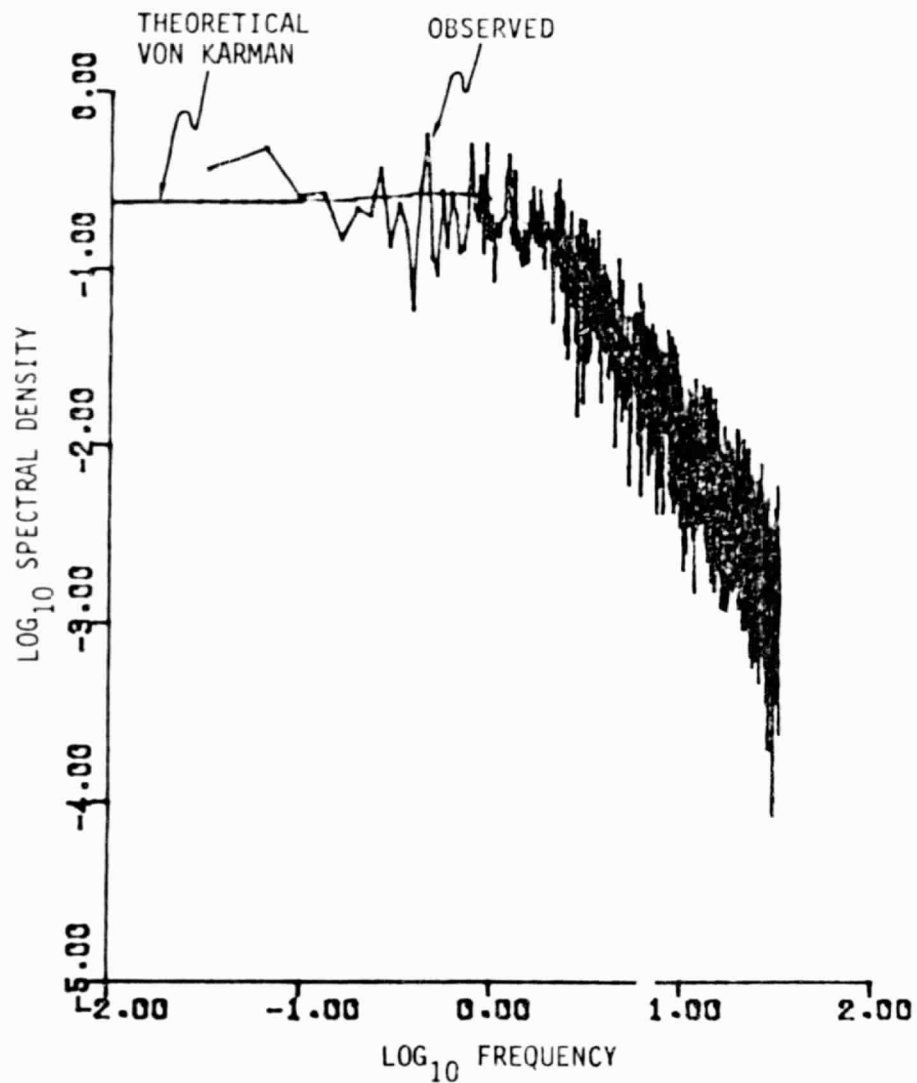
Figure B-7. u_2 - Gust Spectrum, Altitude Band #3
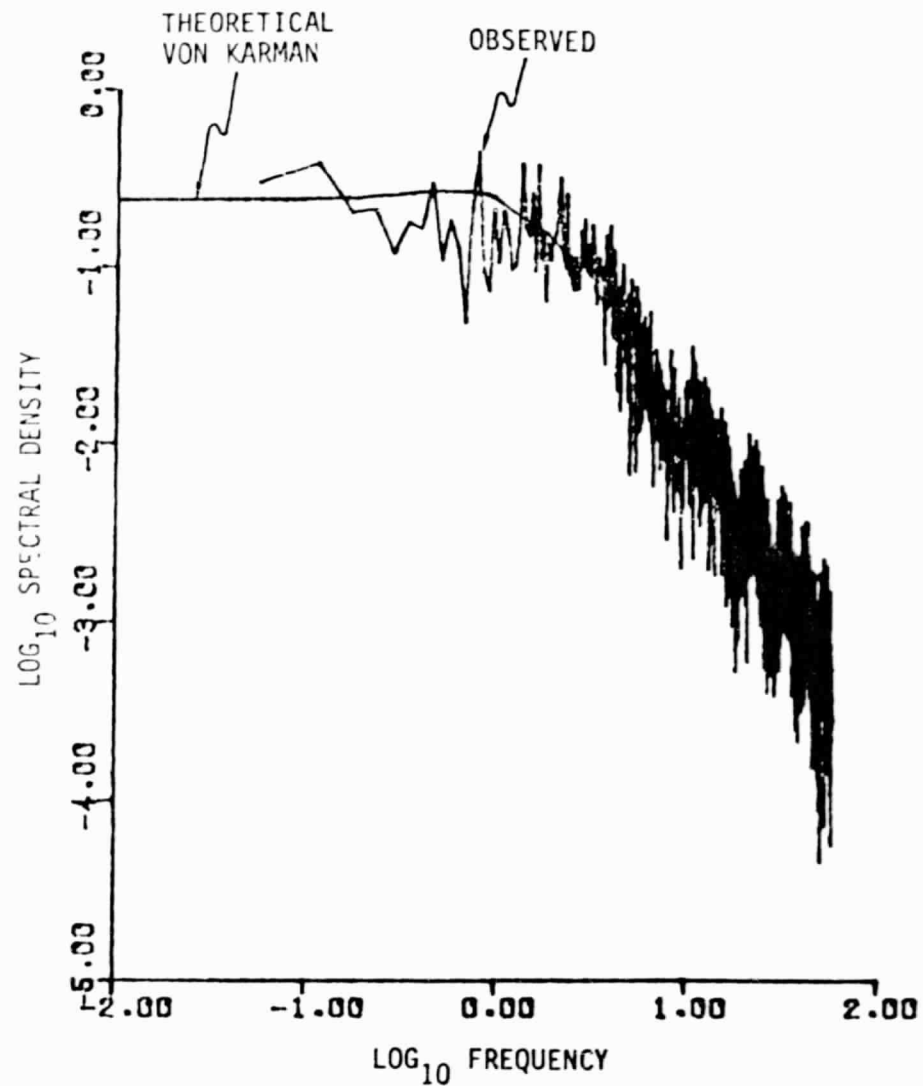
Figure B-8. u_2 - Gust Spectrum, Altitude Band #4

B-5
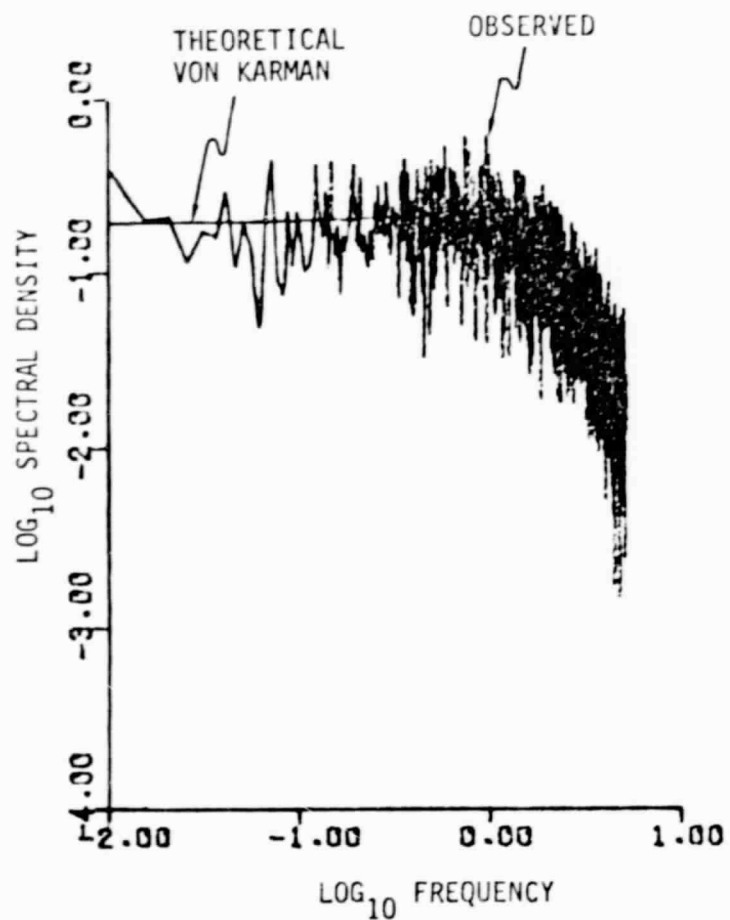
Figure B-9. u_3 - Gust Spectrum, Altitude Band #1
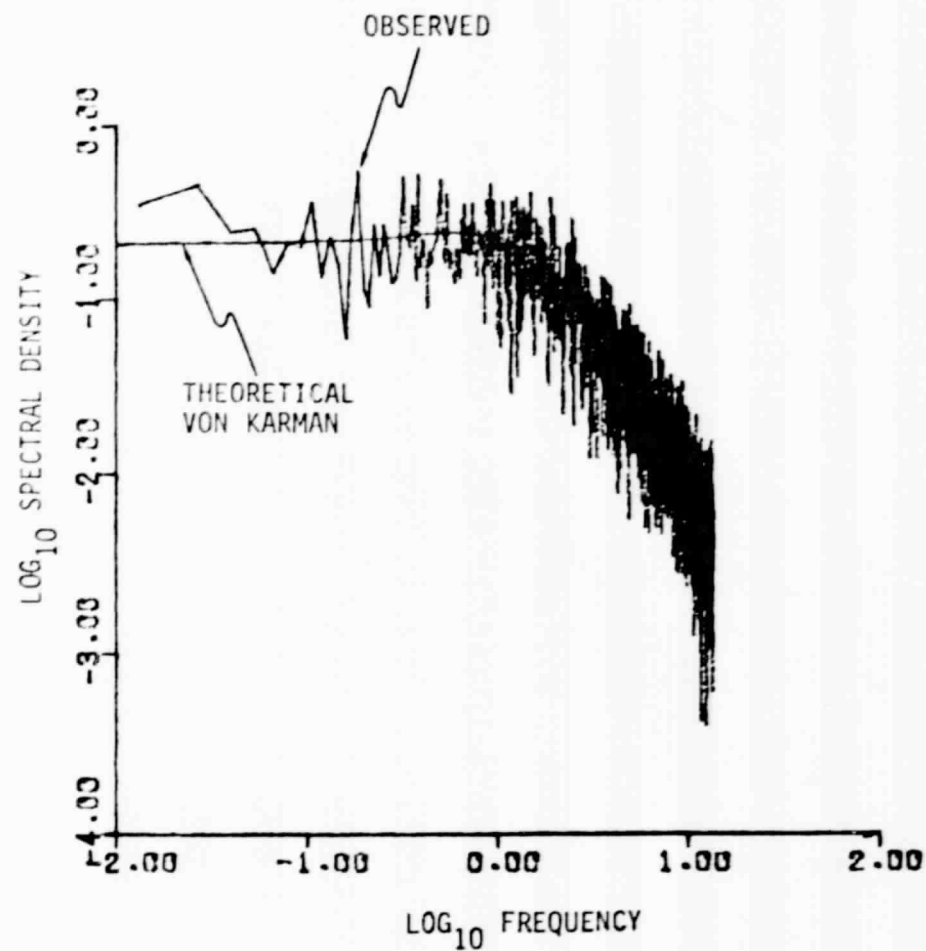
Figure B-10. u_3 - Gust Spectrum, Altitude Band #2
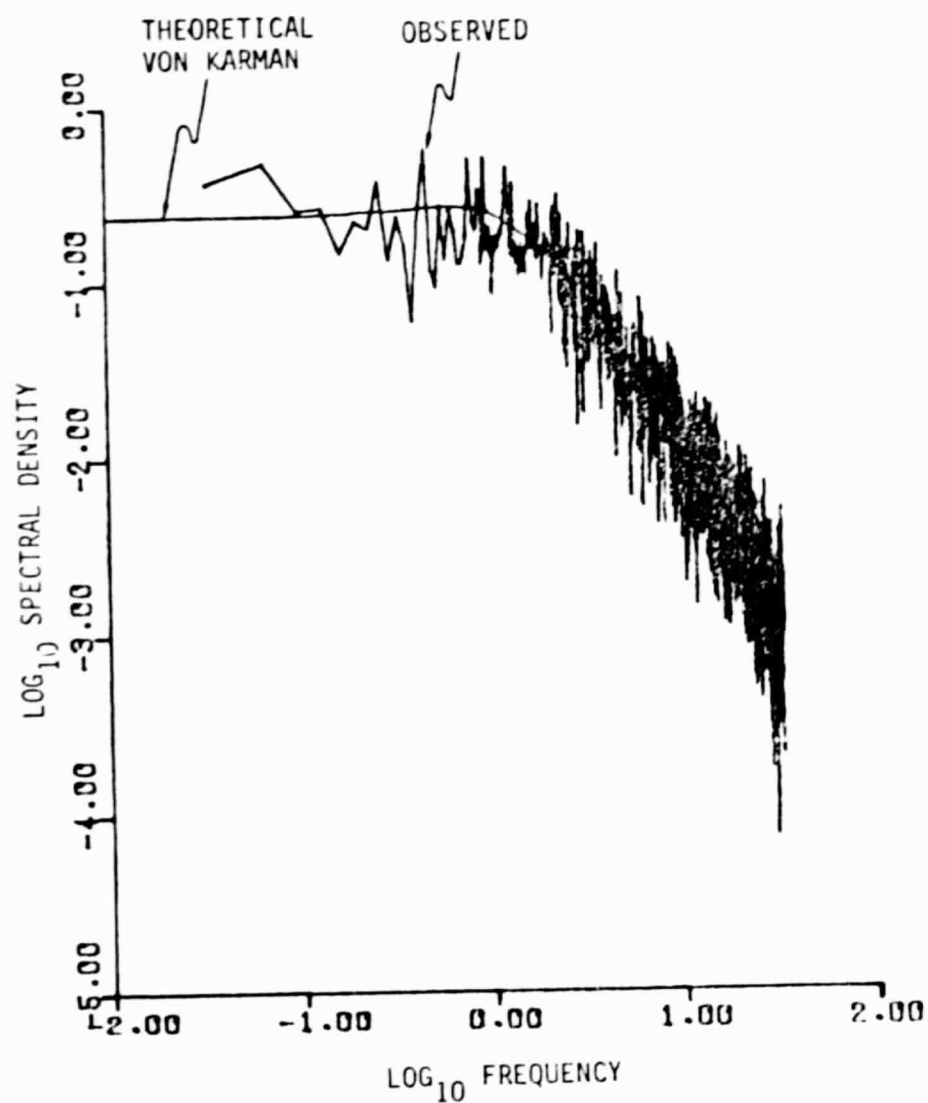
Figure B-11. u_3 - Gust Spectrum, Altitude Band #3
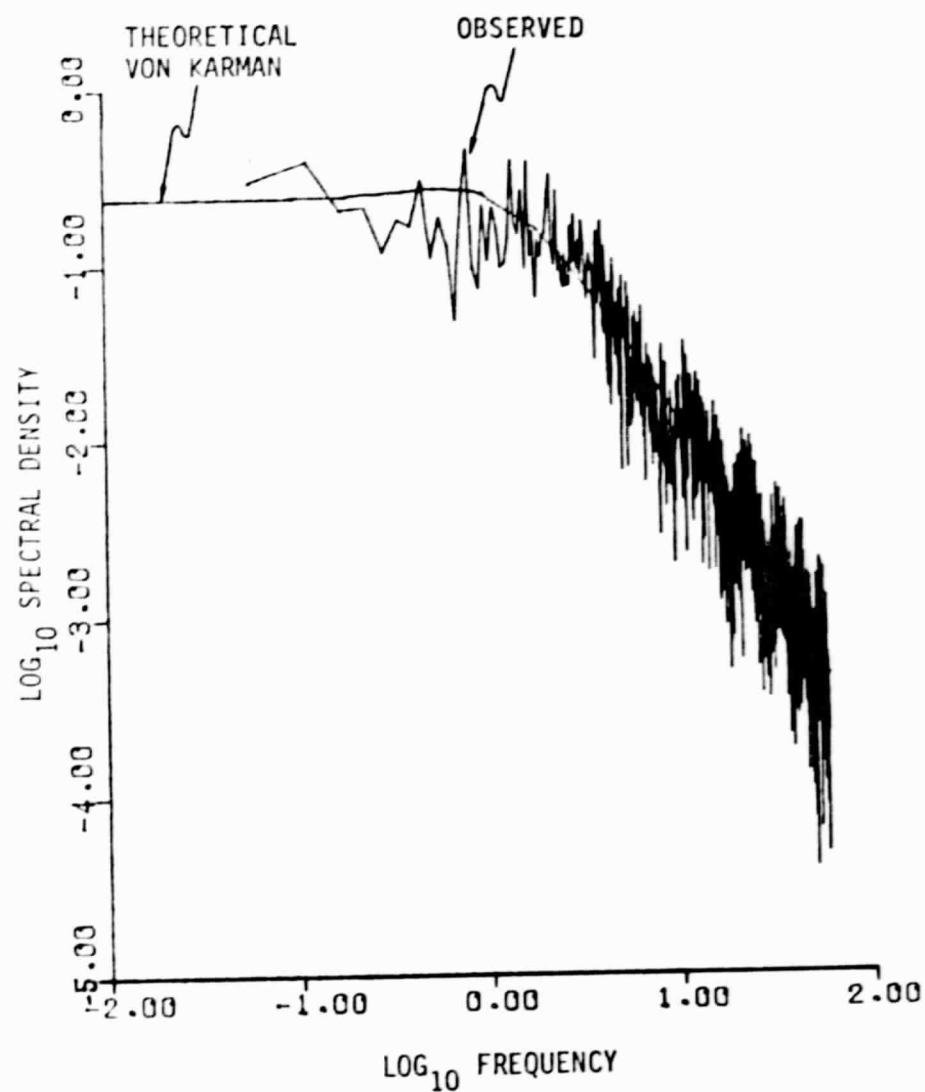
Figure B-12. u_3 - Gust Spectrum, Altitude Band #4
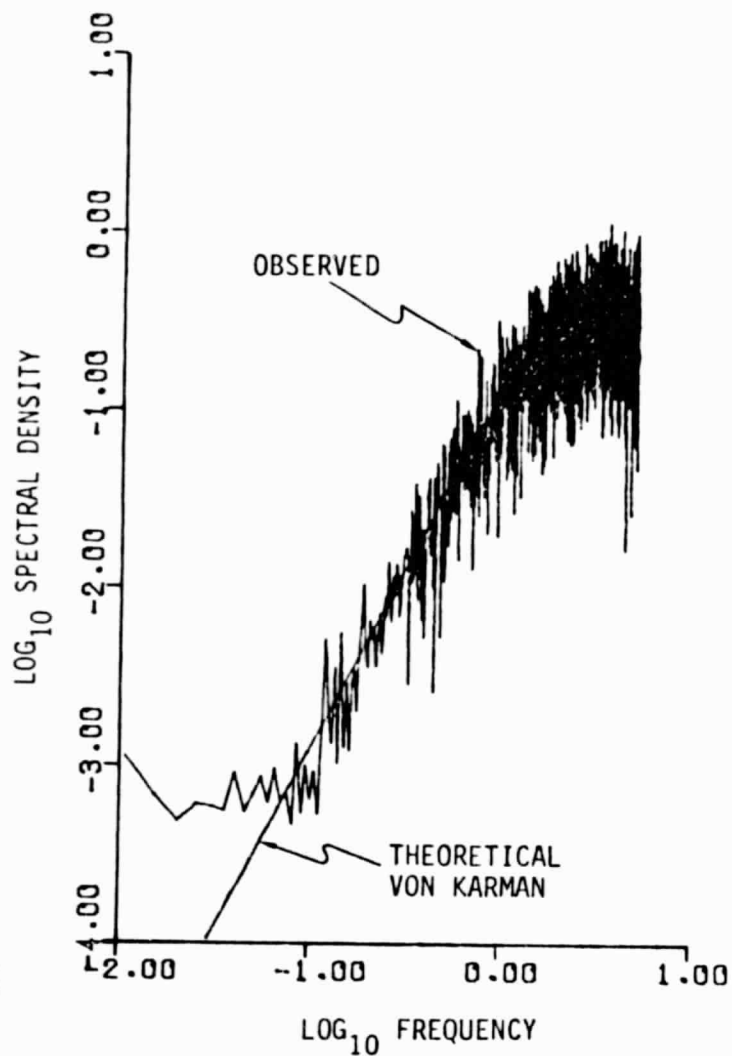
Figure B-13. $\partial u_2/\partial x_1$ - Gust Gradient Spectrum,
Altitude Band #1
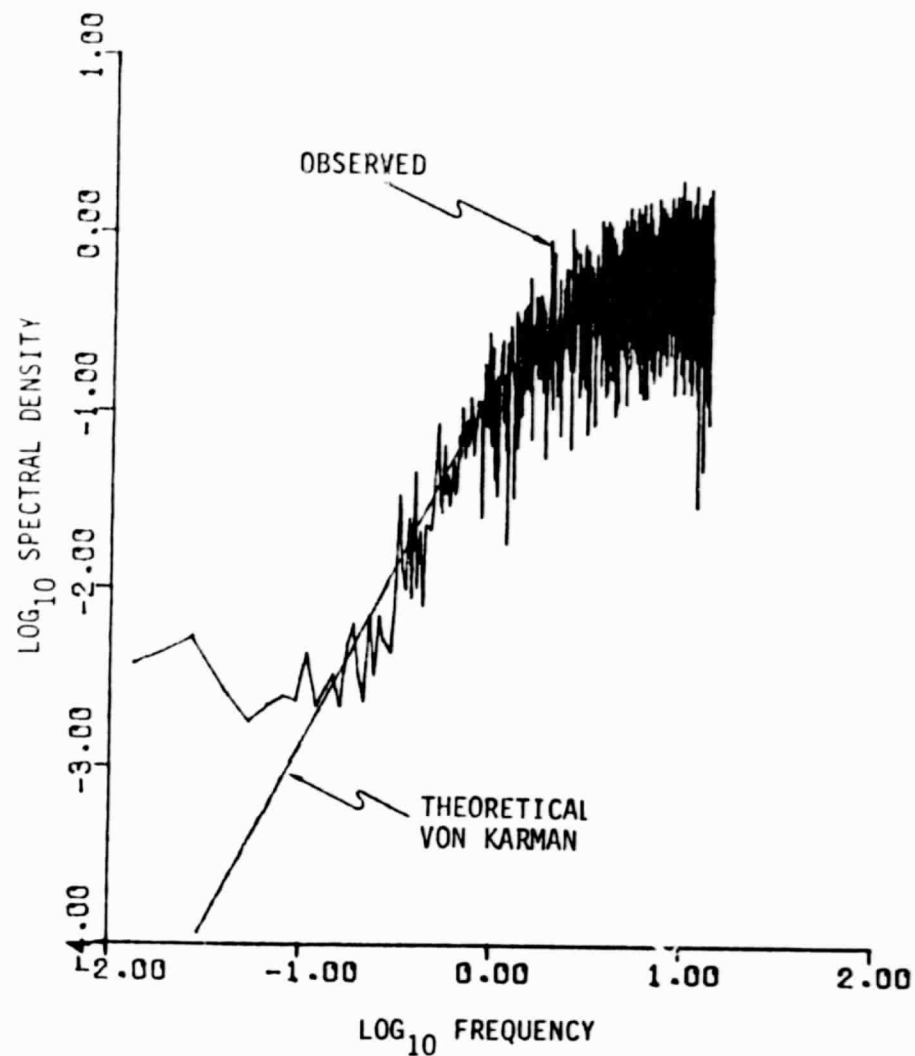
Figure B-14. $\partial u_2/\partial x_1$ - Gust Gradient Spectrum,
Altitude Band #2
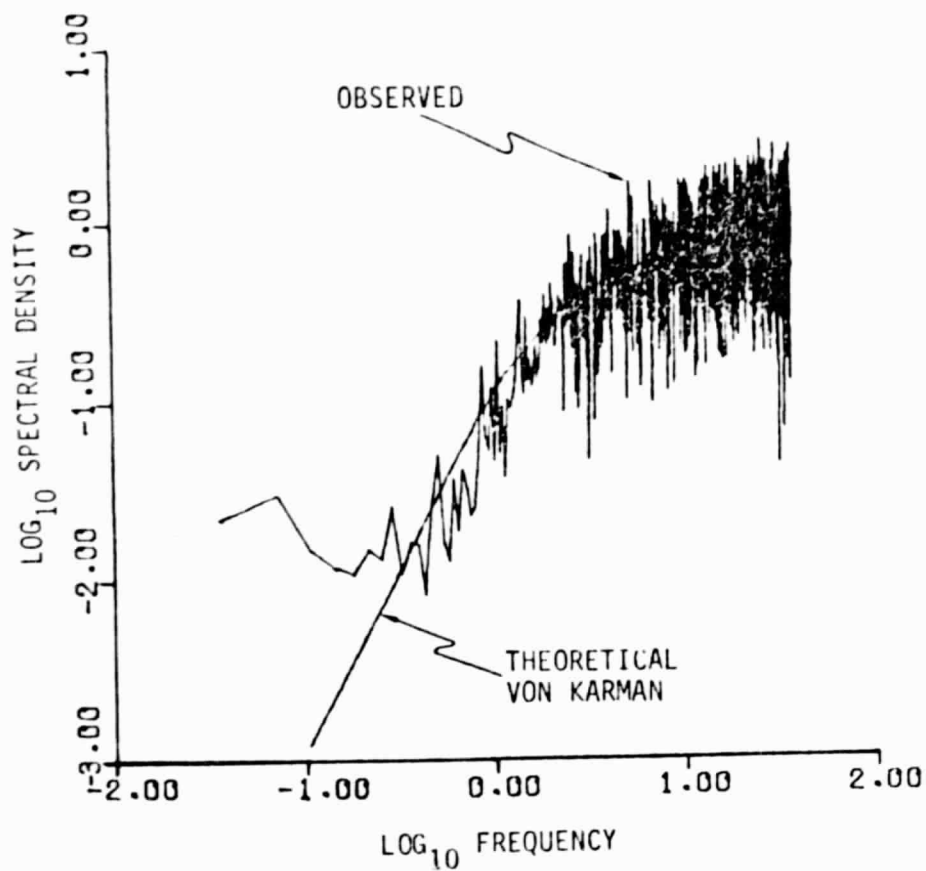
Figure B-15. $\partial u_2/\partial x_1$ - Gust Gradient Spectrum, Altitude Band #3
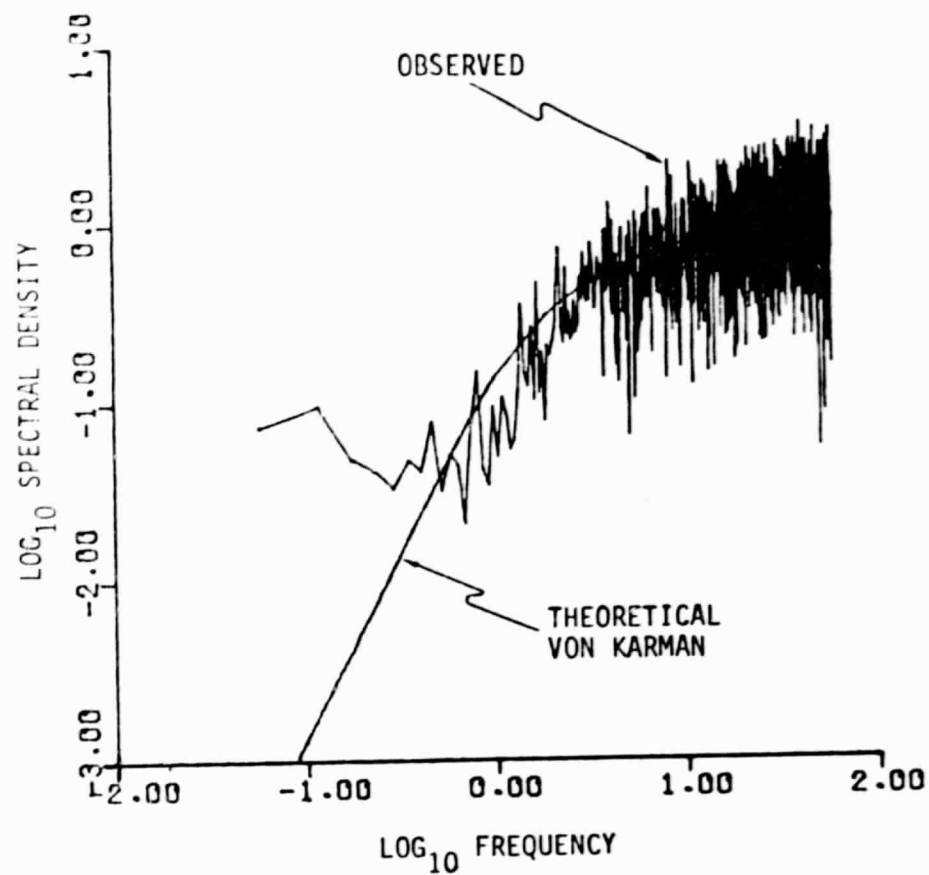
Figure B-16. $\partial u_2/\partial x_1$ - Gust Gradient Spectrum, Altitude Band #4
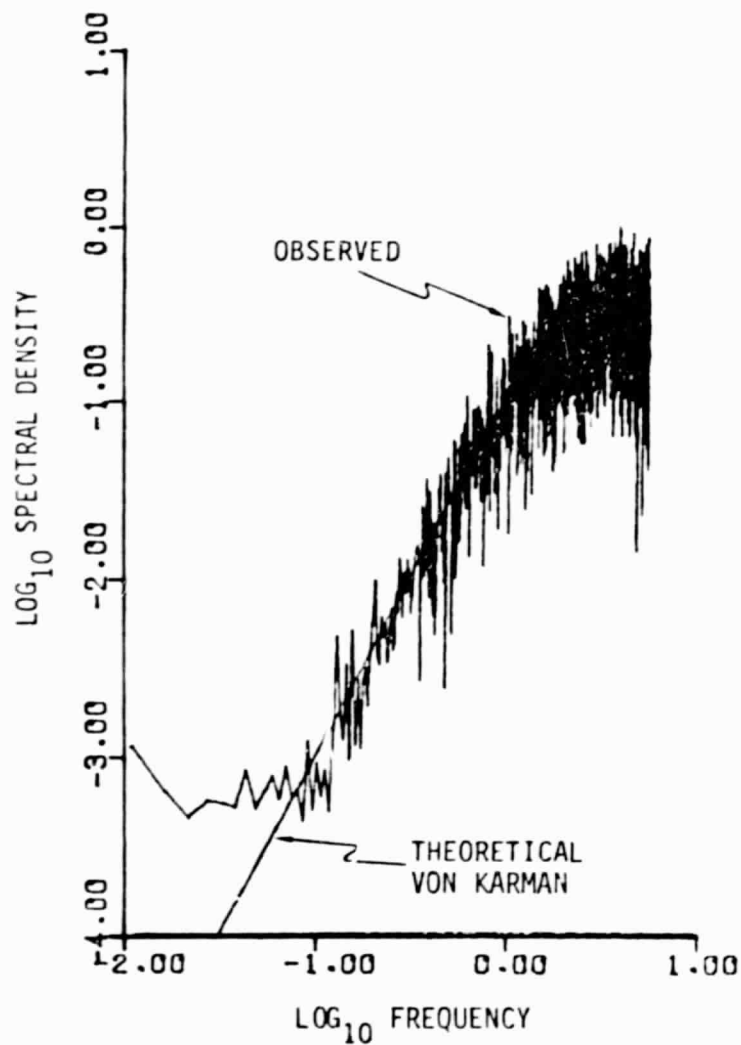
Figure B-17. $\partial u_3/\partial x_1$ - Gust Gradient Spectrum, Altitude Band #1
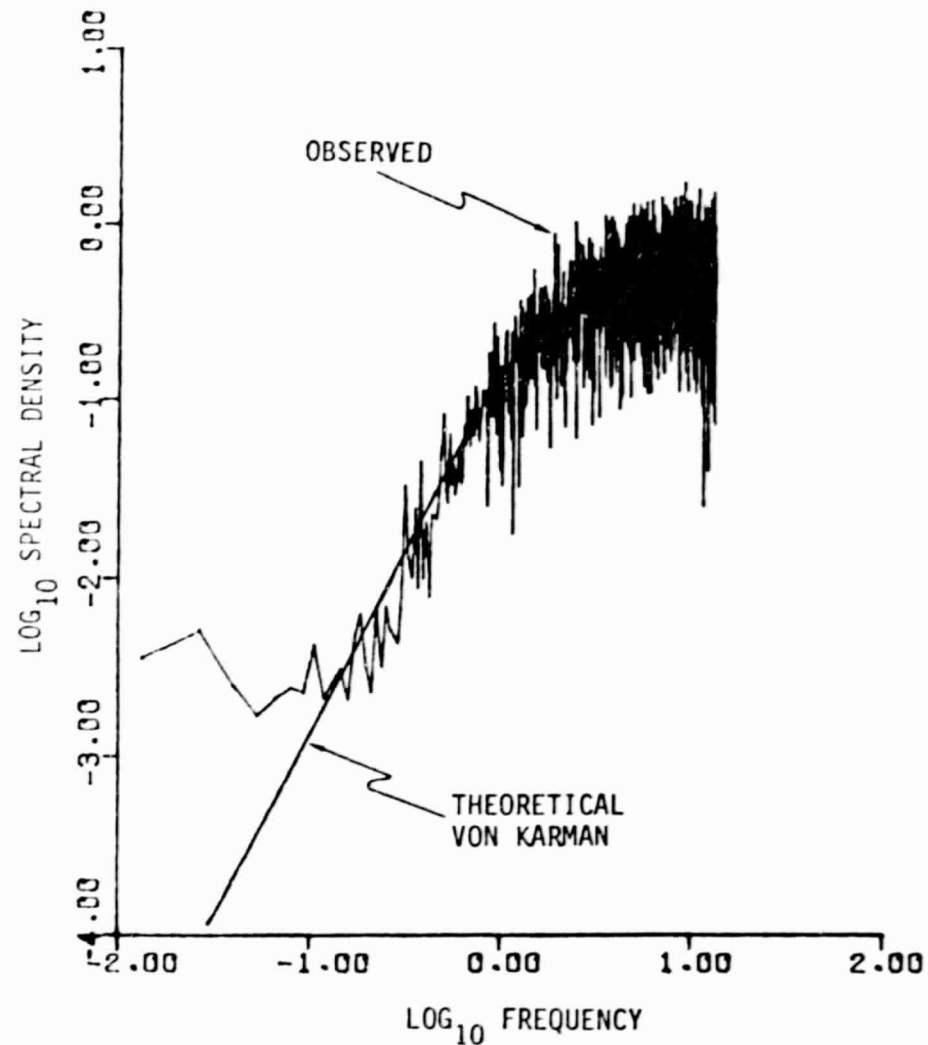
Figure B-18. $\partial u_3/\partial x_1$ - Gust Gradient Spectrum, Altitude Band #2
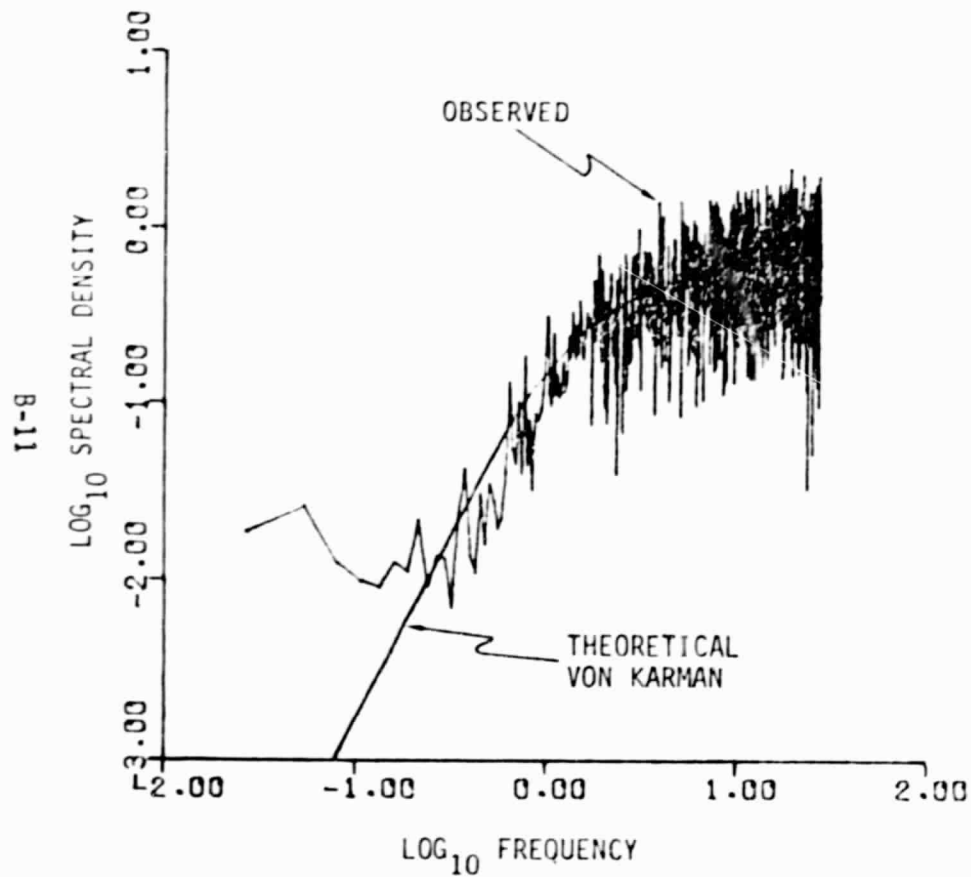
Figure B-19. $\partial u_3/\partial x_1$ - Gust Gradient Spectrum, Altitude Band #3
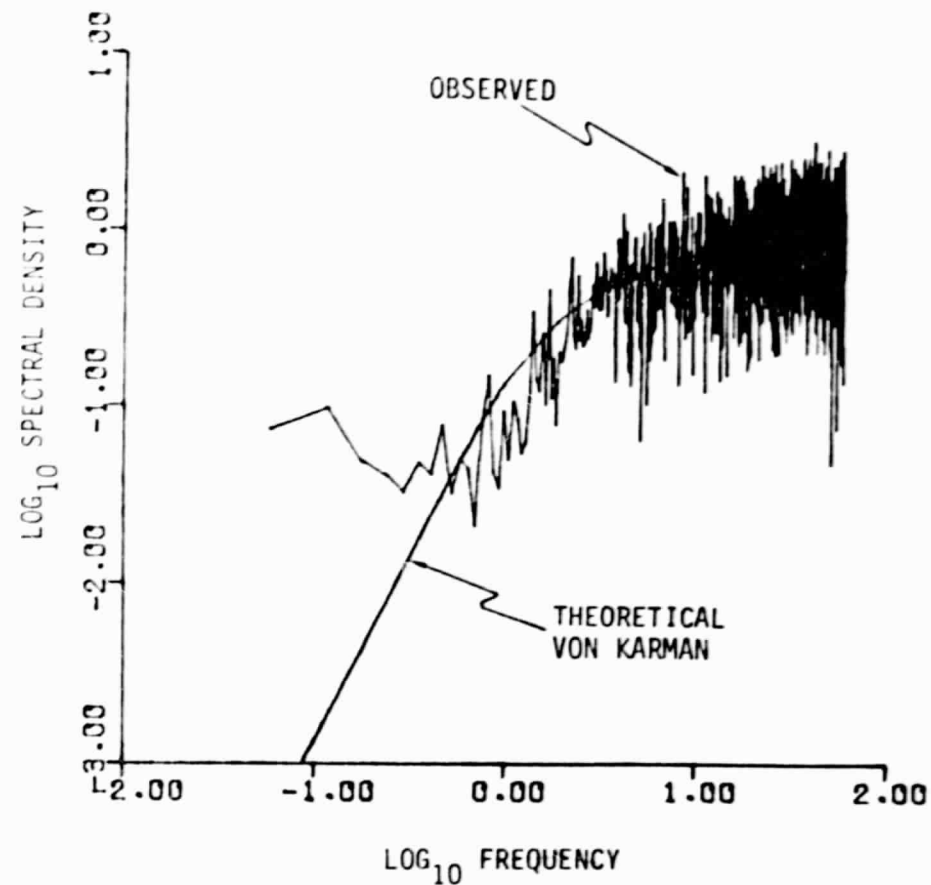
Figure B-20. $\partial u_3/\partial x_1$ - Gust Gradient Spectrum, Altitude Band #4

B-11
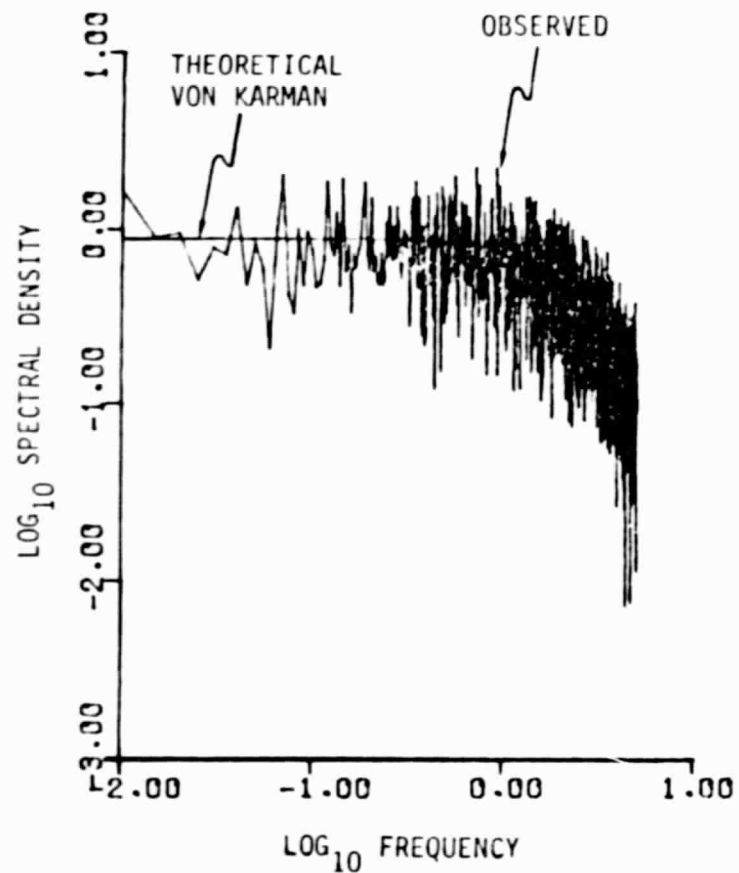
Figure B-21. $\partial u_3 / \partial x_2$ - Gust Gradient Spectrum, Altitude Band #1
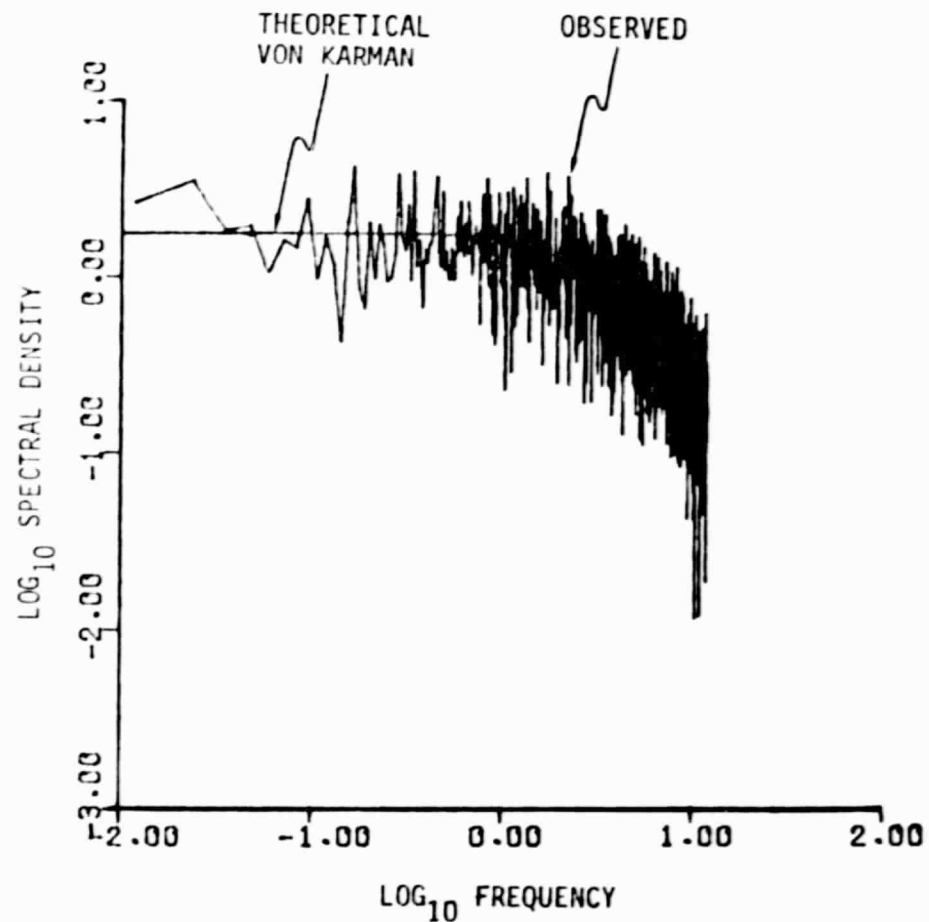
Figure B-22. $\partial u_3 / \partial x_2$ - Gust Gradient Spectrum, Altitude Band #2
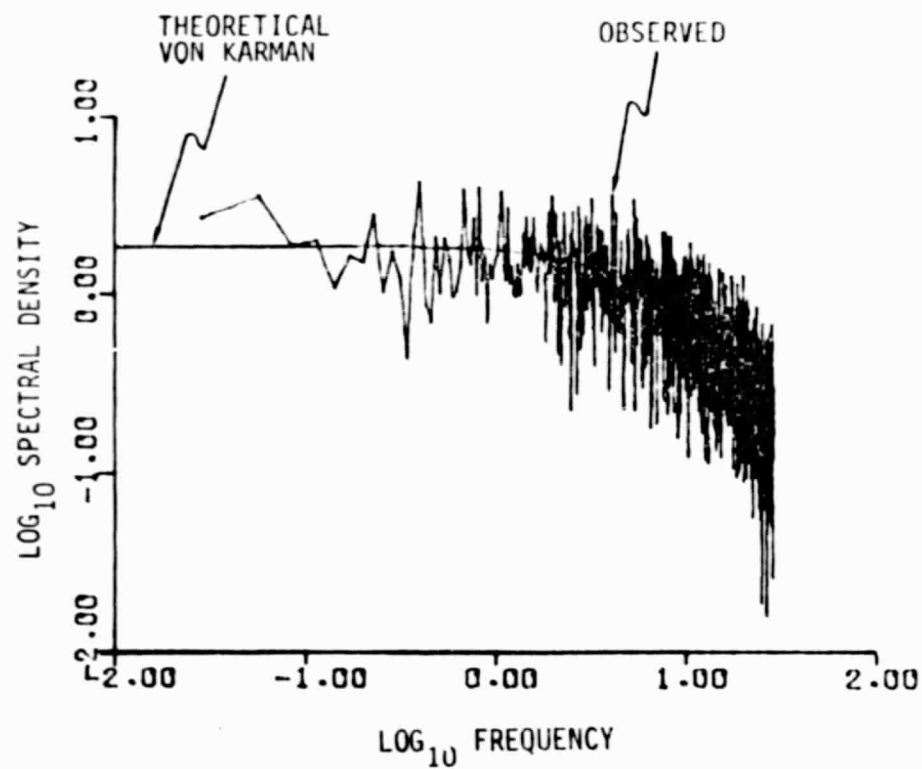
Figure B-23. $\partial u_3 / \partial x_2$ – Gust Gradient Spectrum,
Altitude Band #3
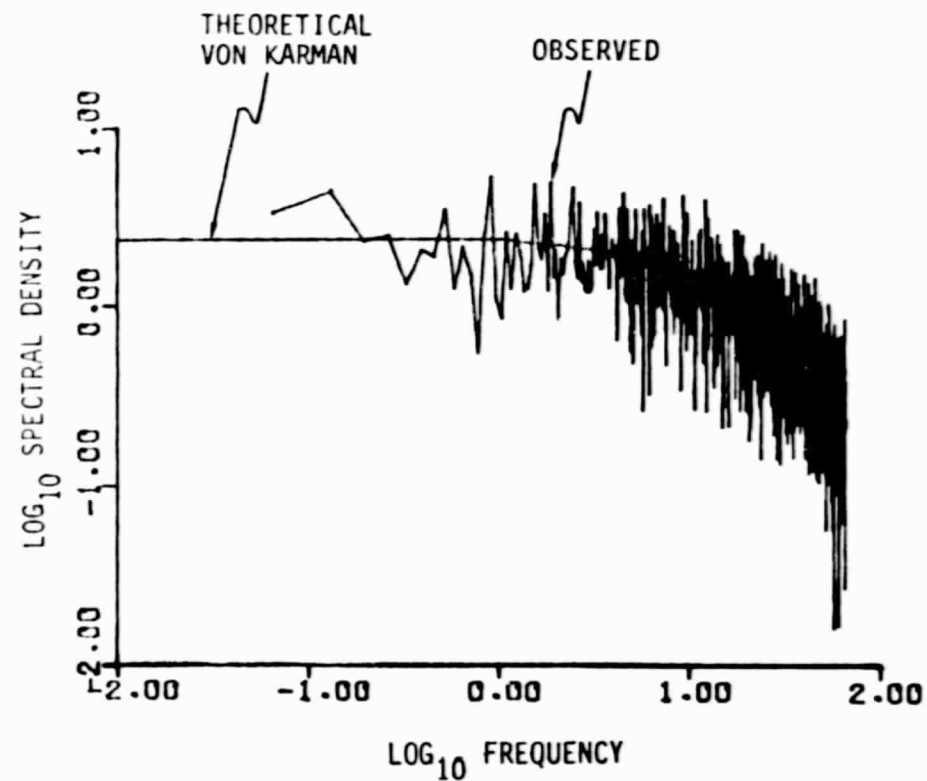
Figure B-24. $\partial u_3 / \partial x_2$ – Gust Gradient Spectrum,
Altitude Band #4

APPENDIX C

STATISTICAL ANALYSIS OF SIMULATED TURBULENCE

By means of standard statistical analysis procedures each of the SSTi has been analyzed to determine its mean value, standard deviation, and probability density distribution. The resulting mean values are presented in Table C-1 while Table C-2 contains the resulting standard deviations. As expected, all mean values were near zero. The standard deviations represent the square root of the energy content. The ratio of the square root of each theoretical energy content (from Table 2-5) to the corresponding standard deviation (from Table C-2) is presented in Table C-3. The agreement appears quite satisfactory.

The gust and gust gradient probability density distributions are presented in Figures C-1 through C-24 in accordance with Table C-4. In each figure the corresponding normal distribution is also presented. The results indicate that both the gust and gust gradient time series are very close to normal distribution.

TABLE C-1. MEAN VALUE OF GUST AND GUST GRADIENTS

SERIES TYPE	ALTITUDE BAND			
	1	2	3	4
u_1	-.006109	-.009637	-.015505	-.020793
u_2	-.005858	-.010306	-.015392	-.018100
u_3	-.005597	-.010238	-.015364	-.018100
$\partial u_2/\partial x_1$	-.000015	-.000269	-.002197	-.006183
$\partial u_3/\partial x_1$	-.000014	-.00027	-.002198	-.006188
$\partial u_3/\partial x_2$	-.006585	-.019388	-.043538	-.064540

TABLE C-2.   STANDARD DEVIATION OF GUST AND GUST GRADIENTS

SERIES TYPE	ALTITUDE BAND			
	1	2	3	4
u_1	.724352	.868642	.927039	.946672
u_2	.756057	.884176	.936133	.947373
u_3	.719277	.867329	.928437	.942133
$\partial u_2/\partial x_1$	1.139887	2.591114	4.999053	7.387333
$\partial u_3/\partial x_1$	1.670499	2.45426	4.777666	7.063241
$\partial u_3/\partial x_2$	.836263	2.225938	4.766939	7.049476

TABLE C-3.   RATIO OF SQUARE ROOT OF THEORETICAL
ENERGY CONTENT[*] TO THE OBSERVED STANDARD
DEVIATION[†]

SERIES TYPE	ALTITUDE BAND			
	1	2	3	4
u_1	1.0134	1.0194	1.0208	1.0186
u_2	1.0048	1.0079	1.0107	1.0177
u_3	1.0050	1.0082	1.0109	1.0179
$\partial u_2/\partial x_1$	.9938	.9951	.9955	.9959
$\partial u_3/\partial x_1$	.9939	.9955	.9960	.9964
$\partial u_3/\partial x_2$	1.0039	1.0041	1.0037	1.0036

[*]Theoretical energy content taken from Table 2-5.

[†]Observed standard deviation taken from Table C-2.

TABLE C-4. MATRIX OF STATISTICAL ANALYSIS FIGURES

SERIES TYPE	ALTITUDE BAND			
	1	2	3	4
u_1	C-1	C-2	C-3	C-4
u_2	C-5	C-6	C-7	C-8
u_3	C-9	C-10	C-11	C-12
$\partial u_2/\partial x_1$	C-13	C-14	C-15	C-16
$\partial u_3/\partial x_1$	C-17	C-18	C-19	C-20
$\partial u_3/\partial x_2$	C-21	C-22	C-23	C-24
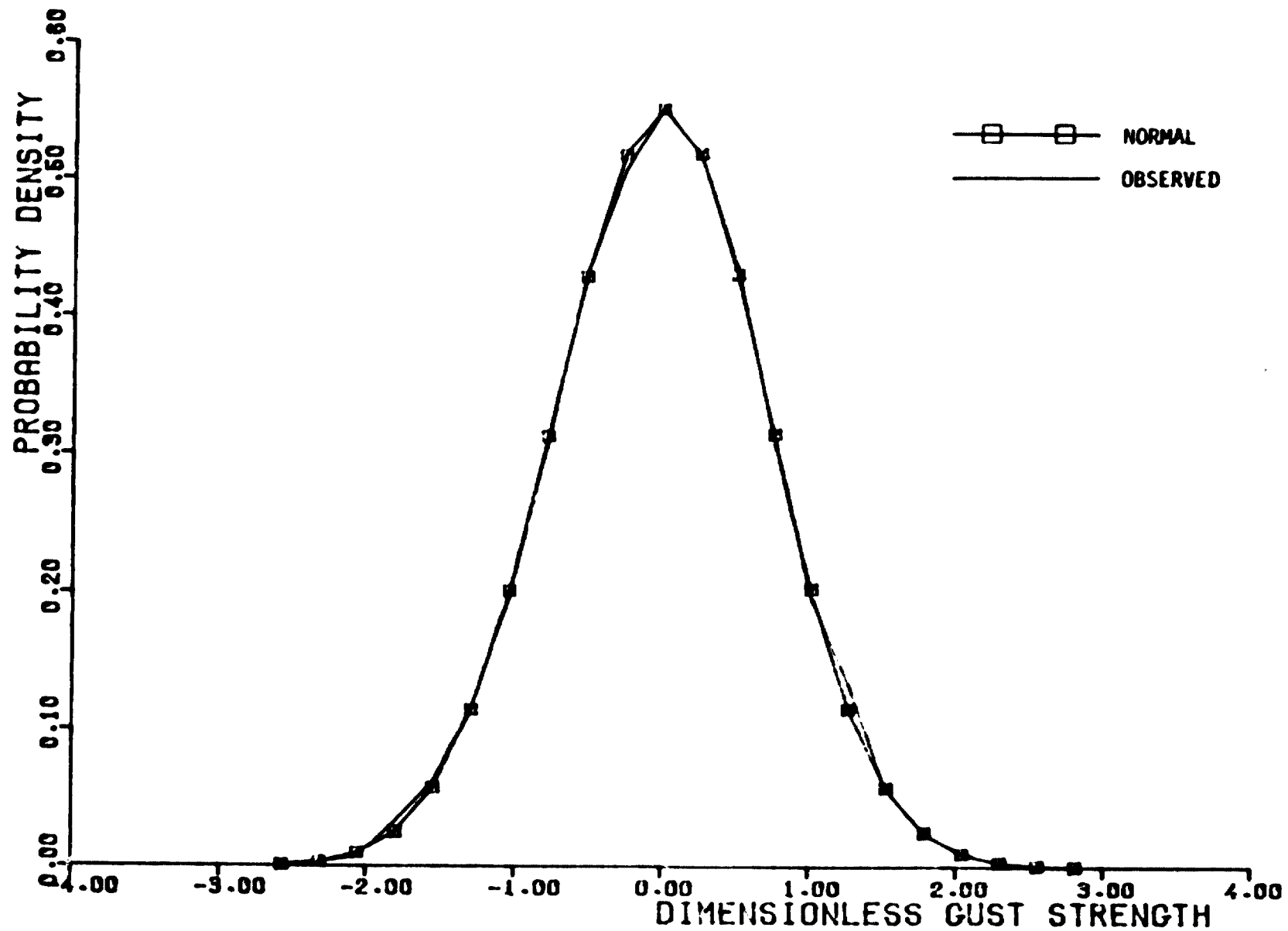
Figure C-1. u_1 - Gust Probability Density Distribution. Altitude Band #1

C-4
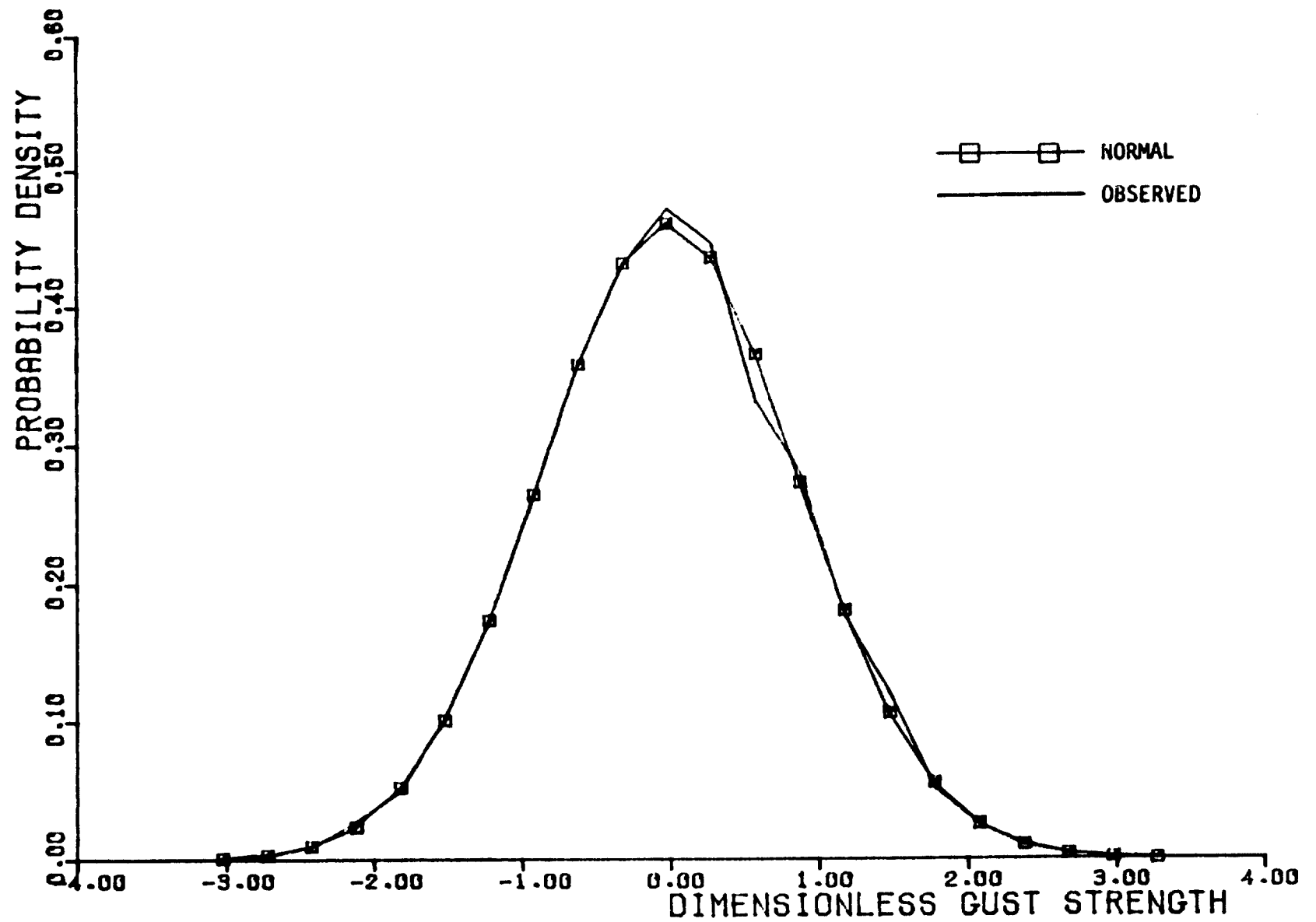
Figure C-2. u_1 - Gust Probability Density Distribution, Altitude Band #2
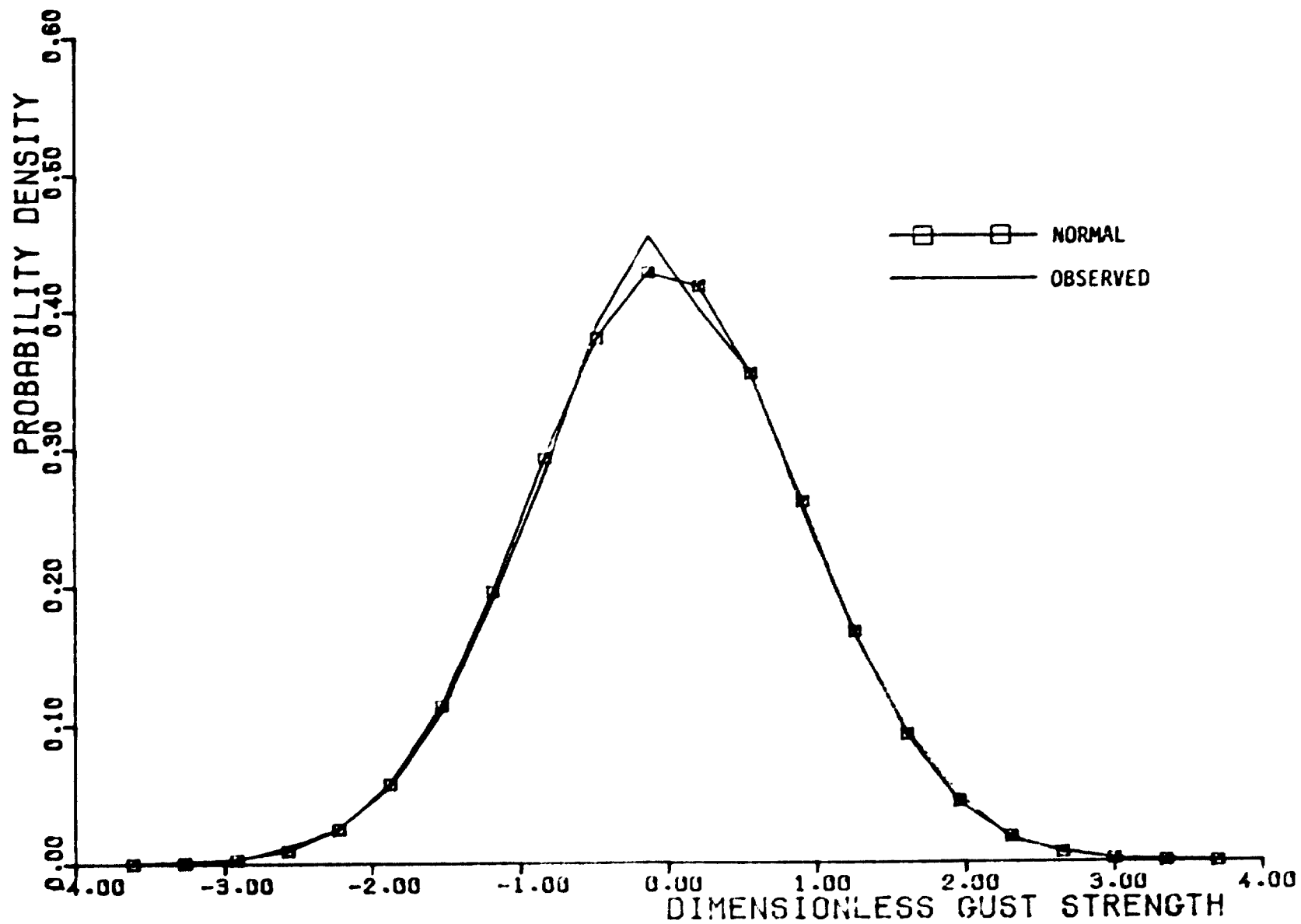
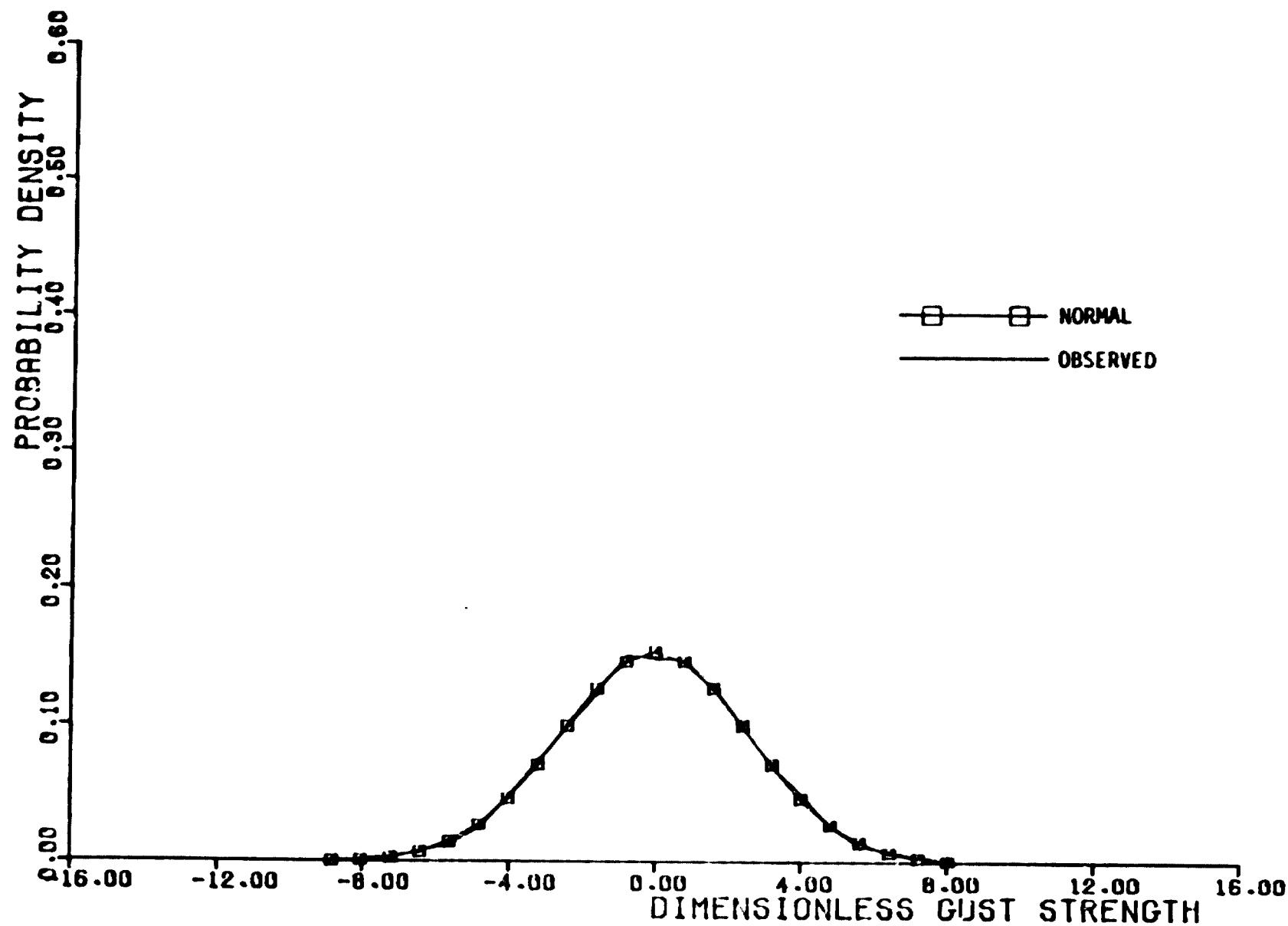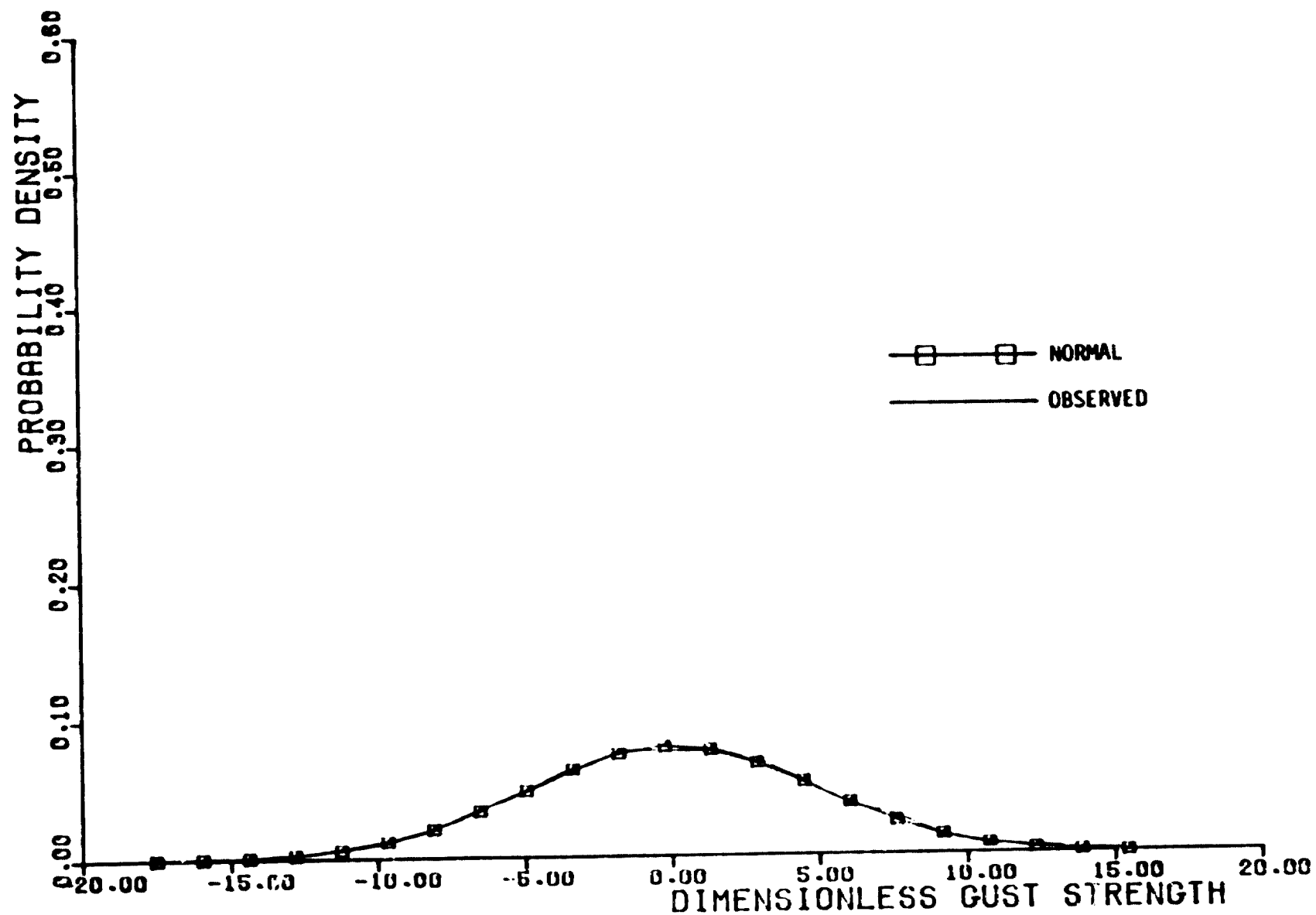Figure C-3. u_1 - Gust Probability Density Distribution, Altitude Band #3
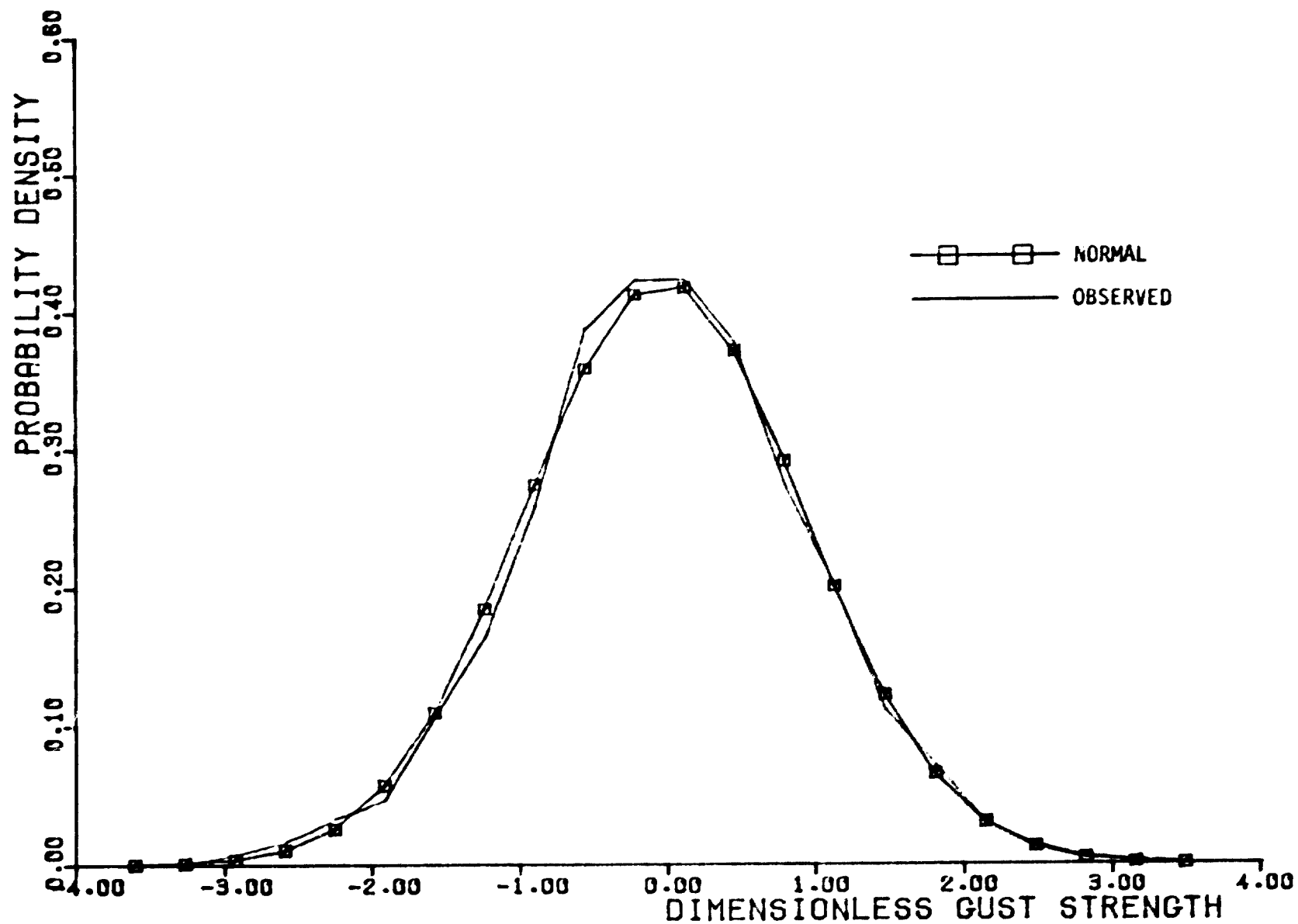
Figure C-4. u_1 - Gust Probability Density Distribution, Altitude Band #4
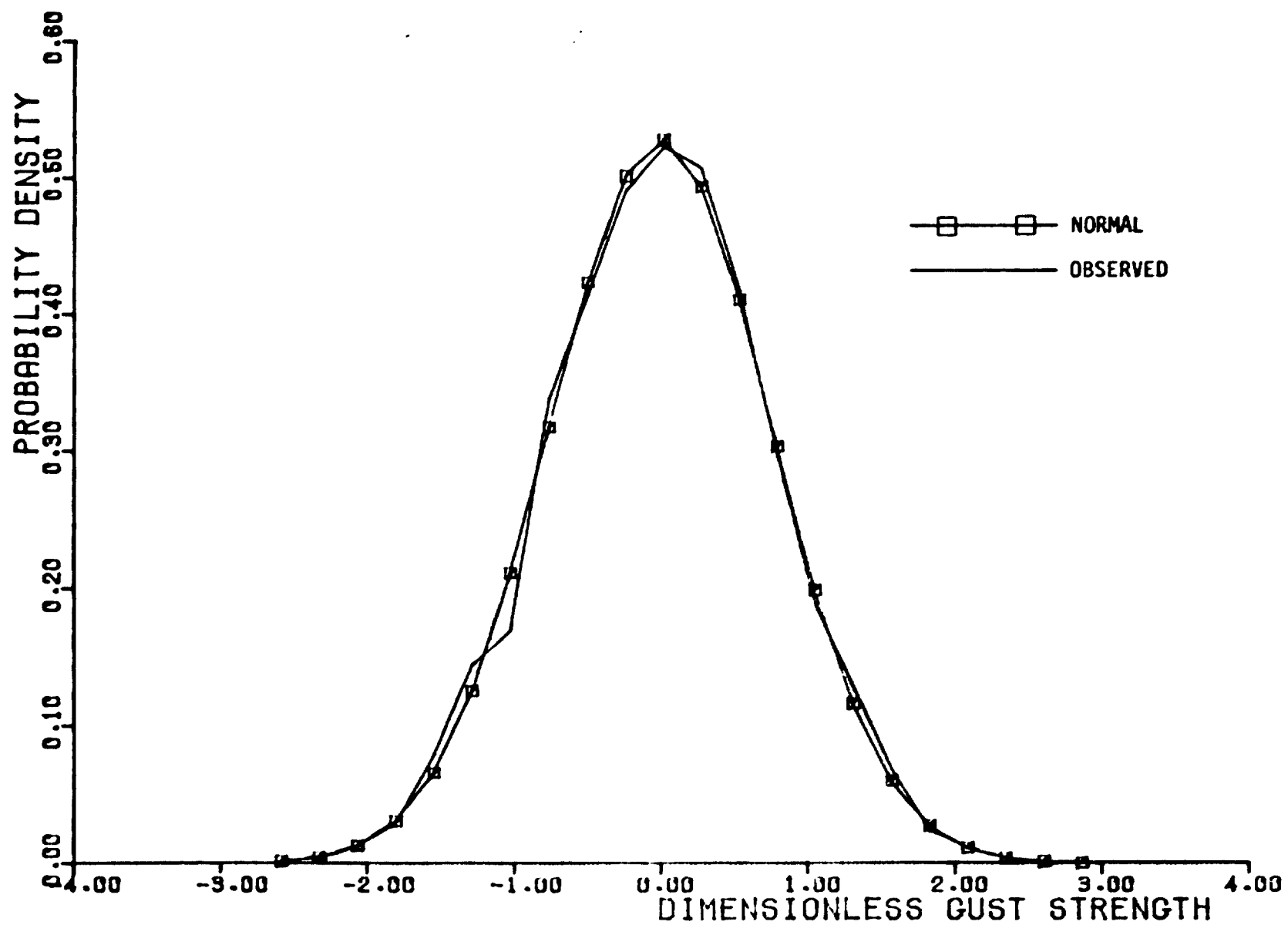
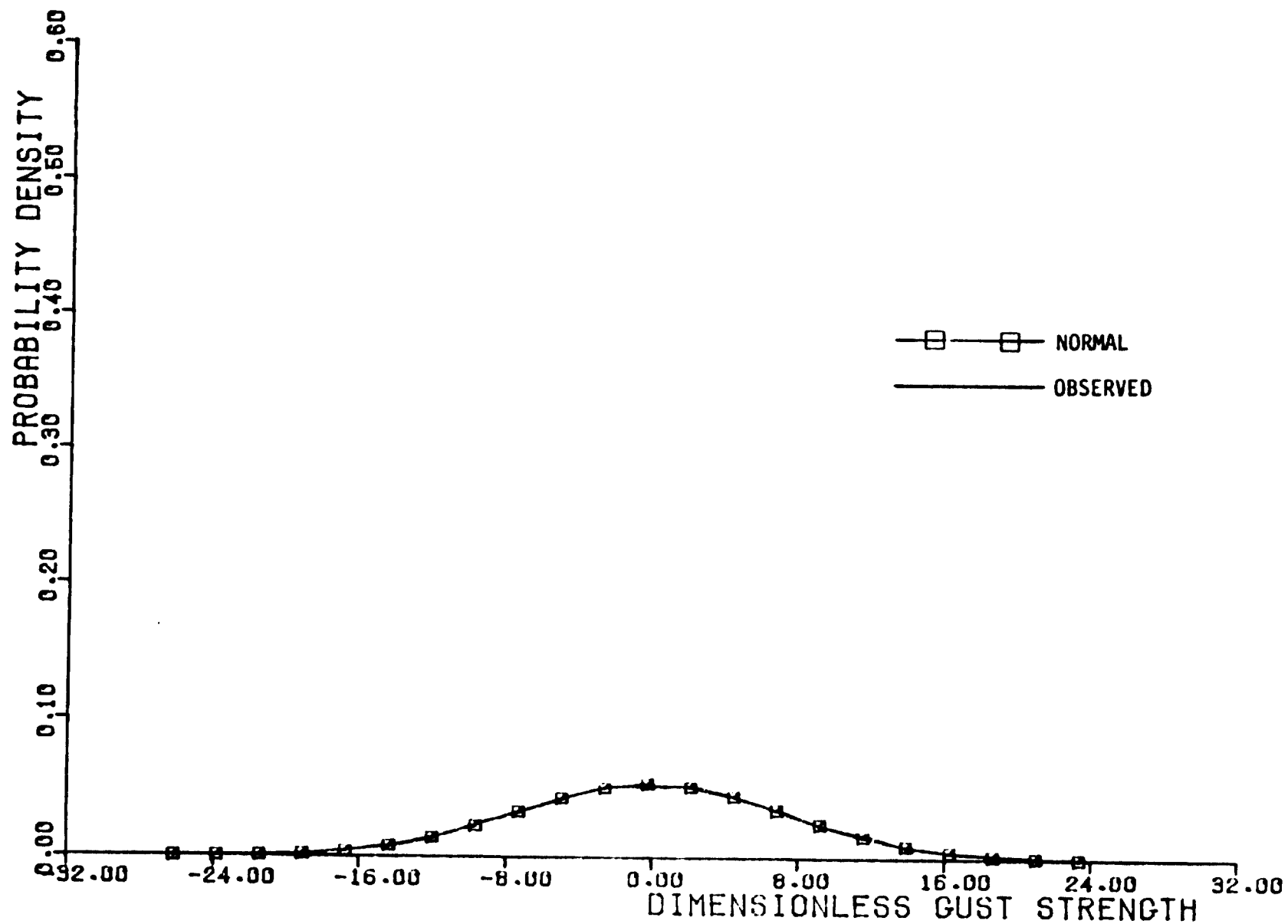Figure C-5. u_2 - Gust Probability Density Distribution, Altitude Band #1
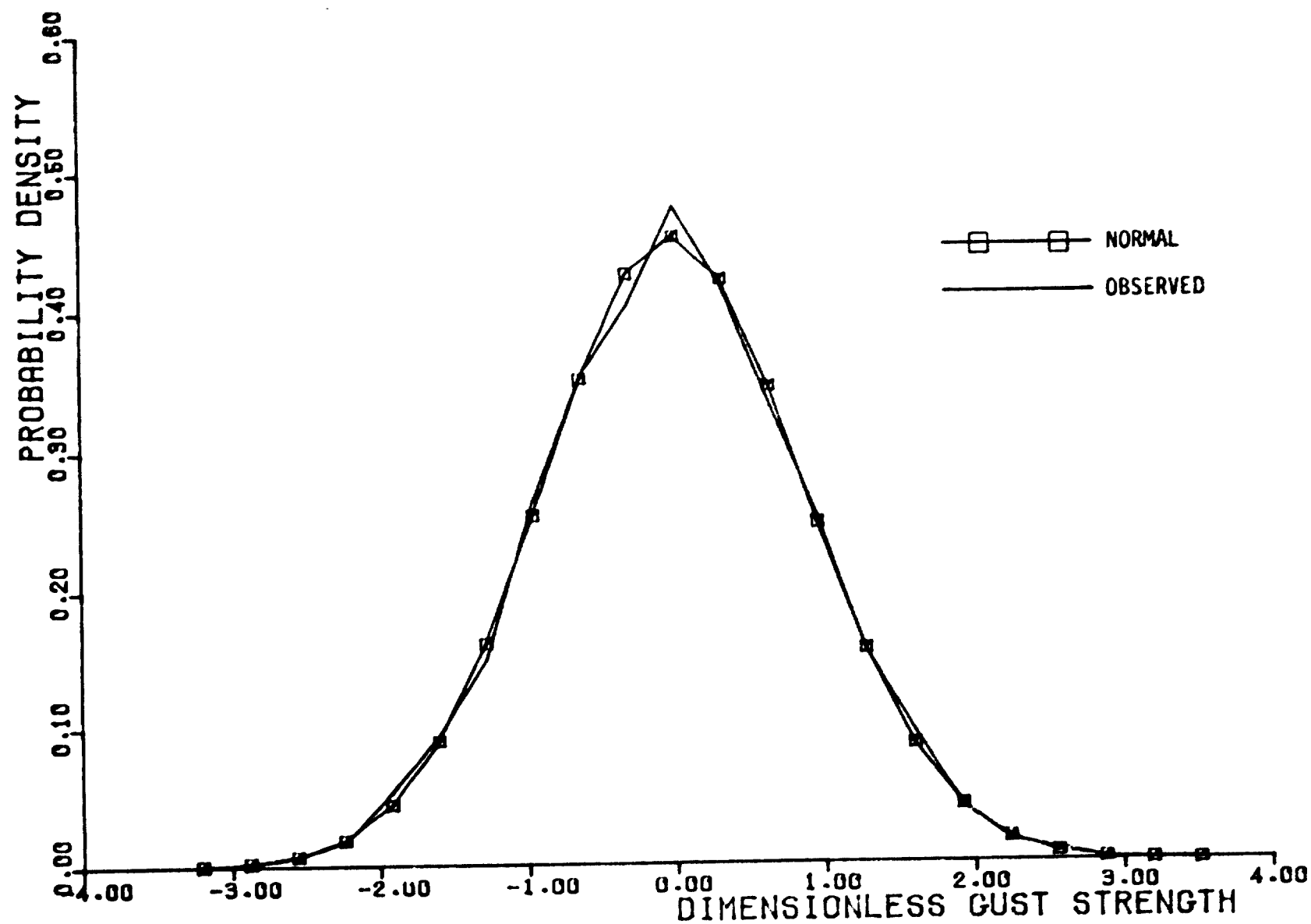
Figure C-6. u_2 - Gust Probability Density Distribution, Altitude Band #2
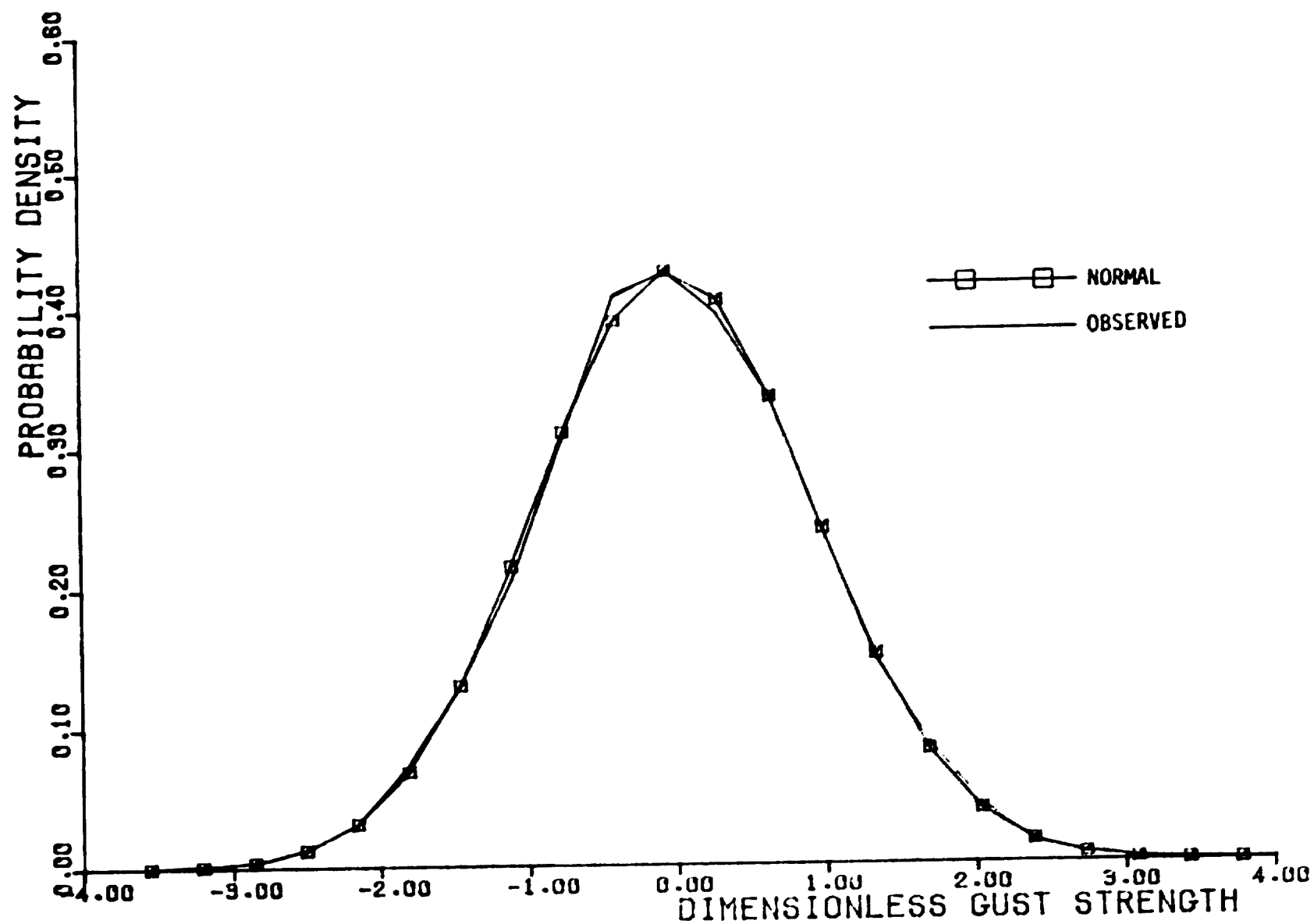
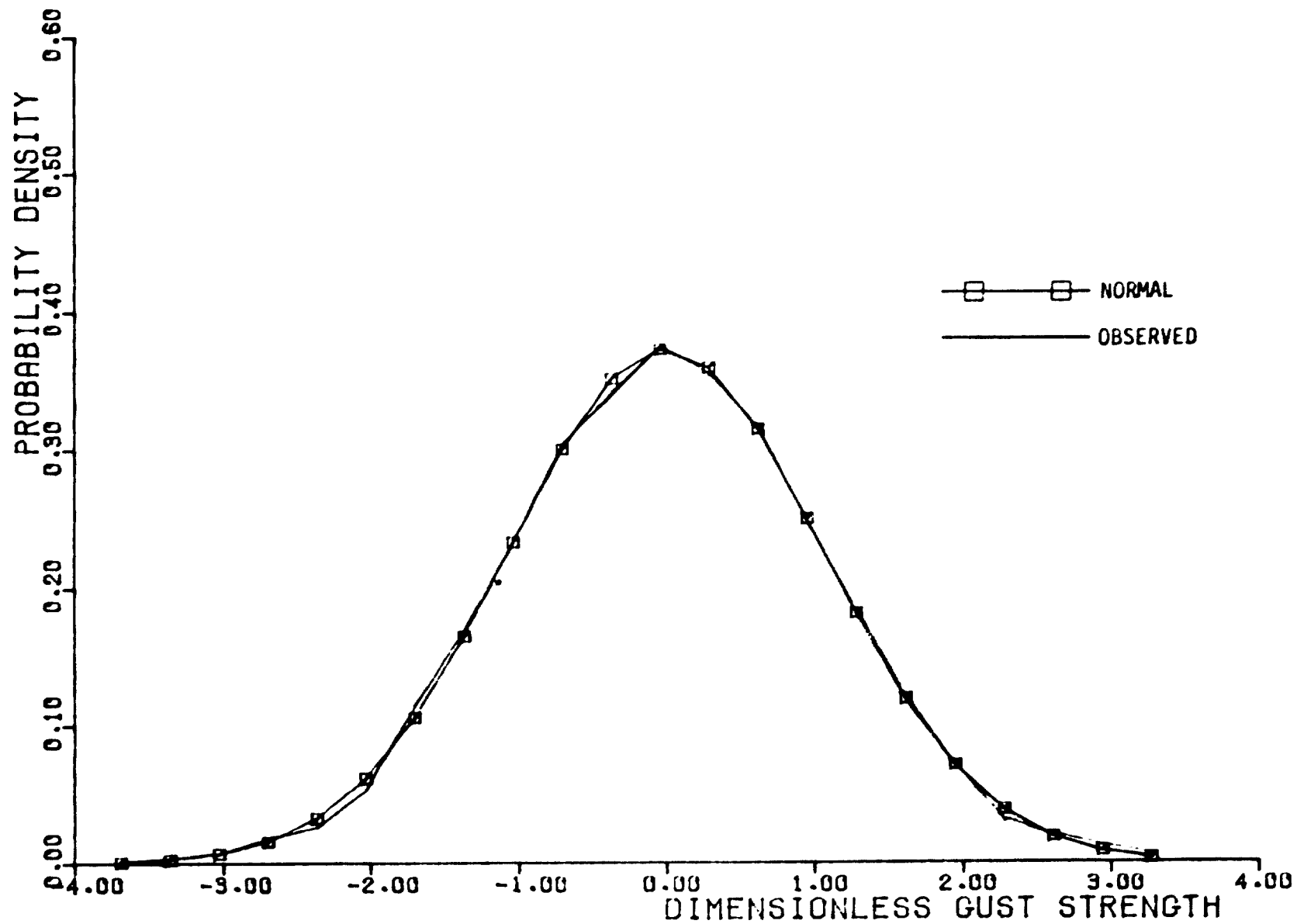Figure C-7. u_2 - Gust Probability Density Distribution, Altitude Band #3

C-10
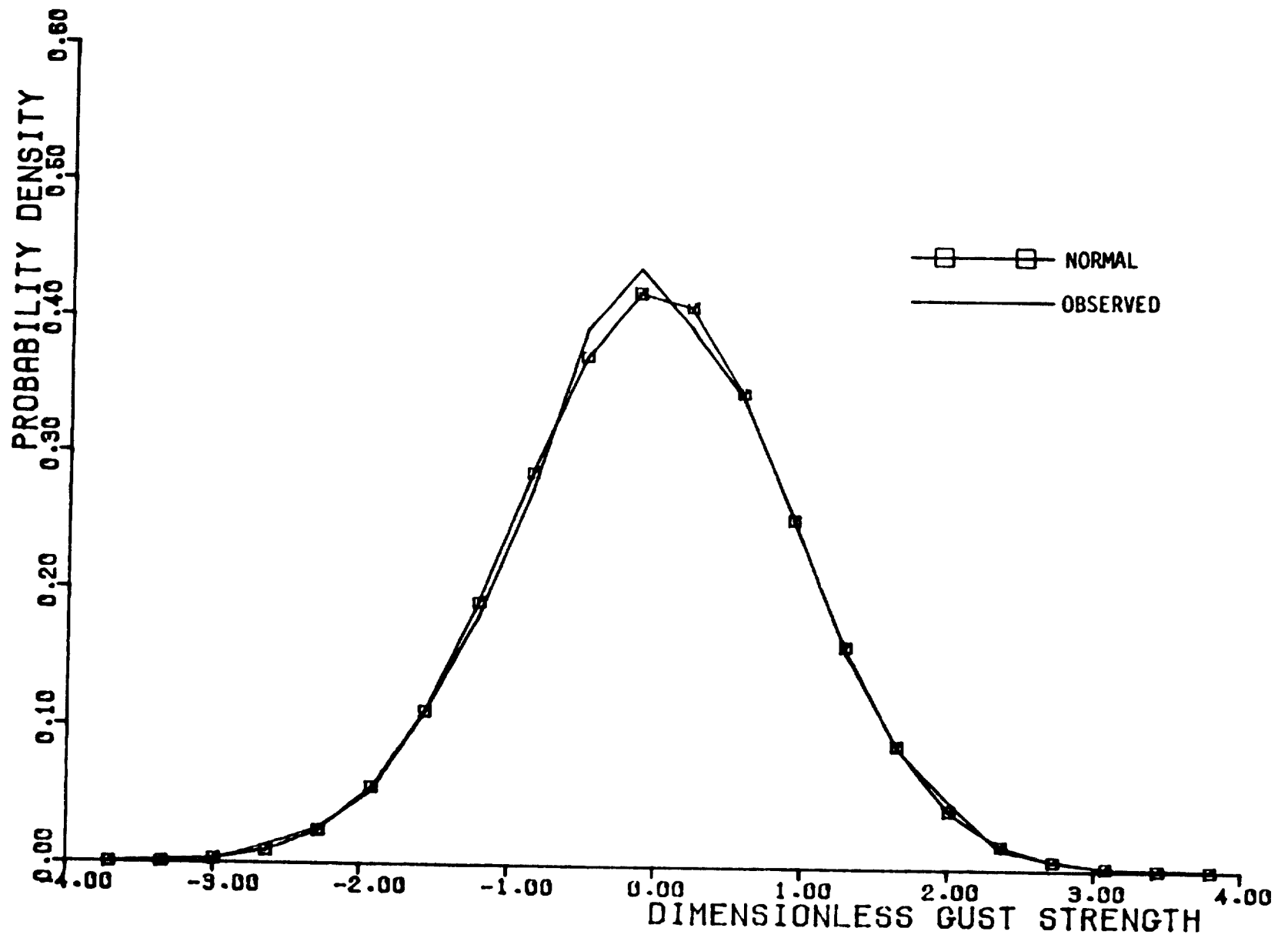
Figure C-8. u_2 - Gust Probability Density Distribution, Altitude Band #4
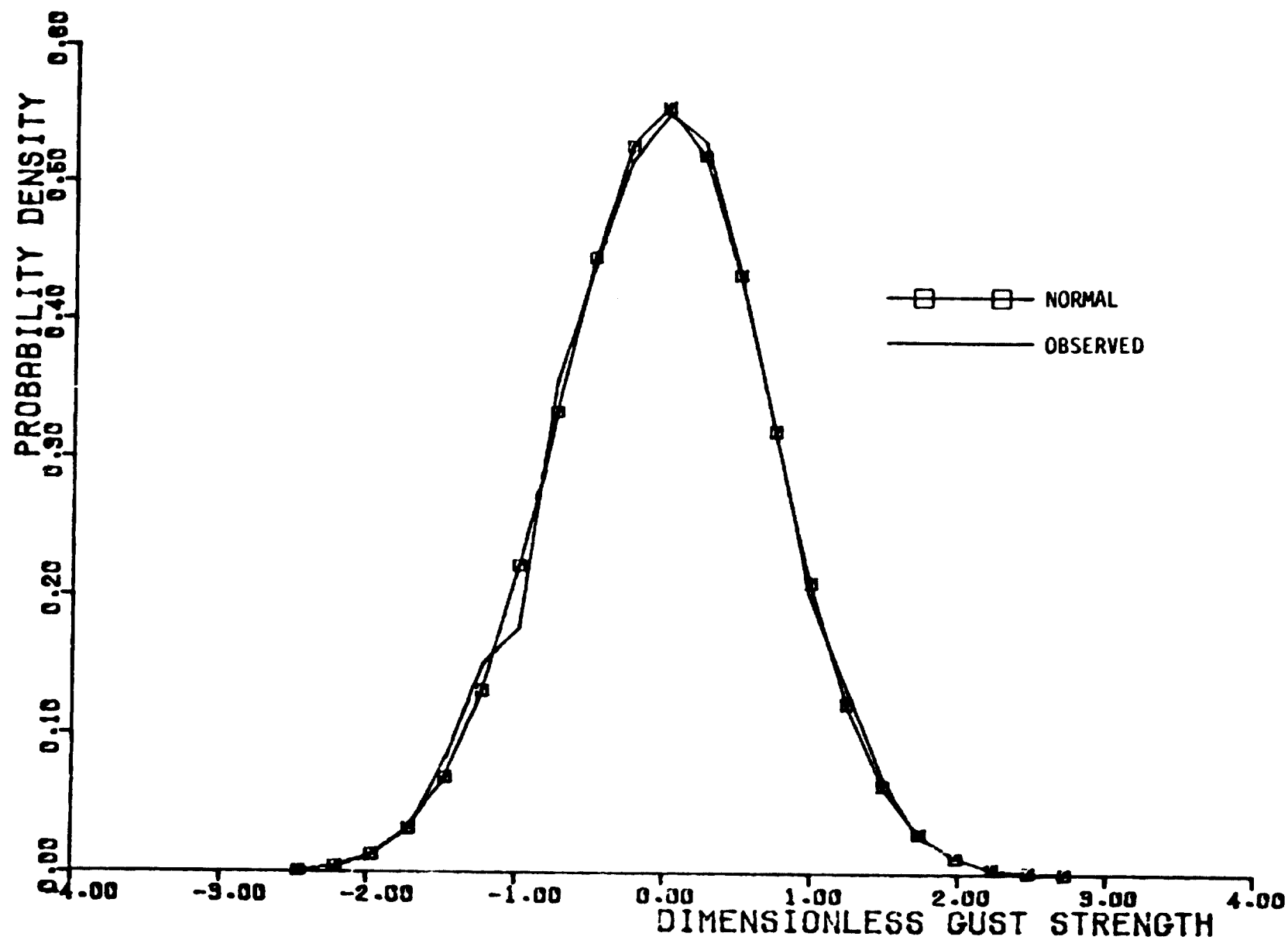
Figure C-9. u_3 - Gust Probability Density Distribution, Atmospheric Band #1
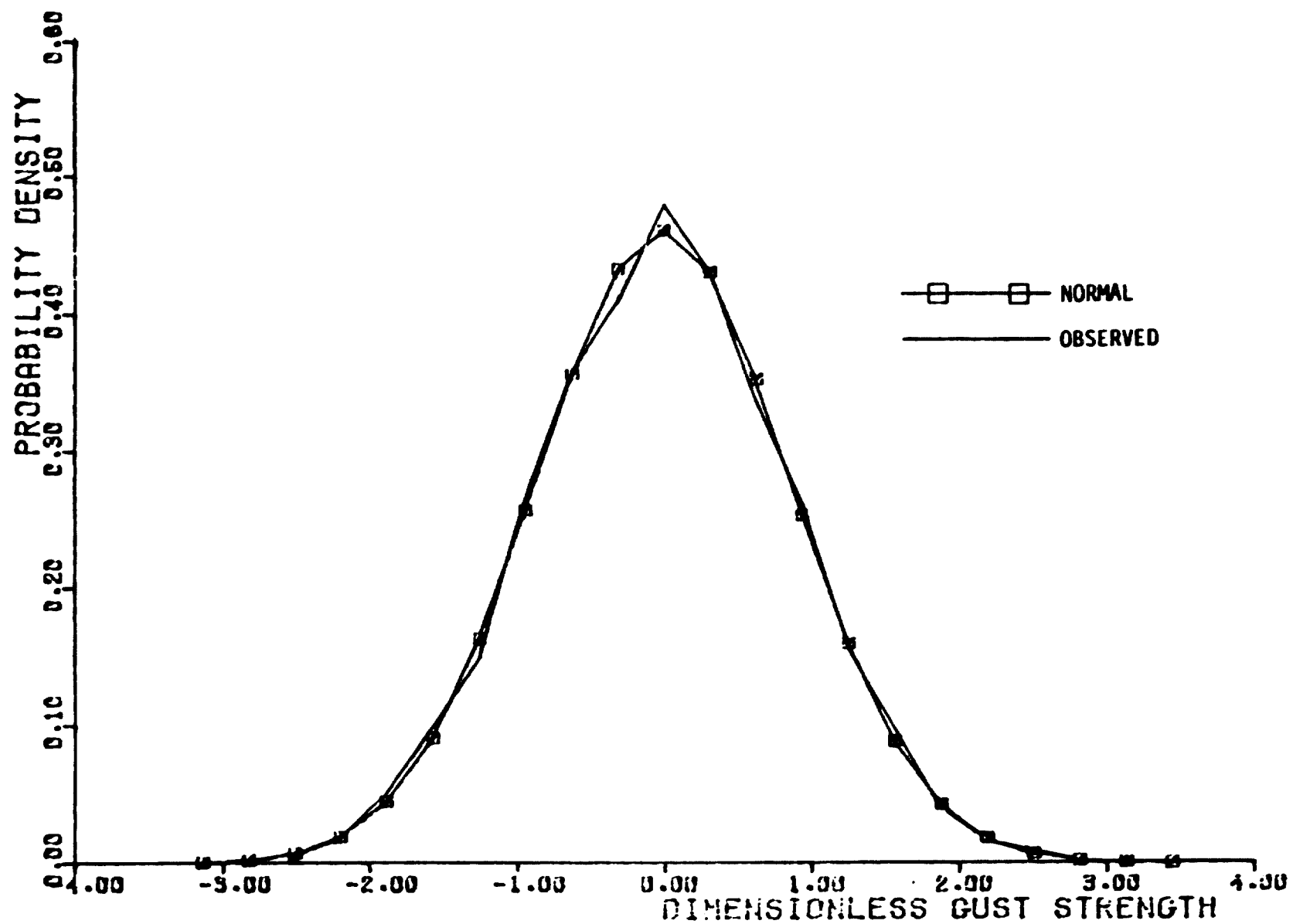
Figure C-10. u_3 – Gust Probability Density Distribution, Altitude Band #2
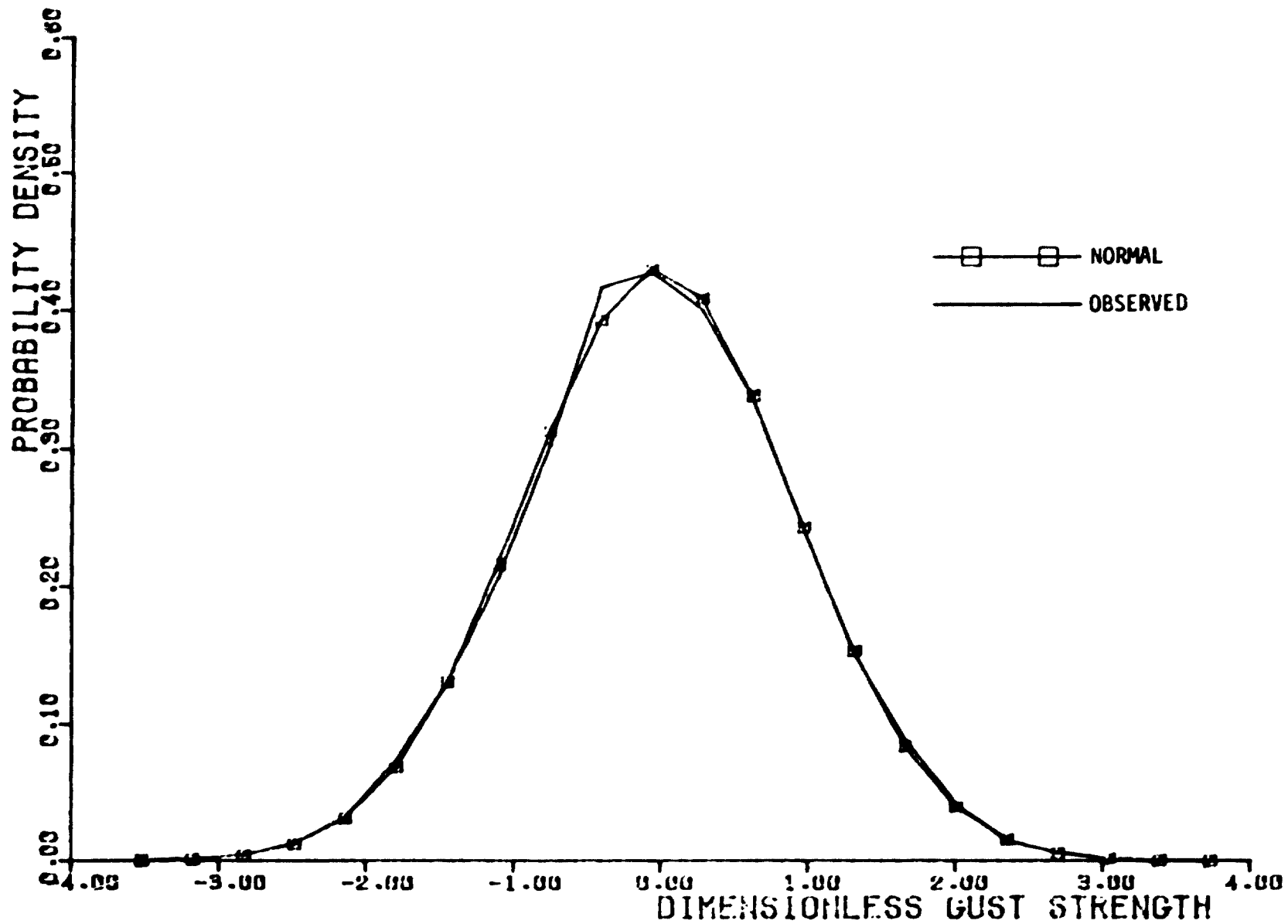
Figure C-11. u_3 - Gust Probability Density Distribution, Altitude Band #3
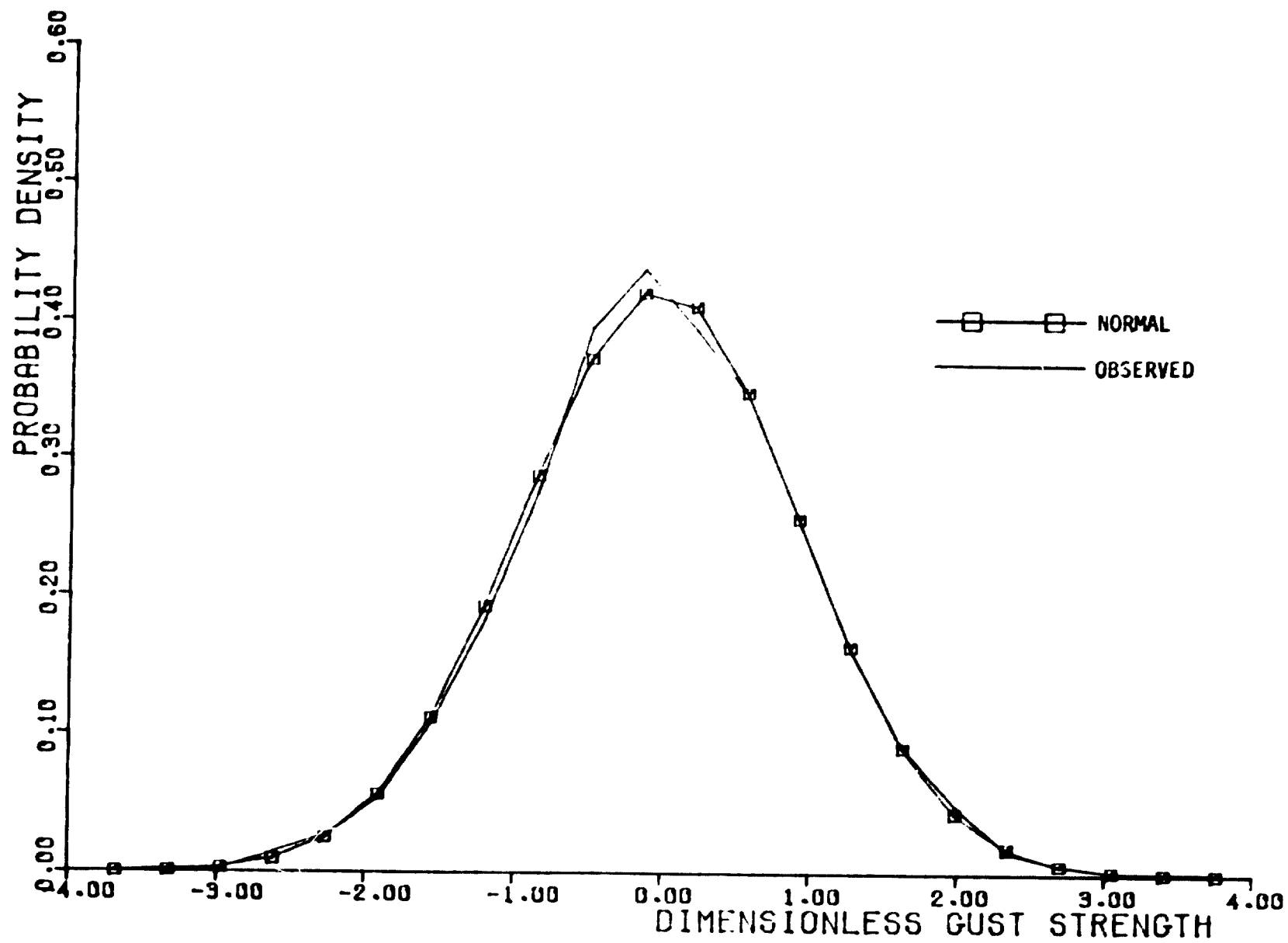
Figure C-12. u_3 - Gust Probability Density Distribution, Altitude Band #4
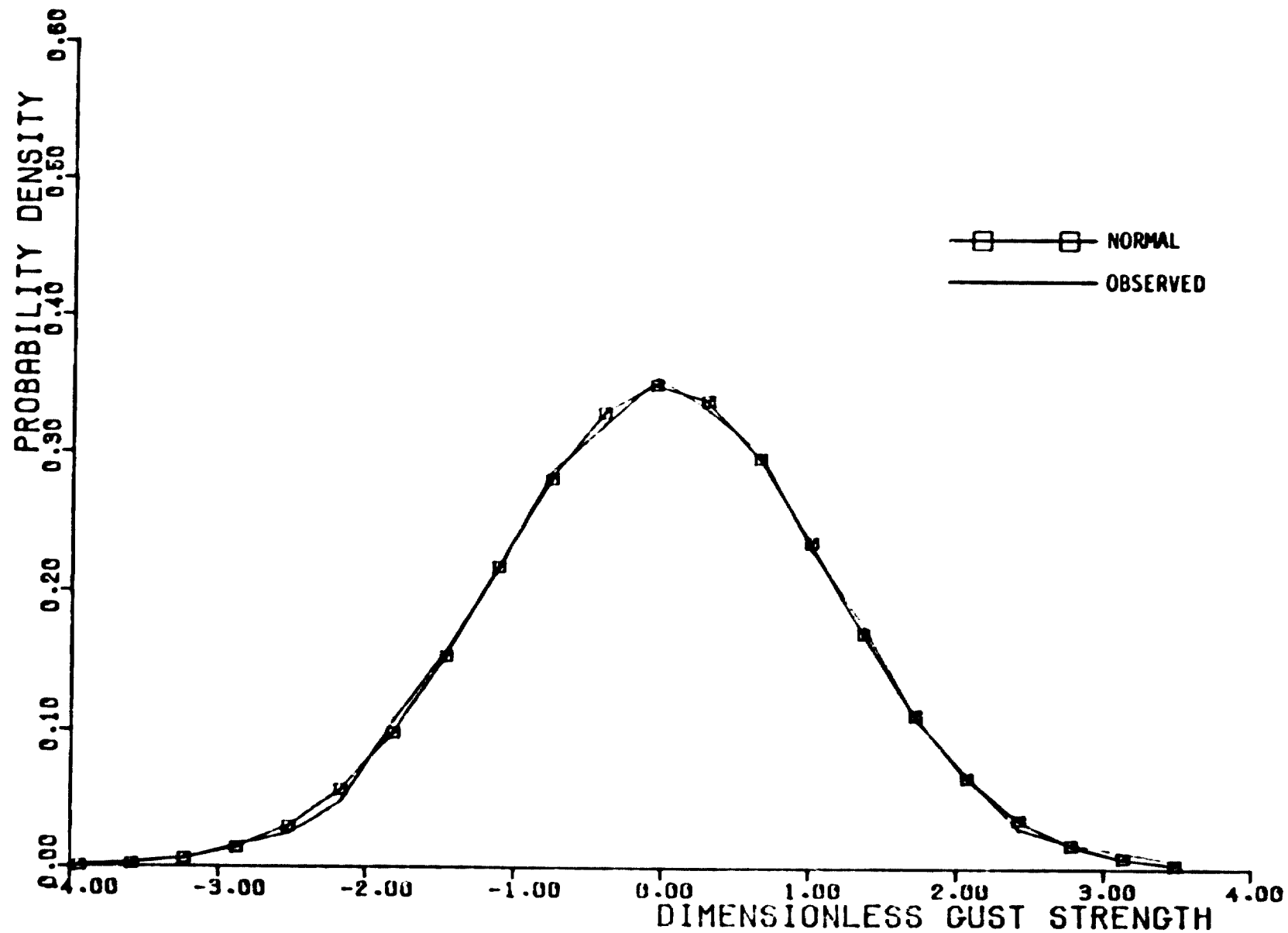
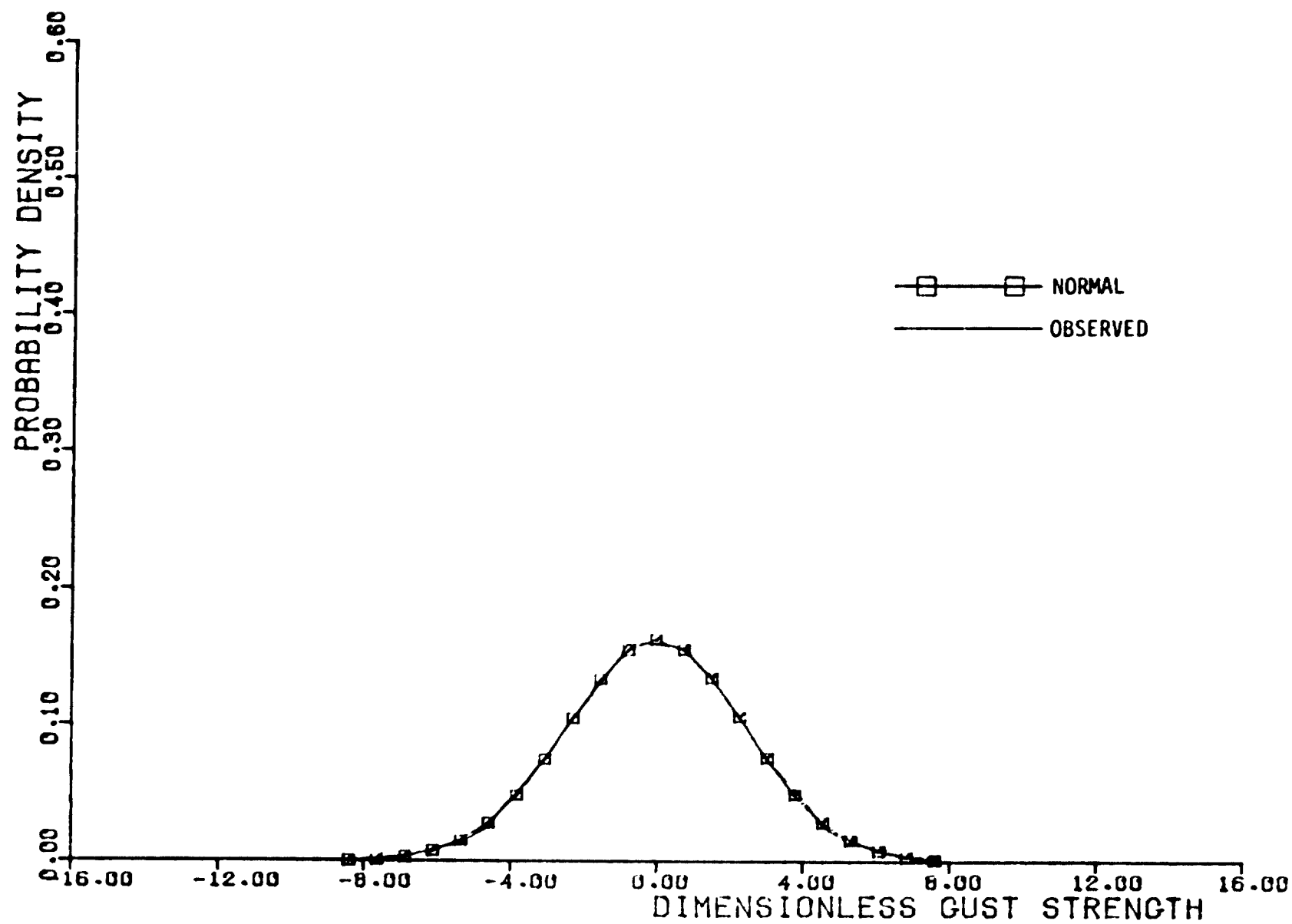Figure C-13. $\partial u_2/\partial x_1$ - Gust Gradient Probability Density Distribution, Altitude Band #1

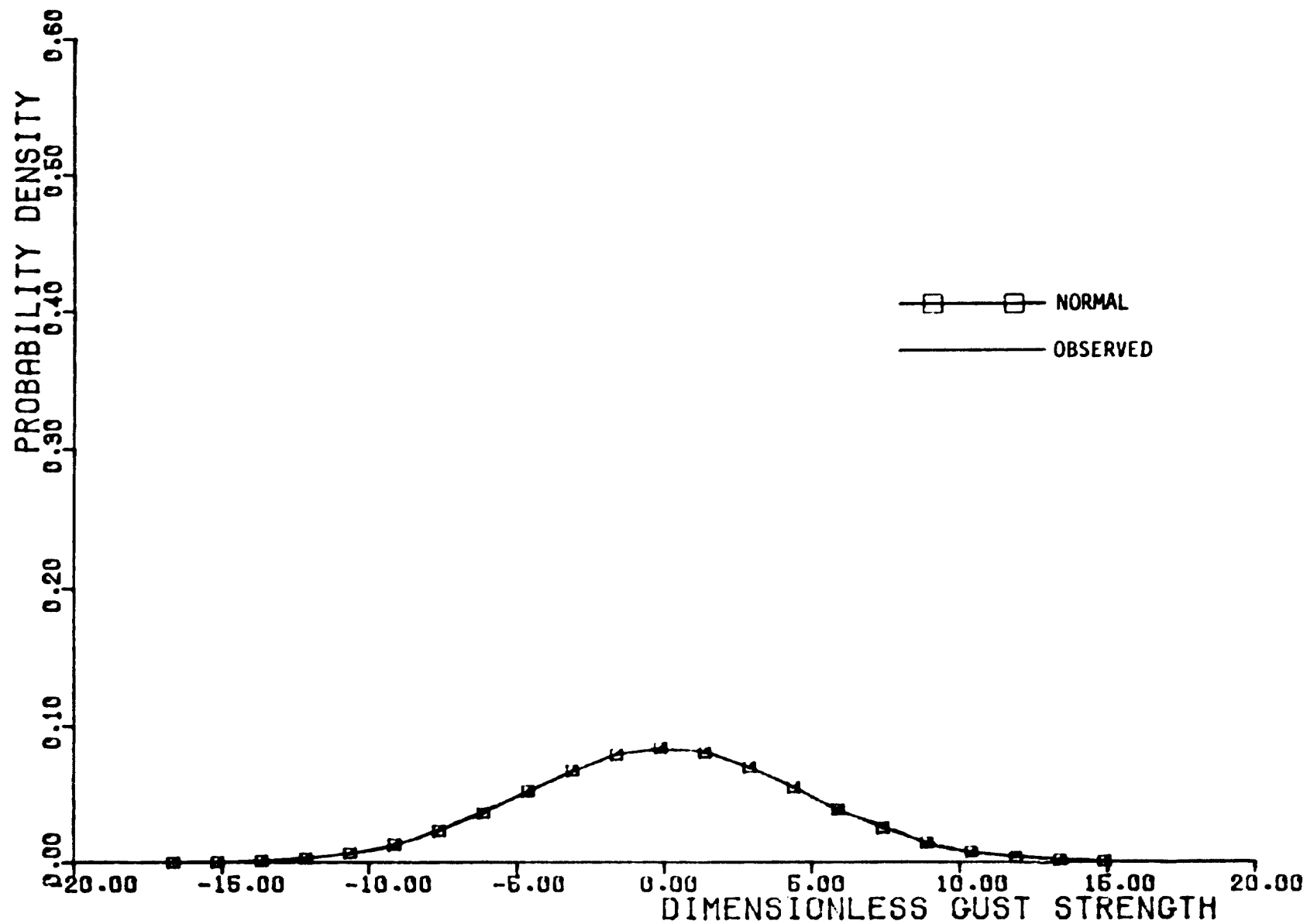Figure C-14. $\partial u_2/\partial x_1$ - Gust Gradient Probability Density Distribution, Altitude Band #2

Figure C-15. $\partial u_2 / \partial x_1$ - Gust Gradient Probability Density Distribution, Altitude Band #3
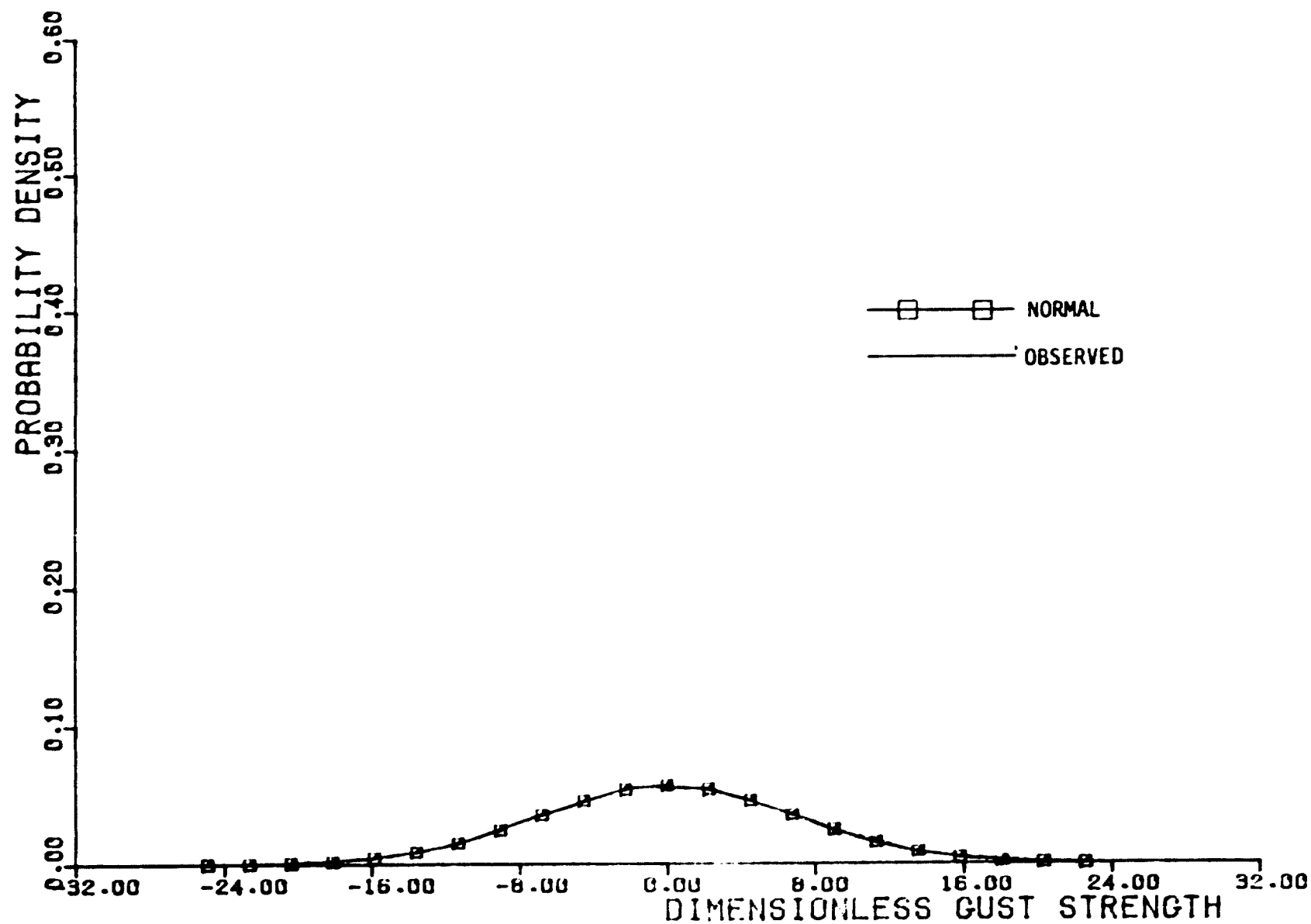
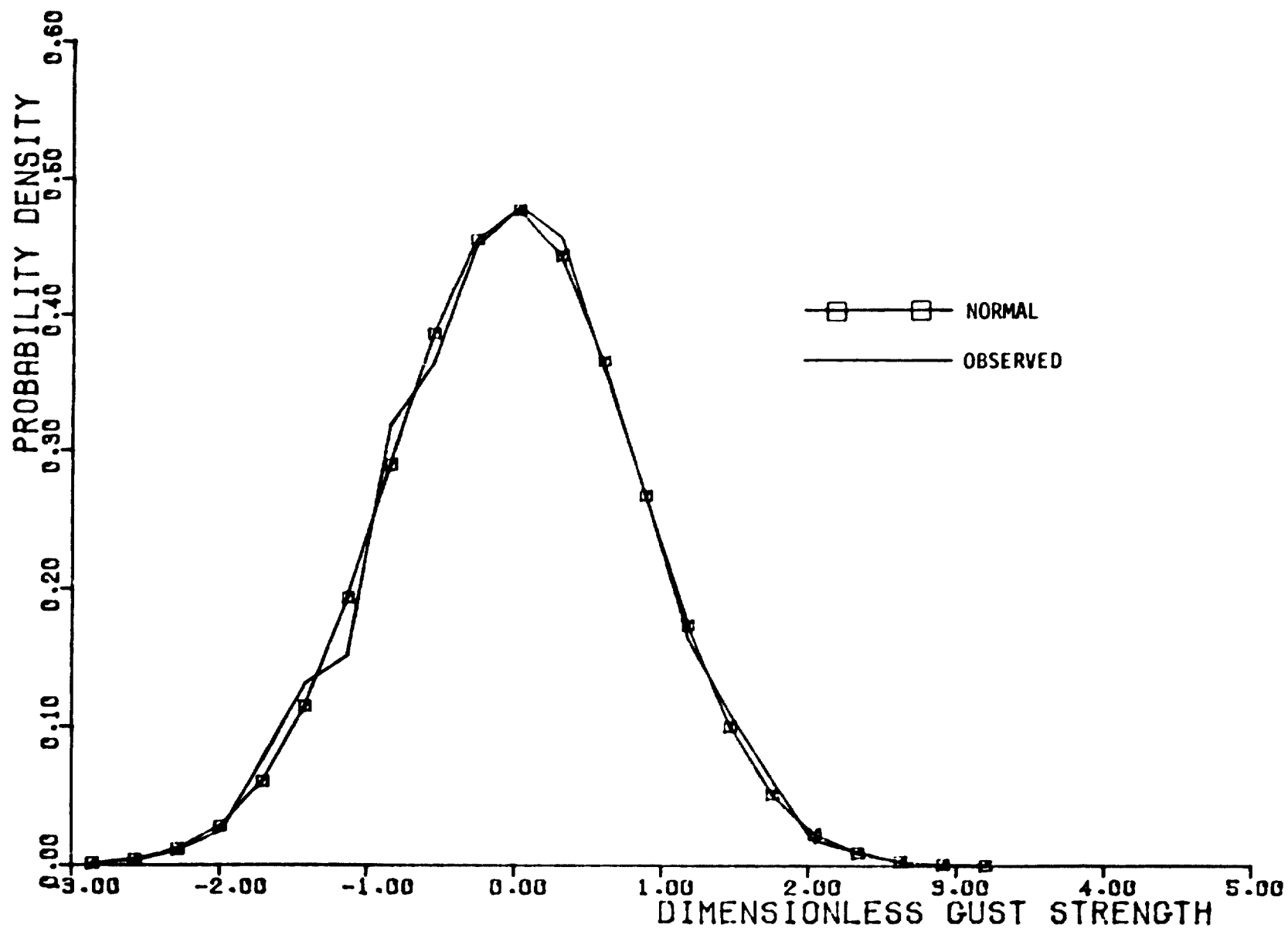Figure C-16. $\partial u_2/\partial x_1$ - Gust Gradient Probability Density Distribution, Altitude Band #4

Figure C-17. $\partial u_3/\partial x_1$ – Gust Gradient Probability Density Distribution, Altitude Band #1

Figure C-18. $\partial u_3/\partial x_1$ – Gust Gradient Probability Density Distribution, Altitude Band #2

Figure C-19. $\partial u_3/\partial x_1$ - Gust Gradient Probability Density Distribution, Altitude Band #3

Figure C-20. $\partial u_3/\partial x_1$ – Gust Gradient Probability Density Distribution, Altitude Band #4

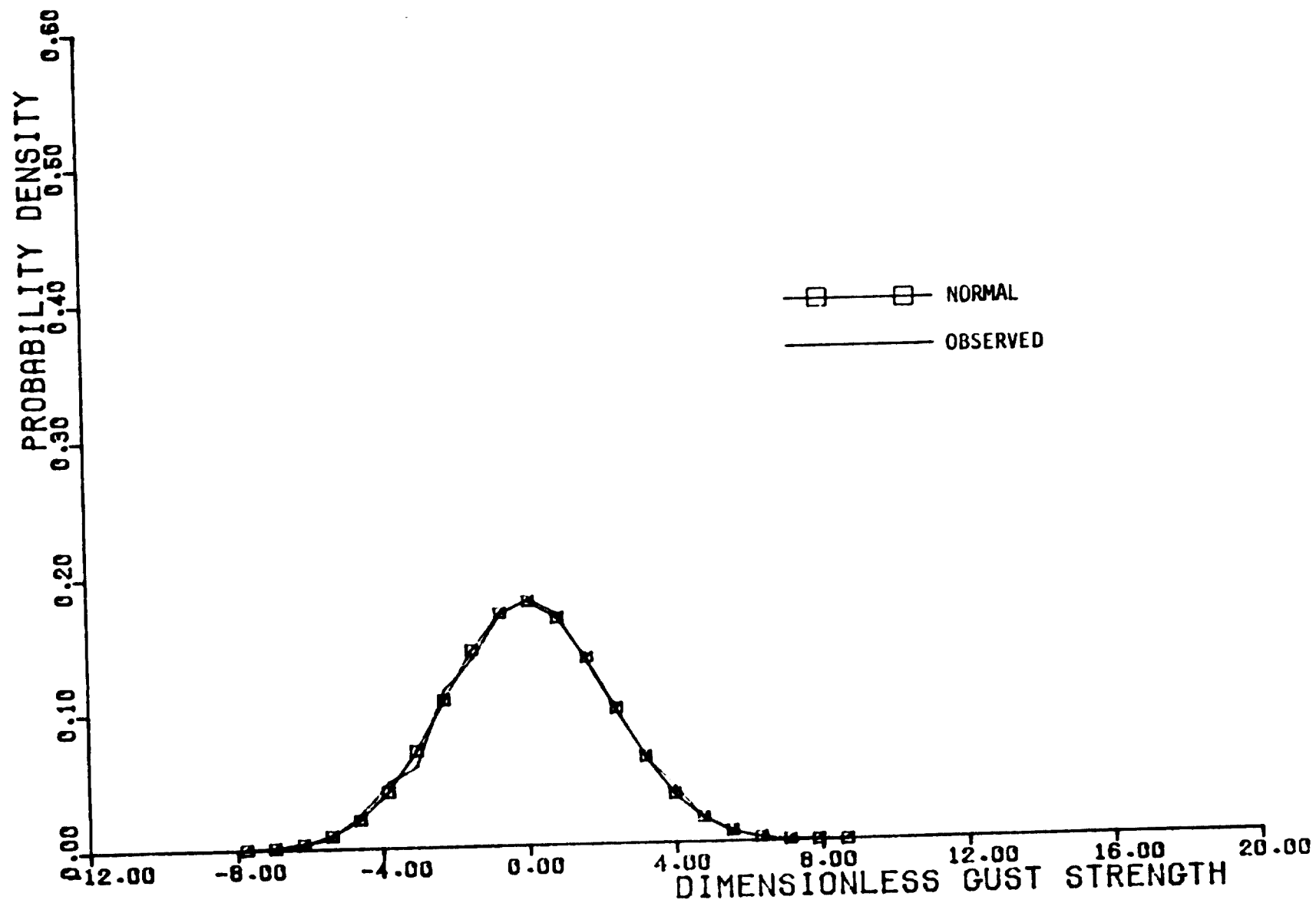Figure C-21. $\partial u_3/\partial x_2$ - Gust Gradient Probability Density Distribution, Altitude Band #1

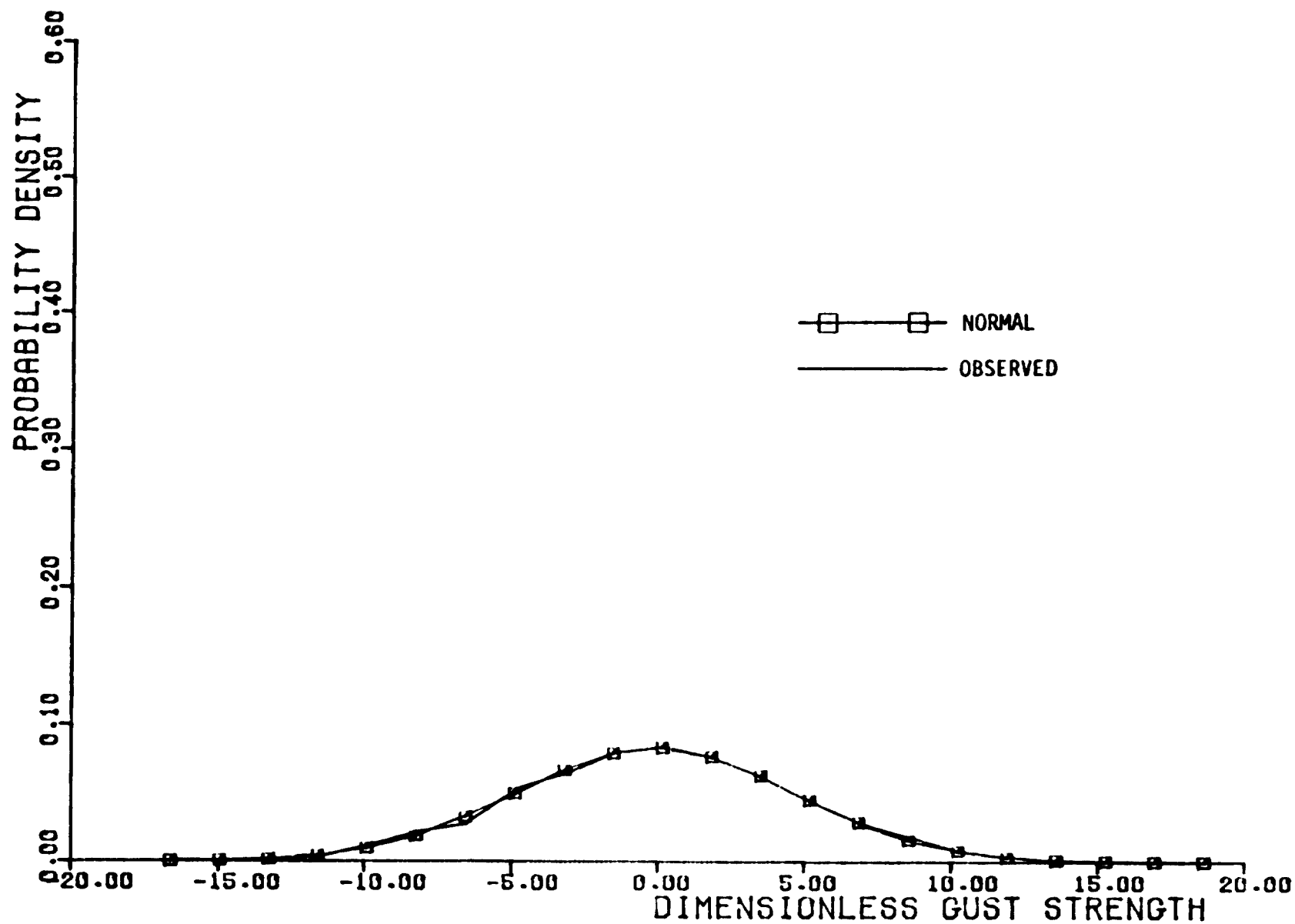Figure C-22. $\partial u_3/\partial x_2$ - Gust Gradient Probability Density Distribution, Altitude Band #2

Figure C-23. $\partial u_3/\partial x_2$ – Gust Gradient Probability Density Distribution, Altitude Band #3
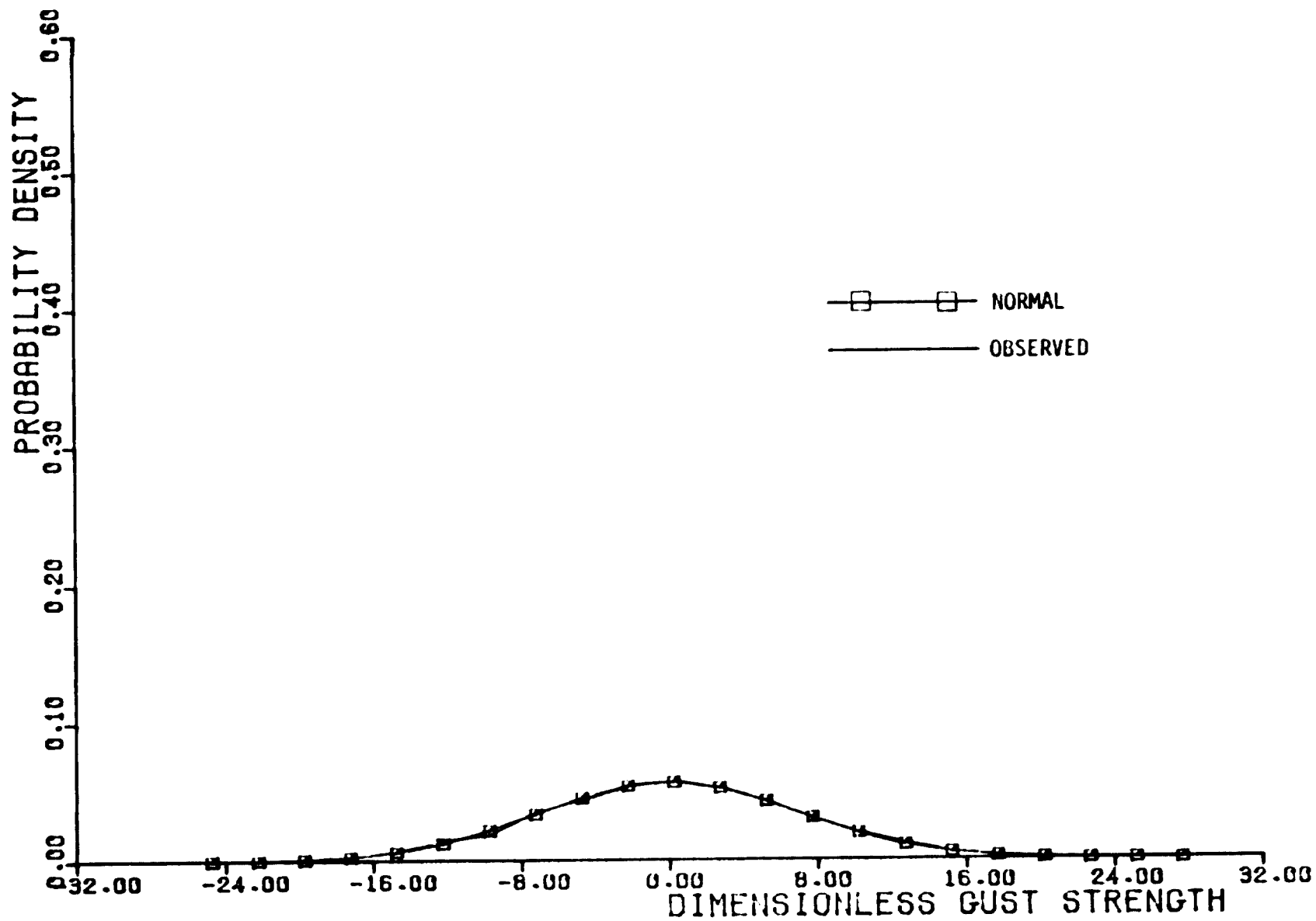
Figure C-24. $\partial u_3/\partial x_2$ - Gust Gradient Probability Density Distribution, Altitude Band #4